RIKAGAKU KENKYUSHO
the Institute of Physical and Chemical Research
Yamato-machi, Saitama Pref., JAPAN

'69

IPCR cyclotron Progress Report 1969

Vol. 3

Edited by Administration Committee of the IPCR Cyclotron

IPCR Cyclotron Progress Report 1969

Vol. 3

The Institute of Physical and Chemical Research
"RIKAGAKU KENKYUSHO" Yamato-machi, Saitama, 351 JAPAN
December, 1969

This volume contains recent information of the IPCR Cyclotron, informal reports and abstracts of papers which will be published at scientific meetings or in publications by staff members, guests,and visitors.

CONTENTS

1. INTRODUCTION

Our cyclotron is mainly operated for use of members of our institute, but it is also used by outside members in two days per month for production of radio isotopes.

Four research groups are studying nuclear physics. Some groups contain outside members who are admitted to work as part time members of our institute. Groups of studying radio chemistry, radiation chemistry, radiation biology, and solid state physics are also using the cyclotron, to which several outside members are contributing much. All these groups are obtaining important results as described in this report.

Maintenance and improvement of the cyclotron and measuring apparata are mainly performed by the members of Cyclotron Laboratory, including the scientific technical staff and operating persons. The stability of the cyclotron is getting better year by year. Especially, this year we succeeded in outstandingly stable operation of heavy ion source and improvement of the nature of beams circulating in the cyclotron.

Hiroo Kumagai

Hiroo Kumagai, Chairman
Administration Committee of
the IPCR Cyclotron

2. MACHINE OPERATION

In the IPCR Cyclotron, no serious fault was found during the third operation year from Dec. 1968 to Nov. 1969. The scheduled machine time in this year was over 230 days, in which the time of unexpected machine stop for repair was less than 5 days even if integrated. Our initial aim to reach the scheduled machine time of 200 days in a year is achieved. Two short periods of overhaul intervened. The time schedule is shown in Table 1. As shown there, the actual beam time is estimated at about 5000 hours a year. Research subjects and their machine times are listed in Table 2.

Several improvements were tried for the cyclotron. One is the new design of the initial acceleration at the central region, which will be mentioned in this Progress Report, and the other is the continuous improvement of the septum system. Under the best conditions, the intensities of deflected beams of protons, alpha particles, and N^{4+} ions were 100, 50, and 2 μA respectively. These values are comparable with those of recent sector focusing cyclotrons. The unexpected variation of deflected currents mentioned in a previous Progress Report (1968) was not completely elucidated. Recently, the dee-voltage has been found to have a few percent variation of 100 cycles and others. This variation will be our next problem to be solved. After that, more precise examinations of the beam emittance, the beam energy resolution and the performance at the central region and at the exit will be undertaken.

Table 1. Machine operating time.

Indication of working time meter		
	Oscillator input power	Ion source input power
Nov. 30, 1968	7415.5 (h)	8113.3 (h)
Nov. 26, 1969	12563.9 (h)	13704.4 (h)
~ 8640 (h)	5148.4 (h)	5591.1 (h)

Schedule for this year (365 days)	
Scheduled machine time	232 (days)
Scheduled time for overhaul and installation	~ 40 (days)
Vacation, holidyas, and sundays	~ 90 (days)

Table 2. Scheduled machine time.

Period IV, Nov. 1968 ~ Nov. 1969

Subject	Days	
Heavy ion reaction	14	
Direct reaction	66.5	
In beam spectroscopy	28	51.5 %
RI production for nuclear spectroscopy	11	
Radiochemistry and RI production	19	
Radiation chemistry and radiation biology	21	
Solid state physics	17	26.5 %
Analysis of nucleid	4.5	
Accelerator physics and machine improvement	22.5	
Experiments of charge exchange	5.5	19.0 %
Machine inspection and repair	16	
RI production for other organizations	7	3.0 %
	232	

The cyclotron was operated on a 24 hours per day system by the operating crew of seven persons under management of five veterans. Their names are shown in the list of personnel at the end of this report. On an occasion of maintenance, overhaul, or improvement of the machine the engineering staff of the Cyclotron Laboratory join the operating group. The engineering members of about 5 persons are usually engaged in the study of accelerator physics, plan of cyclotron improvement and development of nuclear instruments. The members of nuclear physics in the Cyclotron Laboratory also help in some aspects of the machine performance.

3. MACHINE DEVELOPMENT AND ACCELERATOR PHYSICS

3-1. Initial Motion of Ions
Improvements of the Center-Region Geometry and the Internal Beam

Y. Miyazawa, T. Tonuma, A. Shimamura,
T. Inoue, and T. Karasawa

The vertical focusing of internal beam has been experimentally investigated. In the central region of cyclotron the feeler was replaced with a puller arrangement in the spring of 1969. Considerable improvement in the vertical focusing of beam has been obtained by offsetting the ion source and the puller by 10^{o} from the dee line, and thus retarding the phase of the first turn by 10^{o}. Fig. 1 shows the central geometry in the cyclotron consisting of ion source, puller, wing and screen. The puller which is made of a graphite block and put in between two copper plates (10 mm thick) is attached to the copper wing of west dee. The screen which is made of a molybdenum plate (2 mm thick, 70 mm wide, and 50 mm high) is screwed on the supporting tube of the ion source. The positions of ion source and screen are adjustable according to the mass to charge ratio of ion, magnetic field strength and acceleration voltage.

Under the normal operating condition, early orbits are graphically calculated and drawn in Fig. 1.

Beam attenuation curve for 7.2 MeV proton with a usual feeler is shown in Fig. 2(a). The large decrease of beam intensity as seen for the radius below 40 cm depends on the strong vertical electric defocusing force by the feeler. Two separate beams appear for large radius and a part of the beam is lost by collision with a septum due to the precession and phase loss in the region of 65 to 74 cm. Generally speaking, the vertical electric defocusing force is reduced by the 10^{o} offset puller. Beam attenuation curve with 10^{o} offset puller is shown in Fig. 2(b). The beam loss at small radius has been largely reduced by offsetting the ion source and puller by 10^{o} from the dee line so that the first half turn is lengthened from the usual 180^{o} to 190^{o} as shown in Fig. 1. The beam measured without screen and Z-slit decreased somewhat its intensity for the radius below 40 cm, but the beam that reached 40 cm radius was gradually lost for the radius of 68 to 73 cm. Beam measured with screen was hardly lost in the outer region. Useful beam beyond about 28 cm radius, which is selected at the early turns with screen and Z-slit (Z = 10 mm), is well focused and reaches the maximum radius of 74 cm. Beam attenuation curves of d, α, and $^{3}He^{++}$ ions with different energies show the same feature as in 7.2 MeV proton.

At present, the cyclotron is being operated effectively by using the 10^{o} offset ion source-puller arrangement with screen.

The usual beam extraction efficiency is above 30 % in spite of unstabilized dee voltage, in which ripples of about 5 % with a few hundred cycles per second are observed. Reducing the dee voltage ripples is being studied now.

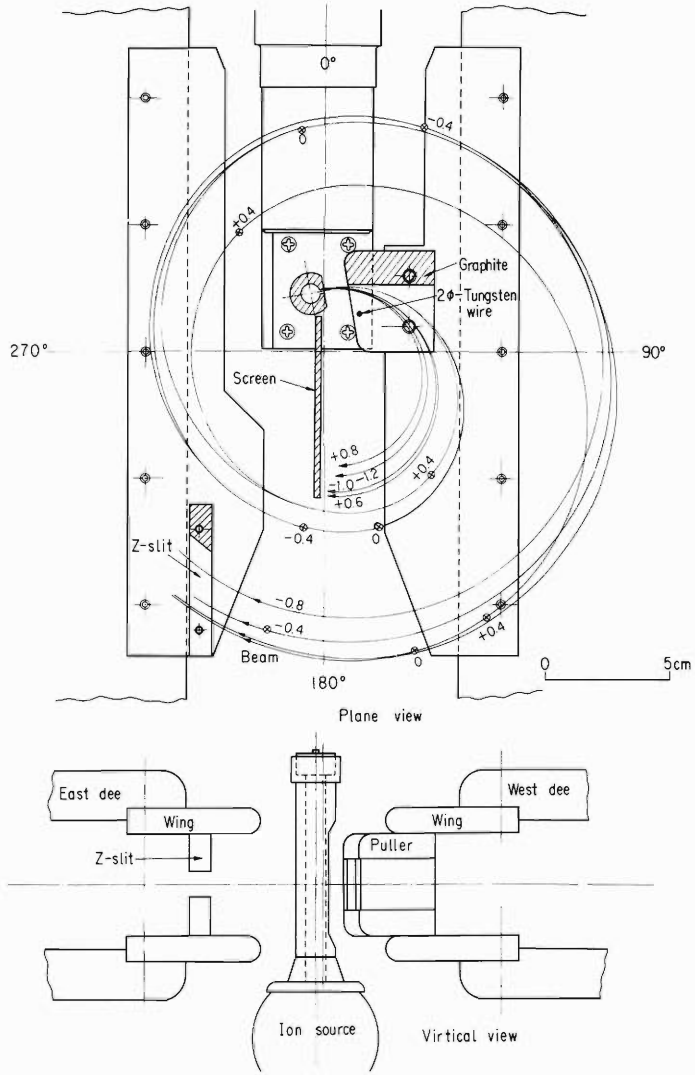

Fig. 1. Plane and vertical views of the cyclotron center with 10° offset ion source and puller. The numerals on the beam orbits show the starting phase of ions.

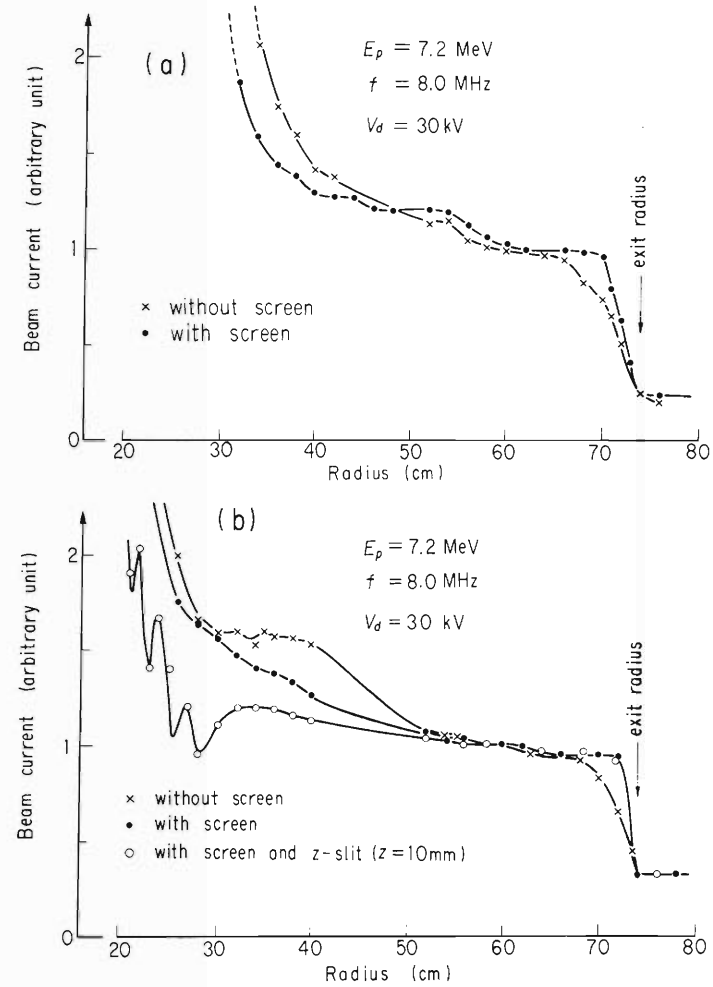

(a) With 0° offset ion source-feeler arrangement.
(b) With 10° offset ion source-puller arrangement.

Fig. 2. Beam intensity versus radius.

3-2. An Improved Heavy Ion Source[1)]

I. Kohno, Y. Miyazawa, T. Tonuma, S. Nakajima,
T. Inoue, A. Shimamura, K. Yoshida, and T. Karasawa

A new type source which has been improved on the old one[2)] is now operating satisfactorily.

Fig. 1 is a cross sectional view of the source. The main improvement is that the graphite anode is replaced with a water-cooled copper anode and this anode is welded to both upper and lower support cases. By this improvement the cathode axis becomes to be aligned with the magnetic field more easily and an ion source life of 20 hours is obtained surely, moreover. O^{4+} particles can be accelerated without C^{3+} particles mixed by not using a graphite cone in the cyclotron. Operation conditions of the new source are almost the same with those of the old one.

At present, several heavy ions are accelerated at sufficient intensity in the cyclotron as shown in Table 1.

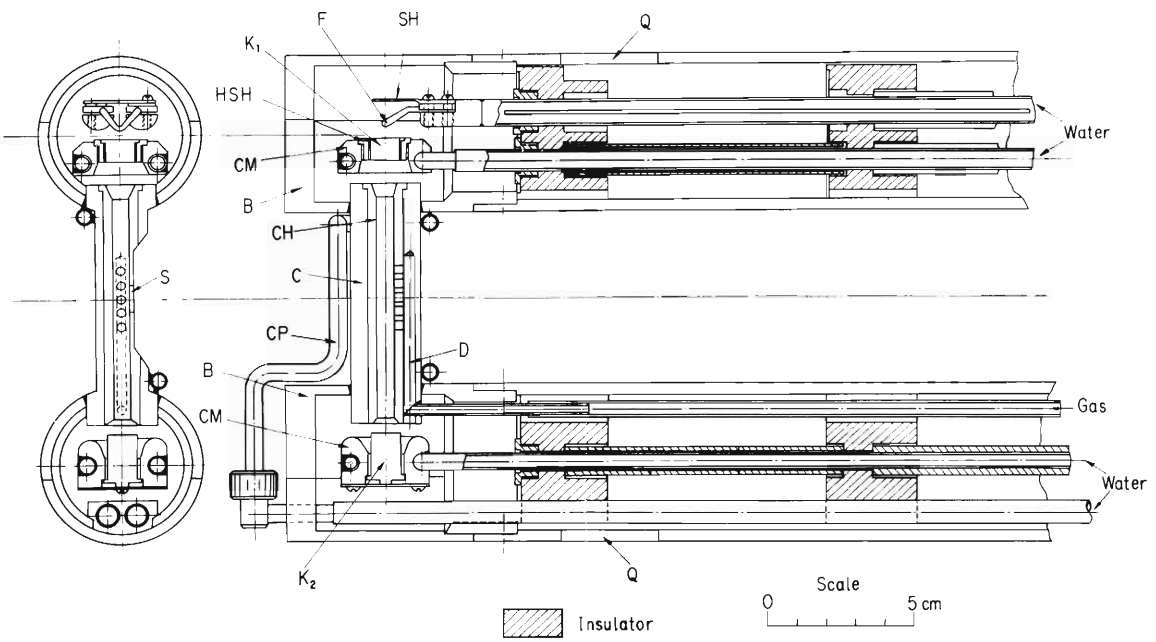

K_1 : Hot cathode (w),
CM : Cathode mount (copper and water-cooled),
SH : Electron shield (Mo),
C : Anode block (copper and water-cooled),
K_2 : Reflector cathode (w),
S : Source aperture,
CH : Anode chimney (copper),
HSH : Cathode heat shield,
Q : Exhaust window,
D : Distribution plenum,
B : Anode box (copper),
F : Filament (w),
CP : Cooling pipe (copper).

Fig. 1. Schematic view of new ion source.

Table 1. Energy and beam current.

	C^{3+}	C^{4+}	N^{4+}	N^{5+}	O^{4+}	O^{5+}
Energy (MeV)	39～75	39～120	45～100	45～160	52～100	52～140
Maximum Current* (μA)	5	4	5	1	2	0.4

* Maximum beam current extracted from the cyclotron.

The photograph of the new type ion source is shown in Fig. 2.

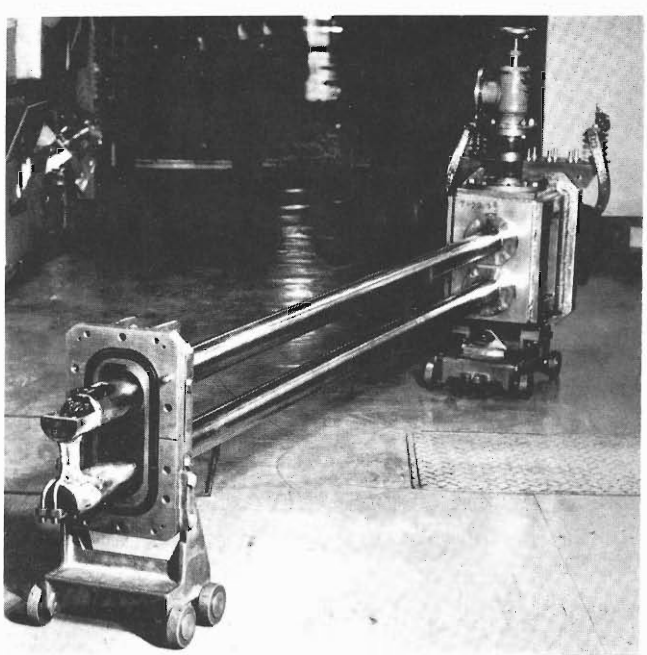

Fig. 2. The photograph of ion source.

References

1) I. Kohno et al.: Proc. 5th Intern. Cyclotron Conf. (1969). (To be published in Japan J. Appl. Phys.)
2) I. Kohno et al.: Nucl. Instr. Methods, 66, 283 (1968).

3-3. The Beam Analyzing Magnet

K. Matsuda, H. Kamitsubo, N. Nakanishi, S. Motonaga,
M. Hemmi, S. Takeda, H. Nakajima, and F. Yoshida

(1) General description

The beam transport and beam analyzing system for the I P C R 160 cm Cyclotron, installed in 1967, was reported in the 1967 Cyclotron Progress Report.

With the increase of experimental necessity, some developments and improvements have been made on the beam transport and analyzing system. Fig. 1 shows the layout of the improved system. Main rearrangement was to provide a place along the beam line in front of the switching magnet to install a beam buncher, which is under construction. The beam courses, #6 and #7, are newly constructed for the gamma ray experiment and the "on-line beta ray" experiment respectively.

The nuclear reaction particle analyzer was constructed, and the experiment with a floating wire technique was performed for determination of the lens properties. Now, the experiment using a known nuclear reaction is under way for the same purpose. A more precise nuclear reaction experiment with the system is to be expected.

(2) Calibration of beam analyzer

Precise nuclear spectroscopic experiments require a beam of particles well defined in energy. The high precision of beam energy has already been obtained with the present configuration. Fig. 1 shows also the arrangement of the beam analyzing system.

To determine the properties of the beam analyzing magnet, two kinds of experiments were carried out, one is the experiment using the well-known Th-α source with energy of 8.766 MeV. Fig. 2 shows schematically the set up in this experiment and alpha spectrum. Alpha particles emitted from Th-α source go into the magnet through the baffle (Ba) and reach the slit (S_D) behind the magnet. The baffle (Ba) limits the particle trajectories, so that each spectrum with a different baffle position does not agree when the slit (S_D) is placed in the unsuitable position as shown in Fig. 3. In this experiment, absolute value of the radius of 1603 mm is obtained and the resolution in energy of $\Delta E/E = 0.11$ % is given with source and slit width of 1.5 and 2 mm respectively.

Energy resolution of the beam analyzing magnet was also measured by the elastic scattering of protons on ^{12}C. It is known that the elastic scattering of proton on ^{12}C shows an isospin forbidden compound resonance at proton energy of 14.255 MeV, and that the width T is less than 1 keV. The result is shown in Fig. 3. The ordinate and abscissa indicate the relative yield of elastically scattered protons and the magnetic field strength of the analyzing magnet, respectively. Error bars indicate the statistical accuracy only. A detector (SSD) used was set at an angle of 165° (lab.) and at this time the slit at the object and image point was set 1 mm in width. Curves in the figure indicate the estimated ones under the assumption of the Temmer's result[1] and of that the incident beam has an energy distribution of Gaussian type with corresponding width. It is concluded from the fitting between the observed resonance curve and the calculated one the energy resolution of the analyzer is 4.9×10^{-4} (FWHM). This value is consistent with the value of 5.0×10^{-4} (FWHM) based on the optical properties of the

analyzing magnet system.

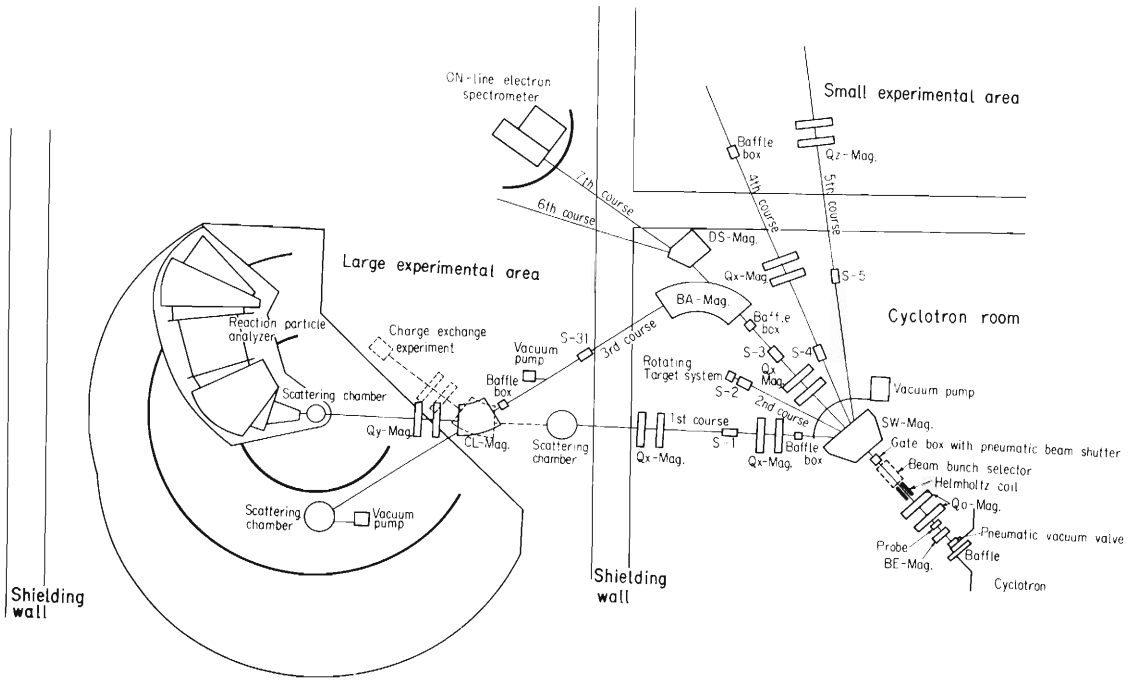

Fig. 1. Beam focusing and analyzing system for IPCR 160 cm Cyclotron.

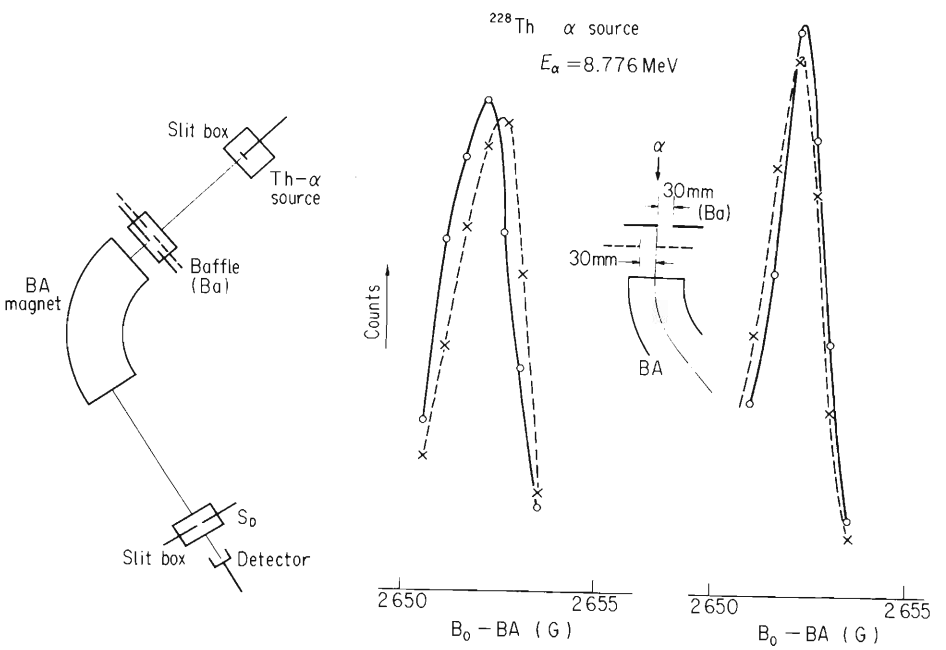

S, S_D : Slit box, Ba : Baffle .

Fig. 2. Test arrangement for calibration of the beam analyzer.

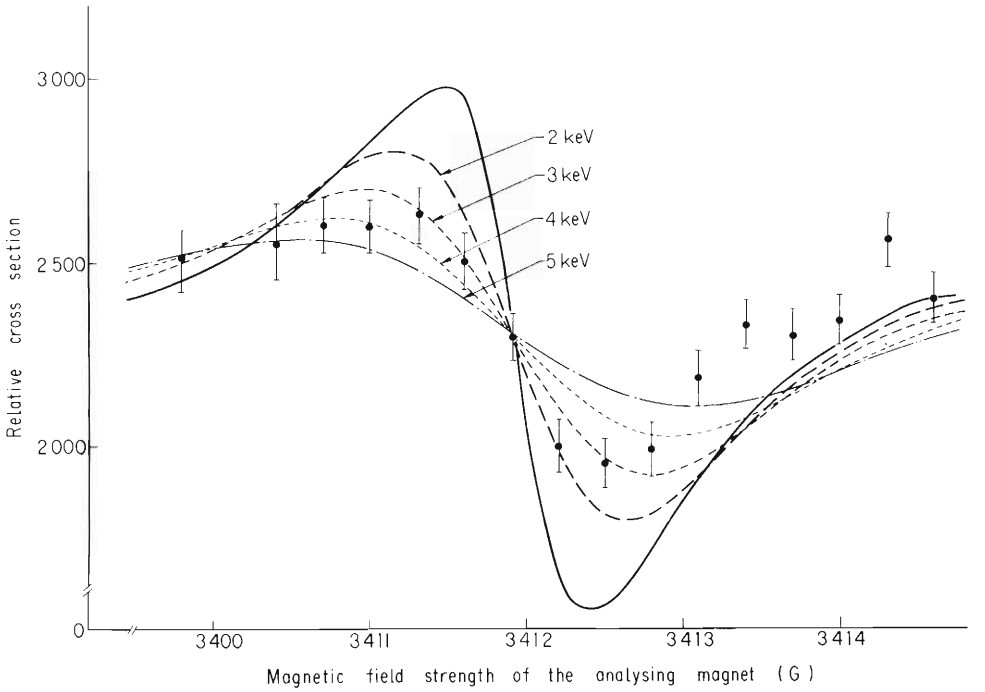

Fig. 3. 14.255 MeV resonance of $^{12}C(p, p)$ at $\theta_{lab.} = 165^{o}$, a real line indicates the excitation curve by Temmer and the other curves the estimated ones based on the assumed beam energy resolution of 2, 3, 4, 5 keV.

Reference

1) G.M. Temmer and R. van Bree: Intern. Conf. Nucl. Phys., Gatlinburg (1966).

3-4. Charge Exchange Experiment (1)

Measurement of Electron Loss Cross Section by Multicharged Ions in Gas

T. Tonuma, Y. Miyazawa, T. Karasawa, and I. Kohno

Experiment of charge exchange gives detailed information on the acceleration or detection of heavy ions.

Electron loss in passage of ions through matter has been studied extensively for ions of hydrogen and helium.[1] Electron loss by heavier ions has been studied mainly at ion energies $E < 0.8$ MeV/nucl.[2] The present paper reports about the cross sections of electron loss in nitrogen gas by carbon and nitrogen ions of 3 to 7 MeV/nucl. accelerated in the IPCR 160 cm Cyclotron.

The cross section is calculated from the charge exchange equation:

$$\frac{dF_k(\pi)}{d\pi} = \sum_j F_j(\pi)\,\sigma_{jk} \quad ,$$

where F_k is the relative number of ions of charge state k in the charge distribution in a volume of one cm^2 cross section along the ion path, ($\pi = \int Ndl$, where N is the number of gas atoms per cm^3 and dl is an ion path element in the gas), and σ_{jk} is the cross section of charge exchange from the charge state j to k.

The charge exchange composition of a three-component ion beam, in which, for example, C^{4+}, C^{5+}, and C^{6+} ions are measured when an incident C^{4+} ion passes through a medium, is expressed by the following equation:

$$\begin{pmatrix} dF_4/d\pi \\ dF_5/d\pi \\ dF_6/d\pi \end{pmatrix} = \begin{pmatrix} -(\sigma_{45}+\sigma_{46}) & \sigma_{54} & \sigma_{64} \\ \sigma_{45} & -(\sigma_{54}+\sigma_{56}) & \sigma_{65} \\ \sigma_{46} & \sigma_{56} & -(\sigma_{64}+\sigma_{65}) \end{pmatrix} \begin{pmatrix} F_4 \\ F_5 \\ F_6 \end{pmatrix}$$

Cross sections for electron loss were measured, using the apparatus shown in Fig. 1. Multicharged ions were accelerated in the cyclotron and arrived at the charge-exchange (collision) chamber, consisting of a cylinder of 2 inches in diameter and 50 cm in length with inlet and exit channels of 4 mm in diameter and 20 mm in length. Gas was admitted to the chamber continuously and the pressure was measured with $10 \sim 20$ % accuracy by a Pirani gauge. The pressure in the collision chamber was varied from 1×10^{-3} to 4×10^{-1} Torr for nitrogen gas.

When a beam of ions with the initial charge i traversed the gas, ions with charges $k \neq i$ resulted from electron capture or loss. The charge distribution in the beam was determined by an analyzing magnet (AM) and a Faraday cup. The analyzing magnet had the radius of curvature of 1.6 meters and bent ions at 35 degrees. Ions bent by the analyzing magnet were focused by a quadrupole magnet and arrived at the Faraday cup apart from about 4 meters. Exciting currents of both the analyzing magnet and the quadrupole magnet were proportional to the charge states of ions. All ions which were separated into respective charge states of ions by the charge exchange in the collision chamber and came out from the exit channel, were focused to a spot of about 1 cm in

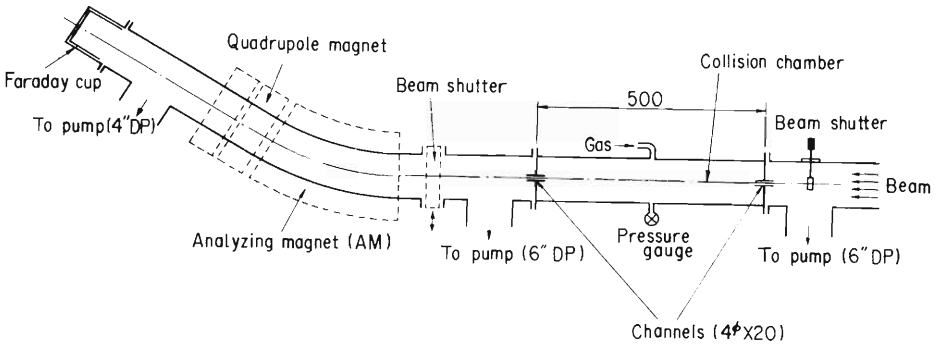

Fig. 1. Diagram of apparatus.

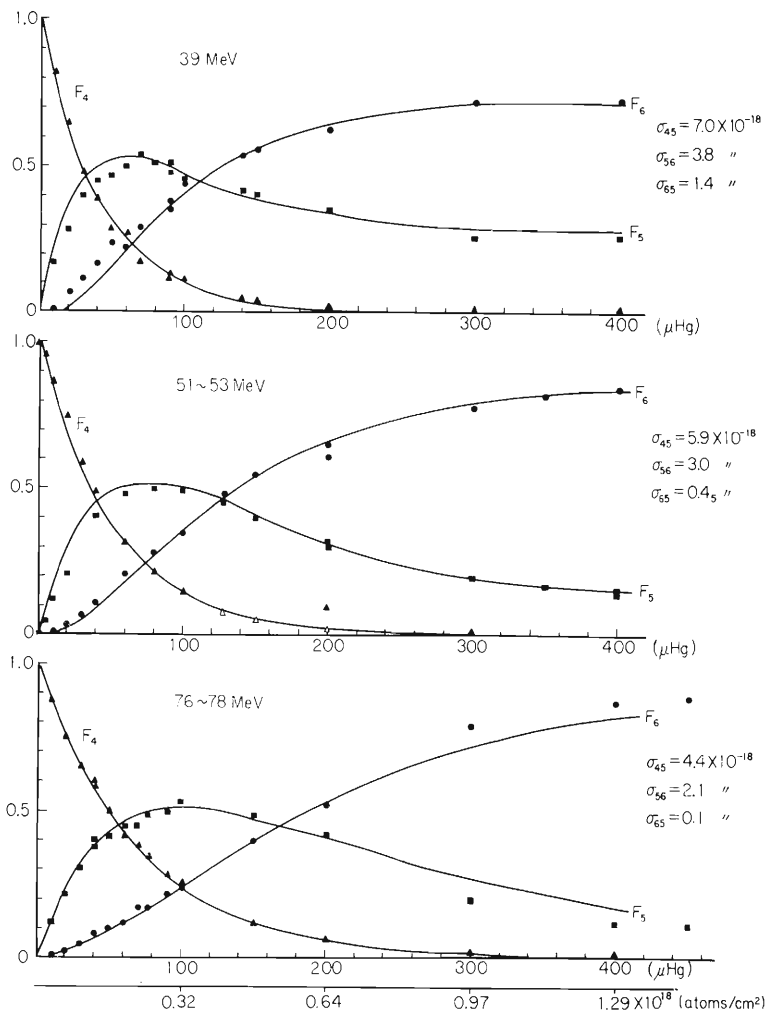

Fig. 2. Charge distribution by carbon ion in nitrogen gas.

diameter on the Faraday cup.

Fig. 2 shows the curves of charge distribution versus pressure of nitrogen gas in the collision chamber by carbon ions, C^{4+} ion being incident particle, and F_4, F_5, F_6 represent the fractions of C^{4+}, C^{5+}, and C^{6+} respectively. From these measurements the cross sections of electron loss are calculated and shown in Fig. 3 (a), where $\sigma_{i,i+1}$ gives the cross section of charge exchange from the charge i to i+1 of carbon ion. It is found that the charge distribution depends on carbon ion energy and the cross section of electron loss decreases with energy. Each of the solid lines in Fig. 2 represents the fraction of carbon ion applied by the cross sections given on the right.

Fig. 3 (b) shows the cross sections by nitrogen ion in nitrogen gas when N^{4+} ion is the incident particle. The data below 0.7 MeV/nucl. are those of Moscow State University.[2] The experimental uncertainty, however, particularly in the $dF_k/d\pi$, makes it impossible to obtain a unique set of values for the cross sections of σ_{56} and σ_{67} as seen in Fig. 3 (b). Therefore, σ_{56} and σ_{67} of N ion should be measured with more sensitive current meters, using an incident particle of N^{5+} ion, of which the intensity is much smaller than N^{4+} ion.

It is intended to measure the pressure of gas with more accuracy and to measure the cross sections of electron loss and capture in the beams of ions of ^3He, ^{12}C, ^{14}N, and ^{16}O in various gases and the equilibrium charge distributions of the ions in gases and some solid media.

Application to heavy ion acceleration-beam attenuation during acceleration caused by charge exchange.

The yield of heavy ions is reduced by charge exchange in collision with residual gas molecules during acceleration. Fig. 4 shows the ratio of N^{4+} beam current measured at 70 cm radius to that at 40 cm radius (maximum radius is 74 cm) versus the pressure of the accelerating chamber of the IPCR Cyclotron. It is found that the ratio decreases rapidly with the pressure. The pressure of the chamber was varied by adjusting the nitrogen gas flow introduced into the ion source. In Fig. 4 is shown the pressure of the

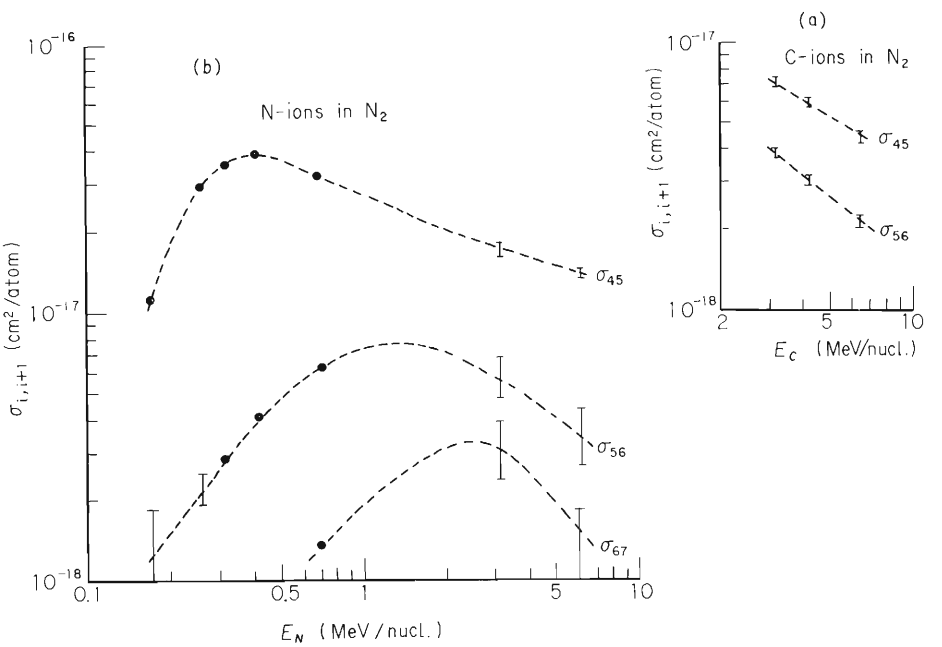

The data below 0.7 MeV/nucl. are those of Moscow State University.[2]

Fig. 3. Cross sections of electron loss .

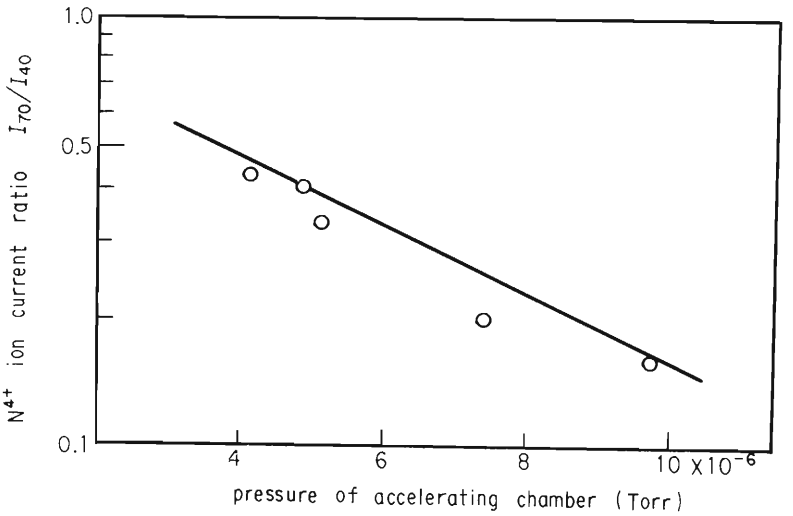

Fig. 4. N^{4+} ion beam attenuation versus the pressure of the accelerating chamber in the IPCR Cyclotron caused by charge exchange.

accelerating chamber near the diffusion pump, but it is noticed that the pressure in dees, where ions are accelerated, is 3～4 times larger than that of the chamber.

When the electron loss cross sections of charge exchange for N^{4+} to N^{5+} in nitrogen gas, the path length of ions during acceleration and the pressure in the dees are given, the ratio of beam attenuation caused by charge exchange can be calculated. In Fig. 4 the solid line represents the result of calculation using the electron loss cross section σ_{45} shown in Fig. 3 (b) and it agrees with the measured value.

If the ratio of the beam attenuation should be kept at larger than a half, it is necessary that the pressure is reduced below 4×10^{-6} Torr. Under the normal condition the pressure of accelerating chamber is $2 \sim 4 \times 10^{-6}$ Torr.

References

1) S.K. Allison: Rev. Modern Phys., 30, 1137 (1958).
2) I.S. Dimitriev et al.: Sov. Phys. JETP., 15, 11 (1962).

4. NUCLEAR PHYSICS
Scattering and Reactions

4-1. Elastic and Inelastic Scattering of ^{14}N and ^{12}C Particles

I. Kohno, S. Nakajima, T. Tonuma, and M. Odera

Differential cross sections of 70 MeV ^{12}C particles elastically and inelastically scattered by ^{12}C and angular distributions of elastically scattered 65, 84, and 90 MeV ^{14}N particles by ^{12}C and ^{27}Al have been measured. The optical model analysis for angular distributions of elastically scattered ^{14}N and ^{12}C particles by ^{12}C, ^{27}Al, ^{28}Si, and ^{58}Ni which were measured since last year have been performed. Throughout the analysis, the automatic search code of optical model parameters programmed by Wada[1] was used.

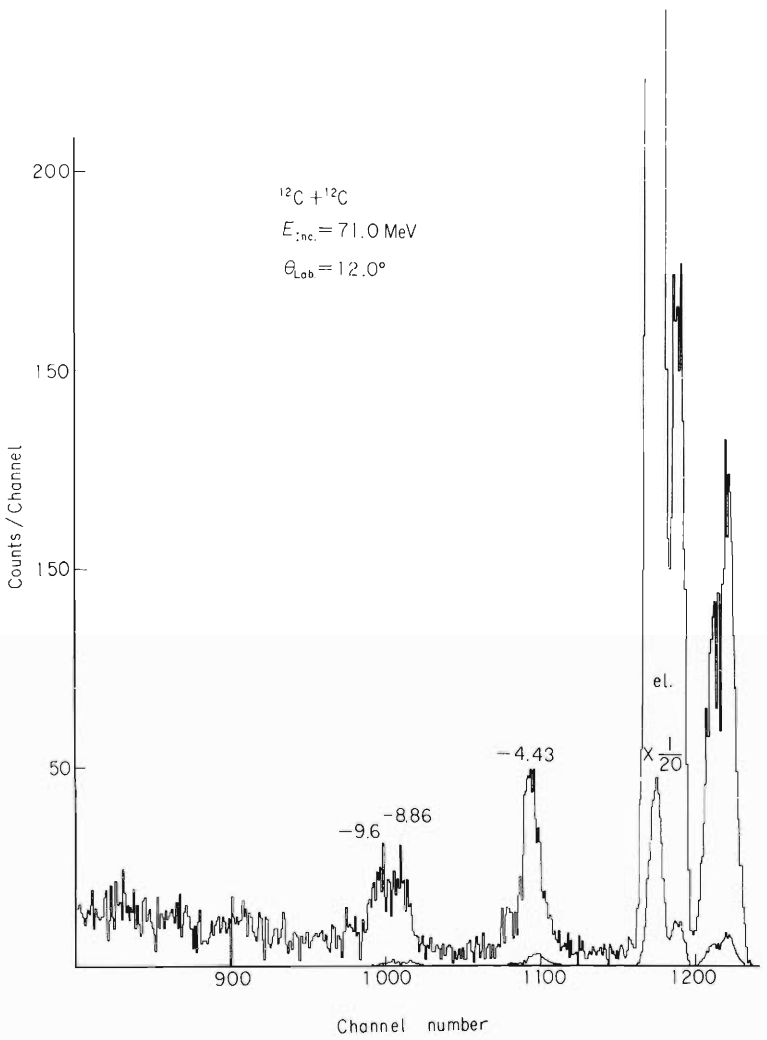

Fig. 1. Spectrum of $^{12}C + ^{12}C$ at energy of 71 MeV.

Experimental arrangement was the same as reported in the last year's Progress Report.[2)]

(1) $^{12}C + ^{12}C$

Fig. 1 is a pulse height spectrum of ^{12}C particles scattered by the ^{12}C target. A doublet is found at the 9 MeV excited level of ^{12}C. One is 9.6 MeV (3^-) excited level of ^{12}C and the other may be mutual excitation to 4.43 MeV (2^+) of both ^{12}C nuclei. In Fig. 2 the angular distributions of each peak in Fig. 1 are shown.

(2) Angular distributions of elastically scattered ^{14}N particles

In Figs. 3 and 4 angular distributions of elastically scattered ^{14}N particles by ^{12}C and ^{27}Al are shown. Incident energies of ^{14}N particles are 65, 84, and 90 MeV, respectively. The form of the angular distribution is changed with the value of Coulomb parameter (η): a relatively smooth dropoff for the $^{27}Al + ^{14}N$ case at the energy of 84 MeV where η is above 6.6, a dropoff with small undulations for the $^{27}Al + ^{14}N$ case at the energy of 84 MeV and $\eta = 5.82$ and a diffraction pattern for the $^{12}C + ^{14}N$ at the

Table 1. Optical model parameters fitted to experimental angular distributions of elastically scattered ^{14}N and ^{12}C particles.

	V_0 (MeV)	r_0 (fm)	a (fm)	W_0 (MeV)	r_{0I} (fm)	a_I (fm)	r_c (fm)	E (MeV)	η
(1) $^{58}Ni + ^{14}N$	60	1.048	0.705	12	1.197	0.516	0.99	84	12.6
(2) $^{28}Si + ^{14}N$	60	1.147	0.527	14	1.163	0.929	0.77	84	6.3
(3) $^{28}Si + ^{14}N$	120	1.009	0.627	14	1.224	0.758	0.833	84	6.3
(4) $^{27}Al + ^{14}N$	70	1.101	0.615	18	1.22	0.738	0.833	90	5.7
(5) $^{28}Si + ^{12}C$	55	1.238	0.4624	10	1.174	0.8114	0.850	49.3	6.53
(6) $^{28}Si + ^{12}C$	55	1.021	0.697	20	1.176	0.671	0.906	70	5.5
(7) $^{28}Si + ^{12}C$	55	1.121	0.631	16	1.201	0.776	0.906	83.5	5.0
(8) $^{28}Si + ^{12}C$	100	1.025	0.6489	16	1.197	0.772	0.906	83.5	5.0
(9) $^{12}C + ^{12}C$	62.3	1.18	0.522	37	1.15	0.464	0.68	71	2.3

η : Coulomb parameter

Optical potential

$$-V(r) = \frac{V_0}{1 + \exp\left(\frac{r - R_0}{a}\right)} + \frac{i\,W_0}{1 + \exp\left(\frac{r - R_I}{a_I}\right)}$$

$R_0 = r_0 (M_1^{1/3} + M_2^{1/3})$, $R_I = r_{0I} (M_1^{1/3} + M_2^{1/3})$, $R_c = r_c (M_1^{1/3} + M_2^{1/3})$

M_1 : Incident particle mass, M_2 : Target mass

M_c : Coulomb radius

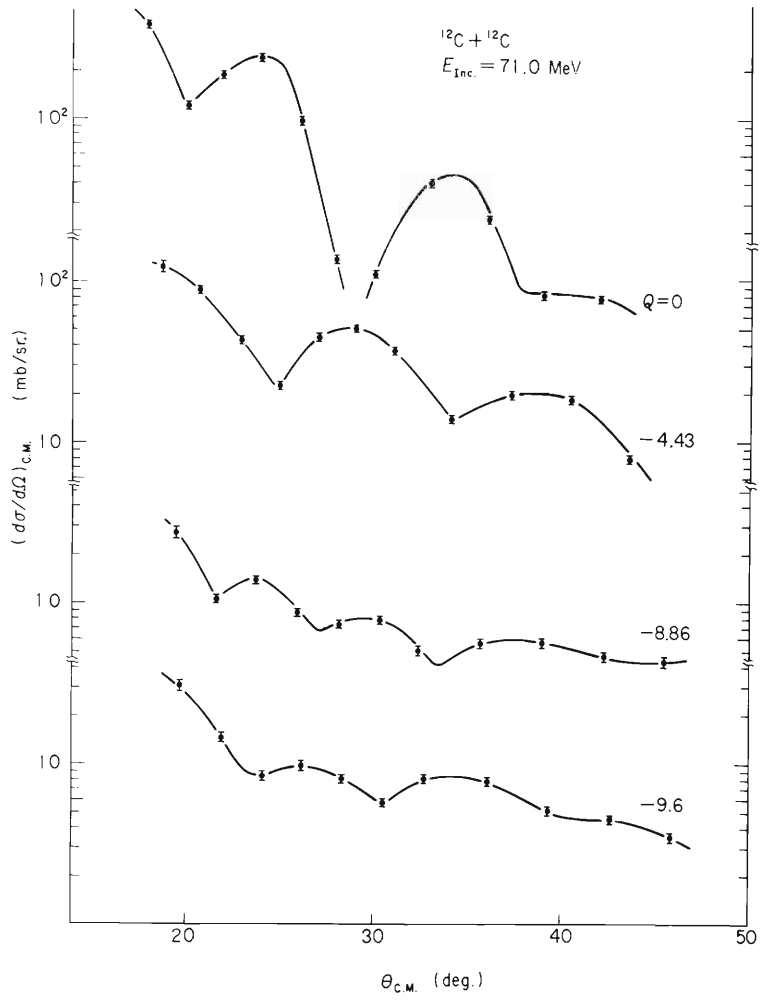

Fig. 2. Angular distributions of ^{12}C elastically and inelastically scattered by ^{12}C at energy of 71 MeV.

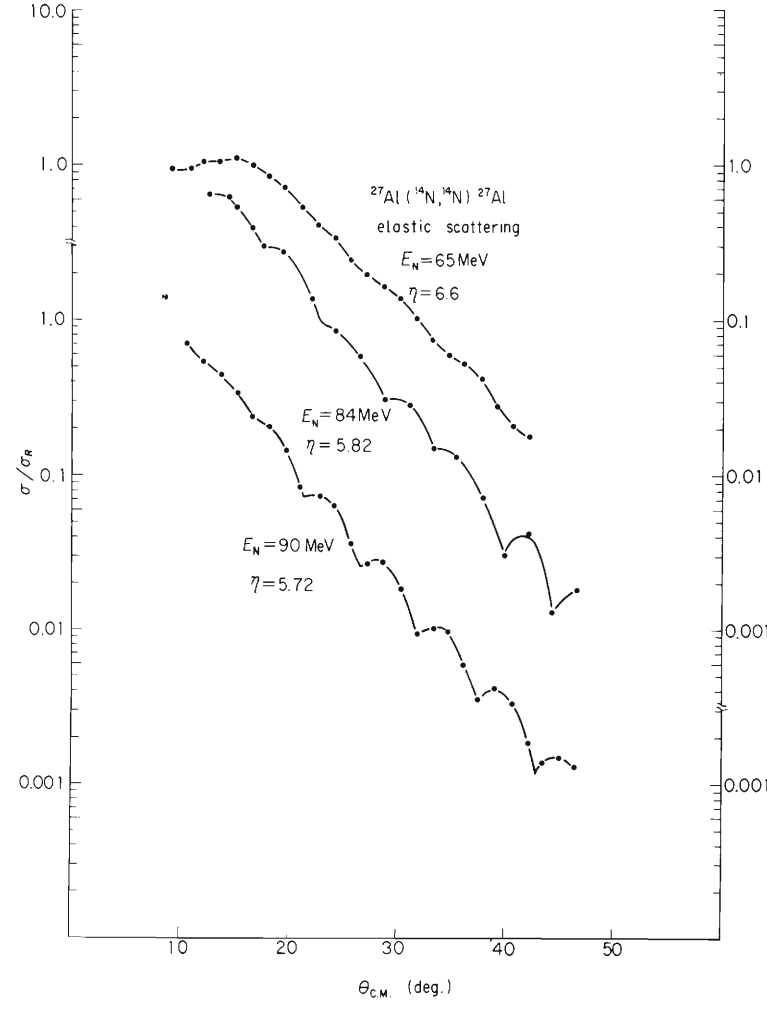

Fig. 3. Angular distributions of ^{14}N elastically scattered by ^{27}Al at energies of 65.84 and 90 MeV.

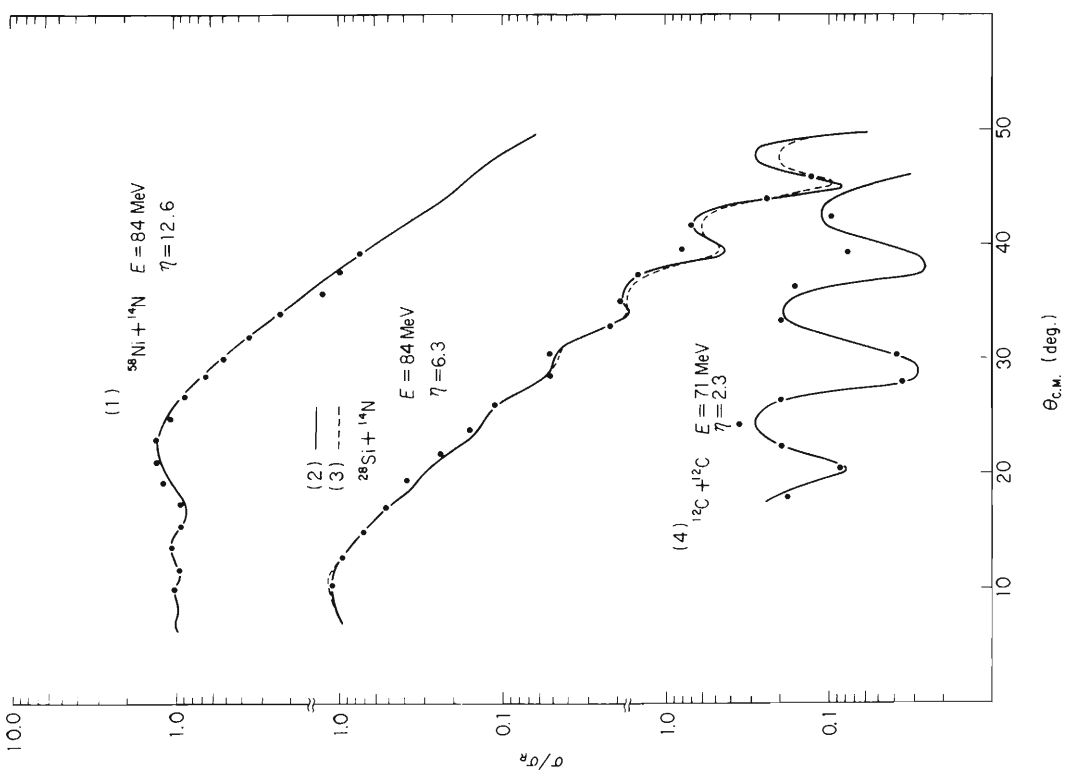

Fig. 5. Optical model analysis of ^{12}C and ^{14}N particles elastically scattered by ^{12}C, ^{28}Si, and ^{58}Ni.

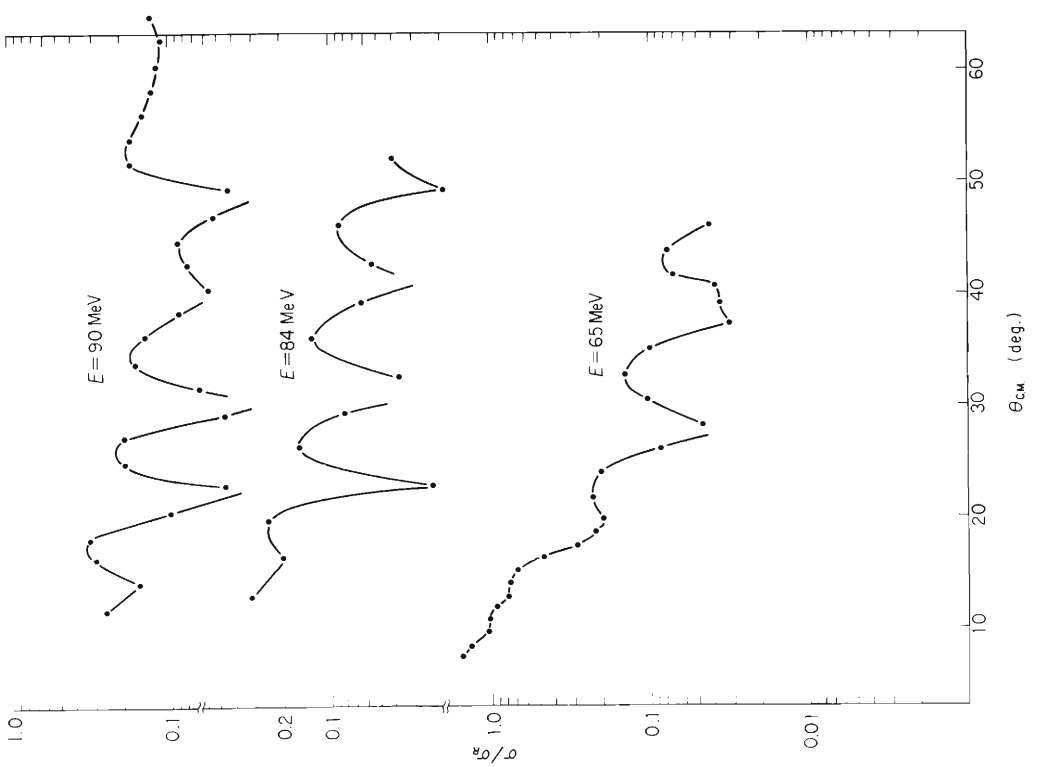

Fig. 4. Angular distributions of ^{14}N elastically scattered by ^{12}C at energies of 65.84 and 90 MeV.

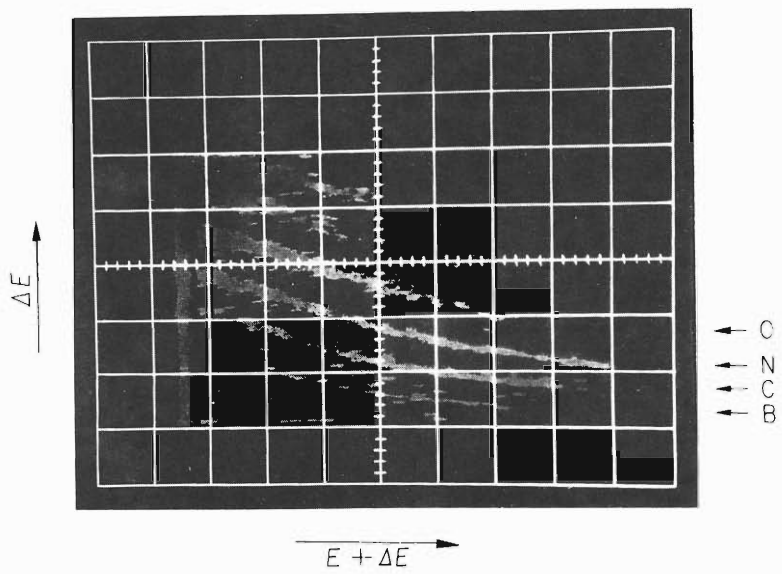

Fig. 6. ΔE viz. E oscillogram at the reaction of 84 MeV ^{14}N on ^{12}C.

energy of 84 MeV and η = 2.77 are found. These three types of scattering are also found in the alpha particle scatterings[3] and their features are almost the same.

(3) Analysis by the search code of optical model parameters

Angular distributions of elastically scattered ^{14}N and ^{12}C particles with variable values of Coulomb parameter have been analyzed by the search code. Their preliminary results are shown in Fig. 5 and in Table 1.

(4) Emitted particle spectrum

The reactions induced by heavy ions should yield a large variety of products with the kinetic energy they carry. A counter telescope consisting of a very thin totally depleted counter 10 μm thick and a 200 μm counter were used to discriminate particle species. Fig. 6 shows a ΔE viz. E oscillogram at the reaction of 84 MeV ^{14}N on ^{12}C. Many species of particles other than incident ions are seen. Using the multiparameter pulse height analysis method the spectrum of each particle can be taken. Thus a peak appearing in ^{14}N + ^{12}C spectrum was identified as that from ^{13}N and ^{13}C (Q value = -5.7) originated from the single proton or neutron transfer reaction.

References

1) T. Wada: IPCR Cyclotron Progr. Rep. 2, 87 (1968).
2) I. Kohno et al.: ibid., p. 48.
3) G. Igo et al.: Phys. Rev., 101, 1508 (1956).

4-2. Spin Flip in the Inelastic Scattering of Protons from ^{12}C at Energies around 13.1 MeV

T. Fujisawa, S. Motonaga, Y. Chiba, T. Wada,
S. Kobayashi*, K. Katori**and A. Stricker***

Proton spin flip probabilities in the reaction $^{12}C(p, p')\ ^{12}C^*(4.43\ MeV)$ were measured in an energy range between 12 and 14 MeV.[1] Elastic and inelastic differential cross sections were also measured. The measurements were done in detail near the resonance in the elastic cross section at 13.1 MeV.[2] In this energy region, the spin flip probability showed remarkable energy dependence in contrast with that of inelastic scattering cross section. The measurements were done by means of the (p, p', γ) coincidence technique.[1]

The proton beam from I P C R variable energy cyclotron was focused on a target in a 75 cm scattering chamber through several Q-magnets and a beam analyzing magnet.[3] The beam current was kept within 30 nA for decreasing the chance coincidence. The energy resolution of the beam through the analyzing magnet was 0.2 %, its horizontal divergence was within 1 degree and the size was 1 mm × 2 mm on the target.

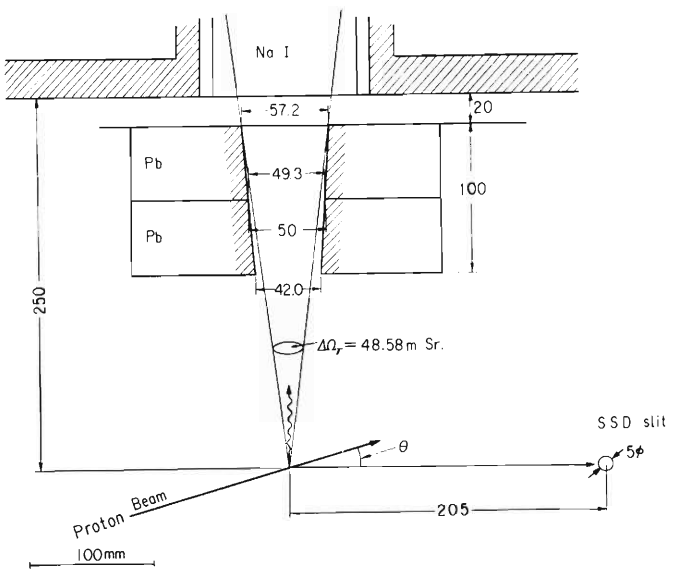

Fig. 1. Schematic diagram of the detector system.

* University of Tokyo.
** Tokyo University of Education.
*** On leave from Basel University in Switzerland.

Fig. 1 shows a schematic diagram of the detector system. A Faraday cup was set 2.5 m away from the scattering chamber and shielded by lead of about 40 cm in thickness and by concrete. The gamma ray detector was a 3 in. $\times$ 3 in. NaI-crystal with a 2 in. photo-multiplier (56 AVP). A slit of the γ-detector was made of lead 10 cm thick with an aperture of 57 mm. The efficiency of the gamma ray detector system was determined experimentally by comparing the cross section of inelastically scattered proton which excited the level of 4.43 MeV with the angular distribution of the gamma ray. The proton detector was an ORTEC 2000 μ m surface barrier unit. Its defining slit has 5 mm ϕ and placed at the position 20 cm apart from the target. A monitor detector was at 90^{o} (lab. angle). The carbon target was made by the cracking method and its thickness was 0.98 mg/cm^2. Fig. 2 shows a schematic diagram of the electronics. The number of true coincidences of inelastic protons with gamma ray and its statistical error were determined by the following equations:

$$NCT = NC_i - \frac{N_i}{N_e} \cdot NC_e$$

and

$$\Delta NCT = (NC_i + (\frac{N_i}{N_e})^2 \cdot NC_e)^{1/2},$$

where NCT and ΔNCT are the number of true coincidences of inelastic protons with gamma rays and its statistical error, NC and N are the measured coincident number and the total number of counts, and suffixes e and i indicate elastic and inelastic scatterings respectively.

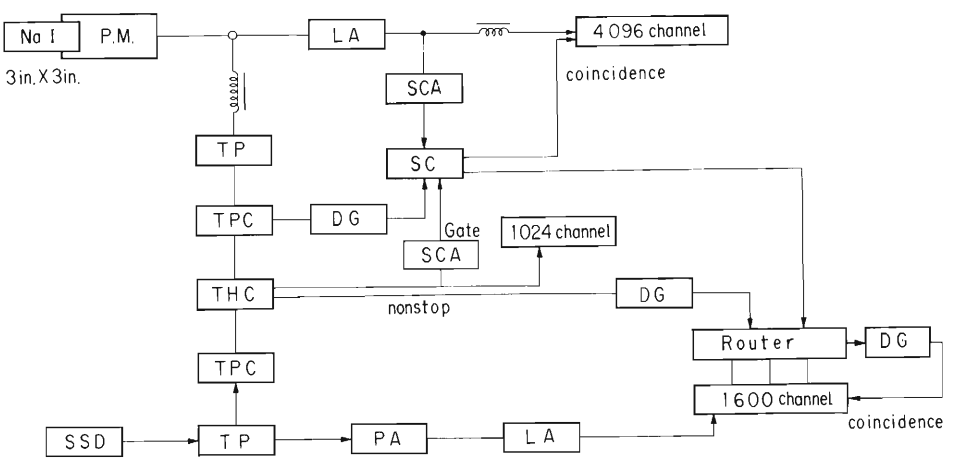

PM :	Photo-multiplier,	S S D :	2000 μ surface barrier unit,
TP :	Time pick off,	T P C :	Time pick off control,
T H C :	Time to pulse height converter,	S C :	Slow coincidence,
D G :	Delay and gate generator,	S C A :	Single channel analyzer.
P A :	Pre-amplifier,	L A :	Linear amplifier.

Fig. 2. Block diagram of the electronics.

In Fig. 3, the excitation curves for the spin flip probabilities and differential cross section are shown. The proton detector was at 90° (lab. angle). In Fig. 4 the angular distributions are shown. The effect coming from finiteness of aperture of gamma ray detector was corrected.

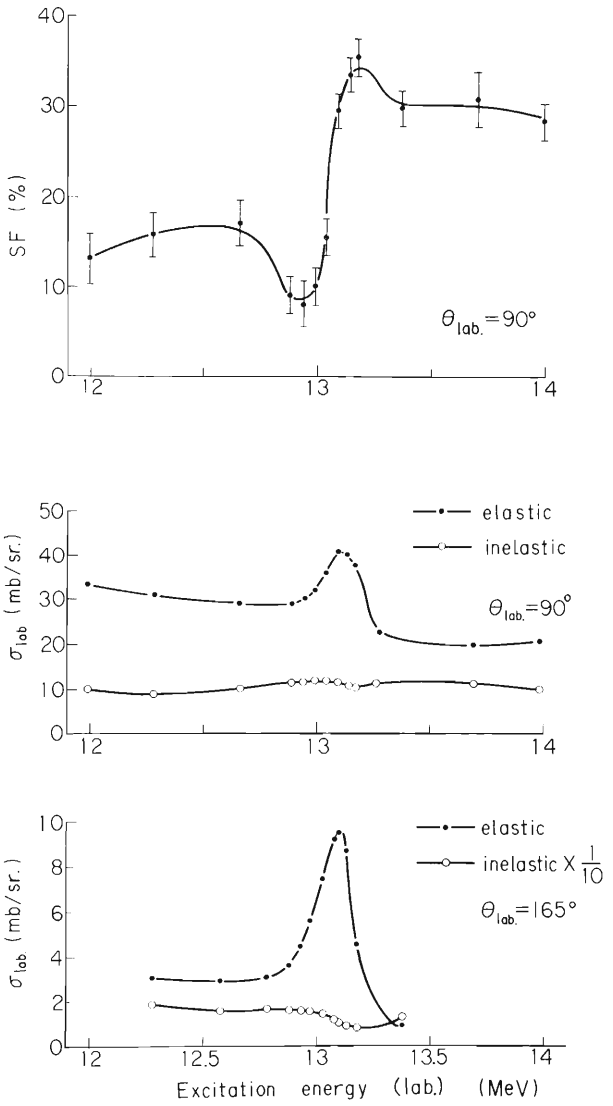

Fig. 3. Spin flip probability and differential cross section for excitation energy.

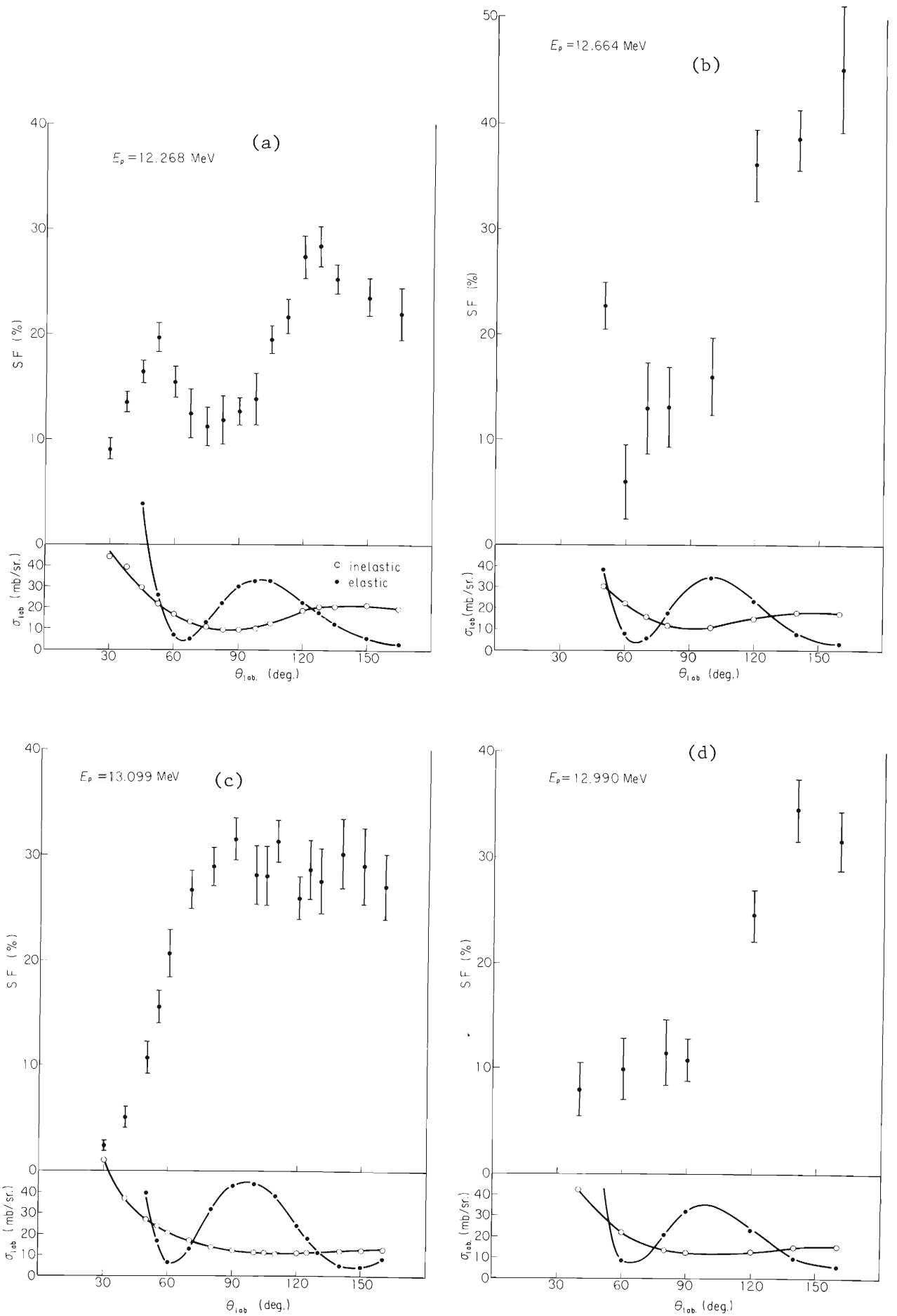
(a)
E_p = 12.268 MeV
(b)
E_p = 12.664 MeV
(c)
E_p = 13.099 MeV
(d)
E_p = 12.990 MeV
S F (%)
σ_{lab} (mb/sr.)
○ inelastic
● elastic
θ_{lab} (deg.)

Fig. 4

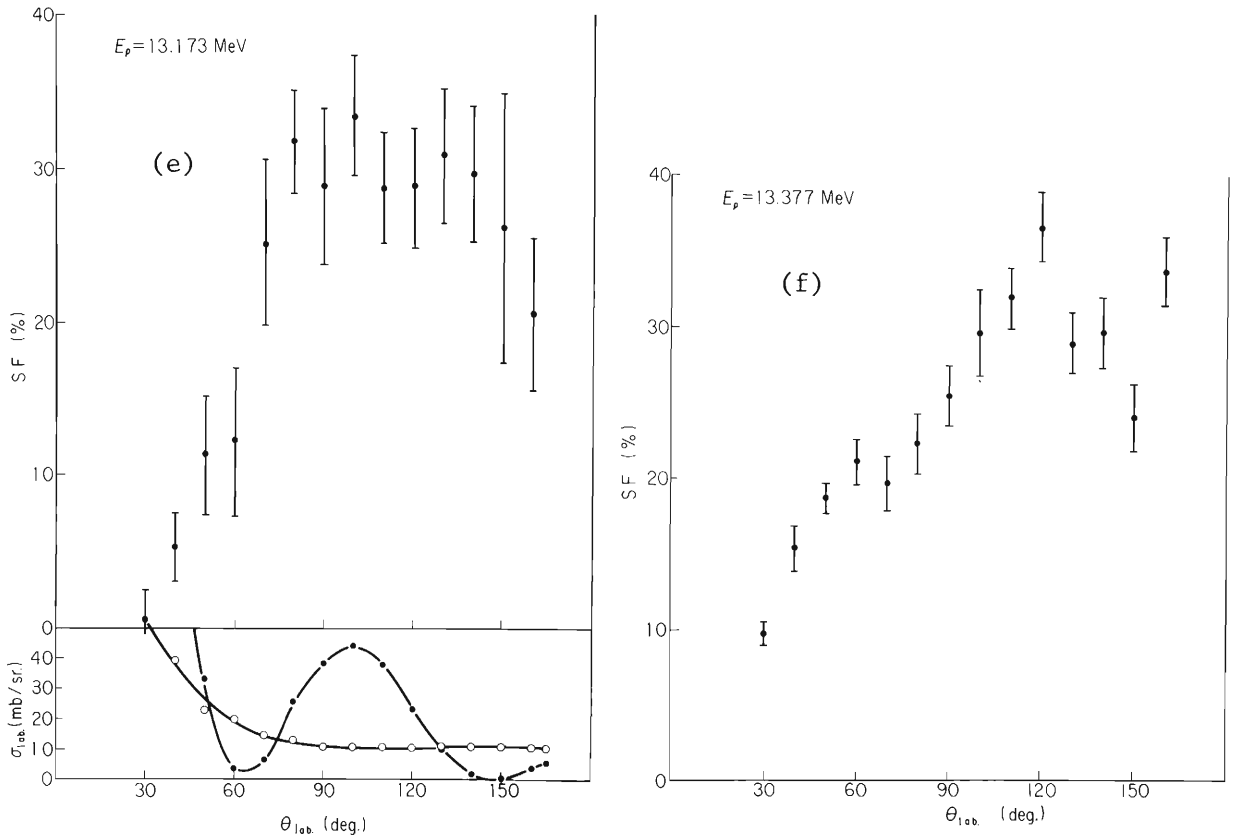

Fig. 4. Angular distribution of spin flip probabilities and differential cross sections.

References

1) F.H. Schmidt et al.: Nucl. Phys., 52, 353 (1964);
J.J. Kolata and A. Galonsky: Phys. Rev., 182, 1073 (1969);
W.A. Kolasinski et al.: ibid., 180, 1006 (1969).
2) Y. Nagahara: J. Phys. Soc. Japan, 16, 133 (1961);
G. M. Temmer et al.: Proc. Intern. Conf. Nucl. Structure, Tokyo, p. 299 (1967).
3) I P C R Cyclotron Progr. Rep. Vol. 1 (1967).

4-3. ^{88}Sr, ^{89}Y, ^{90}Zr, and ^{92}Mo (d, t) Reactions

S. Takeda, K. Matsuda, Y. Awaya, N. Nakanishi,
T. Wada, M. Odera, and I. Kohno

The purposes of the present experiments on the N=50 nuclei are to study how the major shell mixing depends on the number of protons in the nucleus, how the energy levels of neutron hole $T_<$ states change with proton number in N=49 nuclei, and whether or not N=50 is a good closed shell configuration. In the case of the ^{89}Y target, the neutron hole configurations will be coupled in the residual nucleus to the odd proton configurations. Information on the coupling scheme can be derived from the study of the ^{88}Y levels.

Among the neutron pickup reactions that can be used for this type of experiments, the (d,t) and (h,α) reactions are available with the IPCR Cyclotron. The (h,α) reaction, however, shows generally little and fine oscillating angular distribution which makes the assignment of ℓ-value difficult. Also the analysis in terms of the DWBA theory for this reaction presents particular difficulties related to angular momentum miss-matching. [1] Then the (d,t) reaction experiments have been performed preferably.

The reactions were induced by the 21.14 MeV deuteron beam from the IPCR Cyclotron. The beam transport system and the scattering chamber have been described elsewhere. [2] The strontium target was obtained by vacuum evaporation of natural strontium metal onto a thin Formvar backing. In order to avoid the effects of humidity and carbon dioxide, the evaporated strontium target was wrapped with the thin Formvar film. Self-supporting ^{89}Y target was prepared by vacuum evaporation of natural yttrium metal onto a slide glass. The ^{90}Zr and ^{92}Mo targets were obtained from the ORNL Isotope Division. Target thicknesses and enrichments are summarized in Table 1. The thickness of foil was determined by weighing, by Rutherford scattering of low-energy alpha particles, and by energy loss determination of alpha particles. The renormalizations were performed using the same optical potential parameters for each target analyzing the deuteron elastic scattering of forward angles in order to avoid the effects of inhomogeneity of the target thickness. Errors of the target thickness relative to each other were reduced to a few percent using these methods. The reaction products were detected by a (dE/dx)-E counter telescope which consisted of silicon surface-barrier detectors. The zero degree point was established with accuracy of $\pm 0.05^{o}$ by performing left-right measurements of the elastic scattering cross section and adjusting the zero to produce equal results at equal left-right angles. A block diagram of the electronic circuitry is shown in Fig. 1. The over-all energy resolution (FWHM) was found to be about 50 keV. A typical spectrum of tritons for ^{92}Mo (d,t) ^{91}Mo taken at 50^{o} is shown in Fig. 2. Energy levels obtained from the present experiments are shown in Fig. 3 schematically. Theoretical analyses using the distorted-wave Born approximation (DWBA-2) [3] are now in progress. Optical-model parameters used in the DWBA calculation are given in Table 2. The deuteron optical-model parameters are obtained by the analysis of the present ^{92}Mo (d,d) elastic scattering data with the automatic search computor code. [4] Fig. 4 shows the optical-model fit to the data. The angular distributions for the $lg_{9/2}$ levels of each nucleus are shown in Fig. 5 together with the calculated curves. Preliminary results of calculation obtained before the deadline of this annual report are listed in Table 3. Decrease of spectroscopic factors of the first three levels in each nucleus is seen in the Table 3 as the proton number is increased.

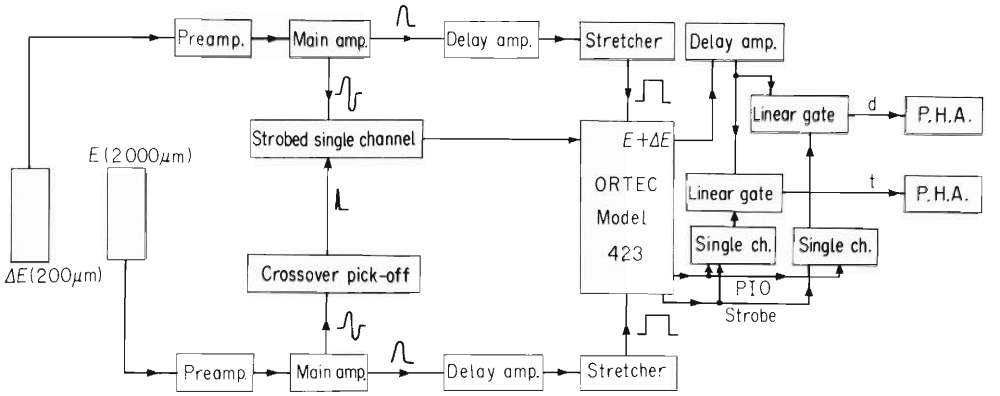

Fig. 1. Schematic drawing of apparatus used for the detection of deuteron and triton particles.

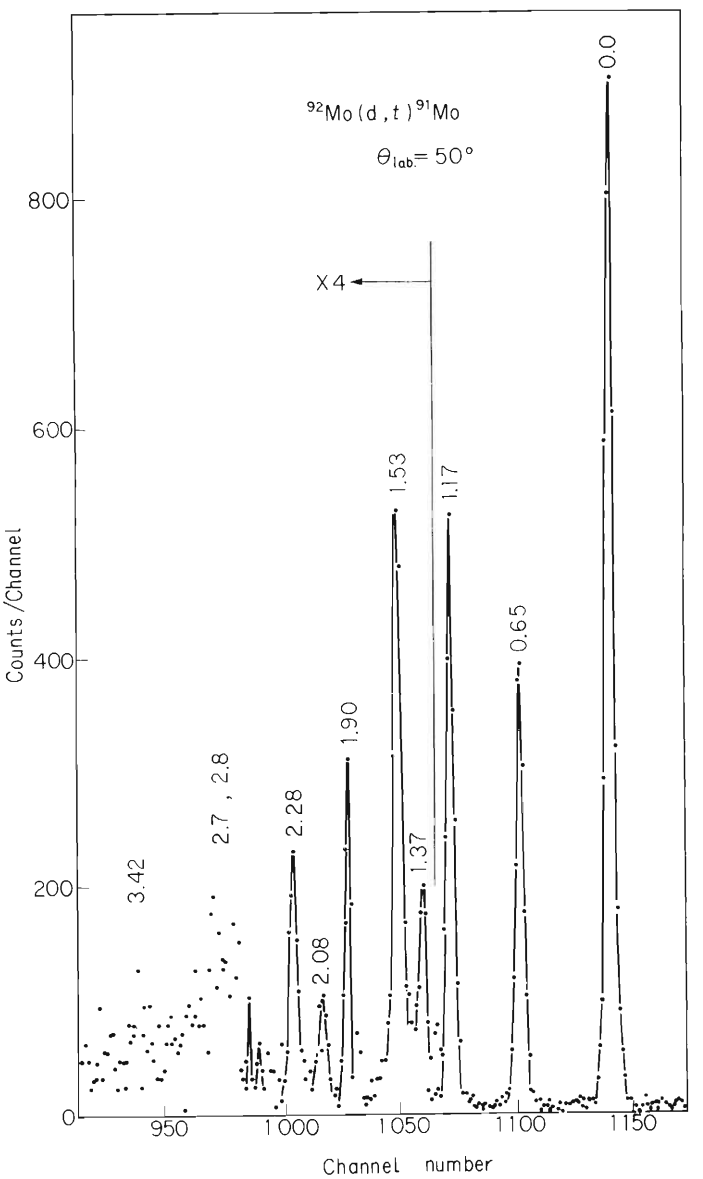

Fig. 2. Triton spectrum produced by 21.14 MeV deuterons at $\theta_{lab.} = 50°$ for ^{92}Mo target.

Table 1. Target thickness and enrichment.

^{88}Sr	^{89}Y	^{90}Zr	^{92}Mo
Natural			
82.6 %	100 %	97.8 %	97.6 %
1.26 mg/cm^2	0.85 mg/cm^2	1.03 mg/cm^2	0.715 mg/cm^2

Transitions from $2d_{5/2}$ level were observed on the ^{89}Zr (1.64 MeV) and ^{91}Mo (1.37 MeV) nuclei and the spectroscopic factors of these transitions are 0.1 and 0.39 respectively. This indicates that there are core excitations in the ^{90}Zr and the ^{92}Mo nuclei, that is, the 1.64 MeV of ^{89}Zr and the 1.37 MeV of ^{91}Mo states can arise from pickup of one of a pair of $2d_{5/2}$ neutrons in the ground states of each nucleus in the form of a two-particle two-hole excitation instead of fully filled shell-model levels. Although the mixing of two-particle two-hole excitation in the ground state of ^{90}Zr is about 5%, the addition of two protons to the ^{90}Zr nucleus induces the mixing of the core excitation as large as 20% in the ground state of ^{92}Mo. Fig. 6 shows the relative excitation energies obtained from the strong excited hole states which show very different level spacing and ordering calculated by a simple shell-model. [5] The $lg_{9/2}$ and $2d_{5/2}$ states change

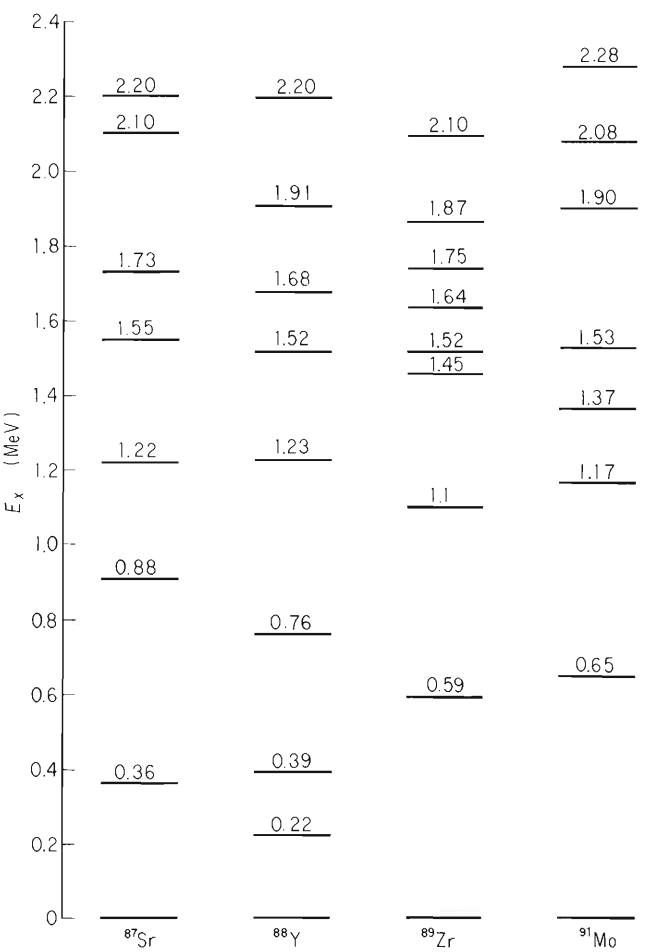

Fig. 3. Experimental level diagrams.

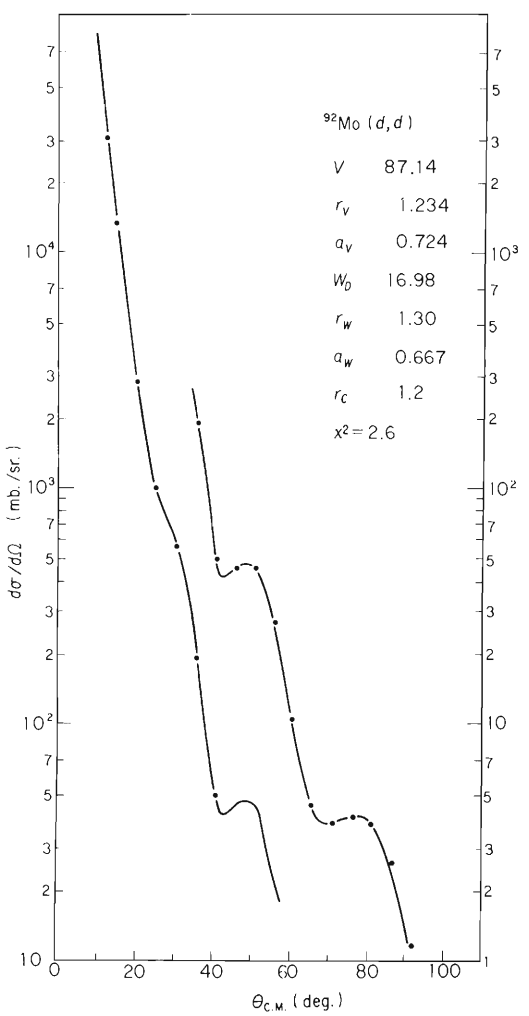

Fig. 4. Comparison of experimental elastic cross sections with optical-model prediction.

distinctly with the proton number, though $2p_{1/2}$ state does a little change.

It is quite possible to assign the 1.23 and 1.52 MeV states of ^{88}Y to 2^+ and 1^+ respectively because of the spectroscopic factors of these states and being not generally populated proton excited states in (d,t) reactions. More drastic shifts of $p_{1/2}$ and $g_{9/2}$ states than those of other nuclei are seem in the ^{88}Y nucleus. Detailed theoretical analyses are now in progress.

Table 2. Optical-model parameters used in the DWBA calculation.

		Deuteron	Triton [6]
V	(MeV)	87.14	170.2
r_0	(F)	1.23	1.16
a	(F)	0.724	0.739
W	(MeV)	—	18.8
W_D	(MeV)	16.98	—
r'_0	(F)	1.30	1.52
a'	(F)	0.667	0.751
r_c	(F)	1.2	1.25

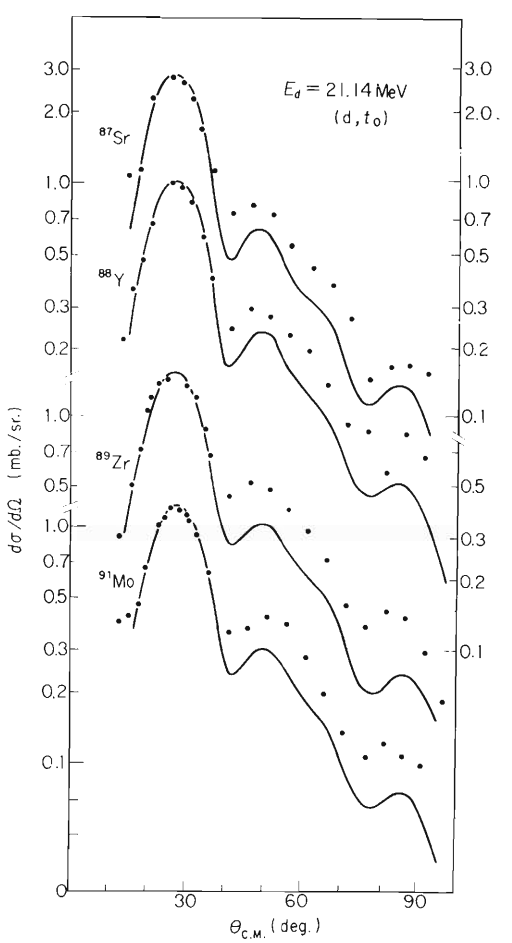

Fig. 5. Absolute differential cross sections for $lg_{9/2}$ ground states of each nucleus.

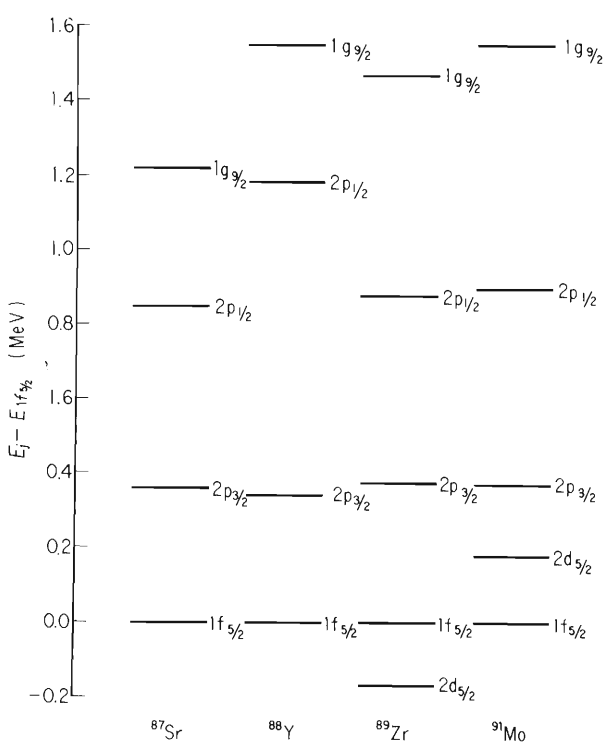

Fig. 6. Relative excitation energies.

Table 3. Spectroscopic factors for the (d,t) reactions on ^{88}Sr, ^{89}Y, ^{90}Zr, and ^{92}Mo.*

Shell-model levels	$^{88}Sr(d,t)^{87}Sr$		$^{89}Y(d,t)^{88}Y$		$^{90}Zr(d,t)^{89}Zr$		$^{92}Mo(d,t)^{91}Mo$	
	E_x(MeV)	C^2S	E_x(MeV)	C^2S	E_x(MeV)	C^2S	E_x(MeV)	C^2S
$1g_{9/2}$	0.0	10.0	0.0	4.10	0.0	8.0	0.0	6.50
		(10.0)		(4.5)		(9.93)		(9.71)
			0.22	5.20				
				(5.5)				
$2p_{1/2}$	0.38	2.0	0.39	1.34	0.59	1.84	0.65	1.56
		(2.0)		(1.37)		(1.88)		(1.8)
			0.76	0.5				
				(0.458)				
$2p_{3/2}$	0.87	3.0	1.23	1.7	1.1	1.6	1.17	1.67
		(3.69)		(2.3)		(3.64)		(3.56)
			1.52	1.12				
				(1.38)				

Numbers in parentheses under each C^2S value indicate sum-rule limit for $T_<$ states.

* All of the data have not been analyzed yet because of deadline of this annual report.

References

1) R. Stock, R. Bock, P. David, H.H. Duhm, and T. Tamura: Nucl. Phys., A104, 136 (1967).
2) K. Matsuda, N. Nakanishi, S. Takeda, and T. Wada: J. Phys. Soc. Japan, 25, 1207 (1968).
3) M. Kawai, K. Kubo, and H. Yamaura: Institute for Nuclear Study Report, PT-9 (1965).
4) T. Wada: IPCR Cyclotron Progr. Rep., 2, 87 (1968).
5) A. Bohr and B.R. Motlelson: "Nuclear Structure", W. A. Benjamin, N.Y., 1, 239 (1969).
6) E.R. Flynn, D.D. Armstrong, J.G. Beery, and A.G. Blair: LA-DC-10367, Sci. Lab. Univ. California, Los Alamos (1969).

4-4. Angular Distributions of $^{27}Al(^{3}He, d)^{28}Si$, $^{27}Al(\alpha, t)^{28}Si$, and $^{27}Al(\alpha, d)^{29}Si$ Reactions

N. Nakanishi, K. Matsuda, Y. Awaya,
S. Takeda, and T. Wada

The two-nucleon transfer reactions (^{3}He,p), (α,d) on a target ^{27}Al have been investigated and proton transfer reactions (^{3}He,d), (α,t) on the same target have been simultaneously studied.

The measurements of the $^{27}Al(^{3}He,d)\ ^{28}Si$ reaction were made under the same condition as in the case of the $^{27}Al(^{3}He,p)\ ^{29}Si$ reaction,[1] that is, the 21.9 MeV ^{3}He-particle energy and the experimental set up. A typical spectrum of the $^{27}Al(^{3}He,d)\ ^{28}Si$ reaction is shown in Fig. 1. It may be seen that the low-lying states of the residual nucleus ^{28}Si are generally hindered. Figs. 2(a) and (b) show the angular distributions corresponding to low-lying states of ^{28}Si. The $\ell_p = 2$ transition only is allowable to the ground 0^+ and 4.97 MeV 0^+ states but angular distributions leading to these states are somewhat different in the forward angle region. It was reported that the 4.61 MeV 4^+ state was excited through the pure $\ell_p = 2$ transition and that the other states show the ℓ_p-value mixture to 37.7 MeV ^{3}He-particle energy.[2] The lowest curve in Fig. 2(b) is a composite one of the 6.88 and 6.89 MeV doublet.

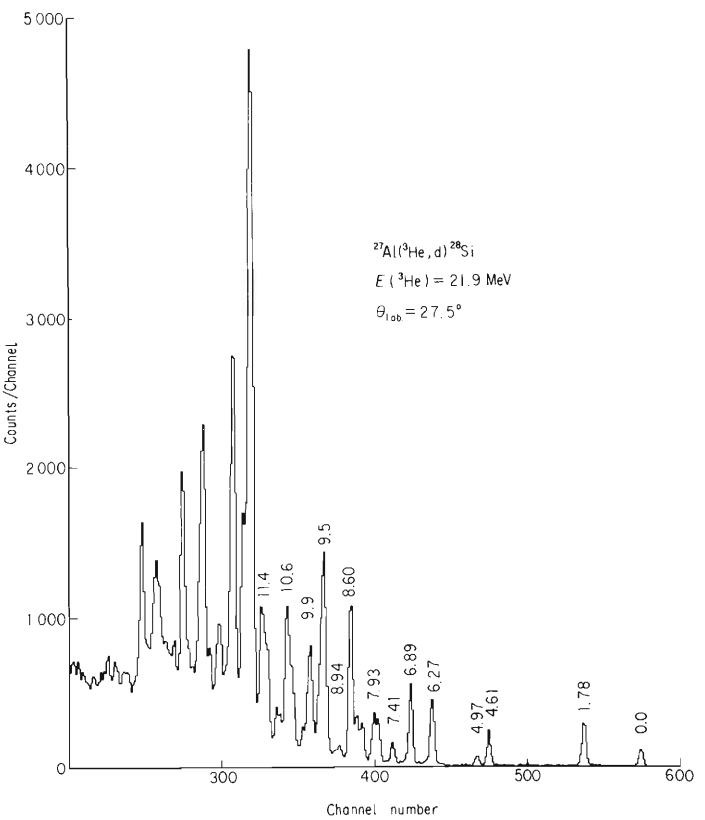

Fig. 1. A deuteron spectrum of the $^{27}Al(^{3}He,d)\ ^{28}Si$ reaction at E (^{3}He) = 21.9 MeV and $\theta_{lab.} = 27.5°$.

For the (α,t) and (α,d) reactions the same target was bombarded with 37.2 MeV alpha particles from the IPCR 160 cm Cyclotron. Emitted tritons and deuterons were detected using a $\Delta E - E$ solid state counter telescope, which was composed of a 300 μm totally depleted silicon surface barrier detector and a 3000 μm Li-drifted detector, and discriminated by a particle identifier (ORTEC Model 423). Fig. 3 shows a triton spectrum at the scattering angle 27.5° (lab.). Low-lying states of the nucleus ^{28}Si are excited strongly. Figs. 4(a) and (b) show the angular distributions with excitation energies, spins and parities corresponding to the ground and first five excited states of the residual nucleus ^{28}Si. Each of angular distributions of the ground 0^+ and 4.97 MeV 0^+ states has a different pattern. The angular distributions of 6.9 MeV doublet resemble those of 4.61 MeV 4^+ state for both reactions going on to the nucleus ^{28}Si, and therefore the 6.89 MeV 4^+ state may predominate in the doublet.

A deuteron spectrum of the ^{27}Al(α,d) reaction is shown in Fig. 5. In Figs. 6(a) and (b) are shown angular distributions leading to the ground and first six excited states of the residual nucleus ^{29}Si. It may be seen that these angular distributions show structureless patterns and that some of them are enhanced in the backward angle region.

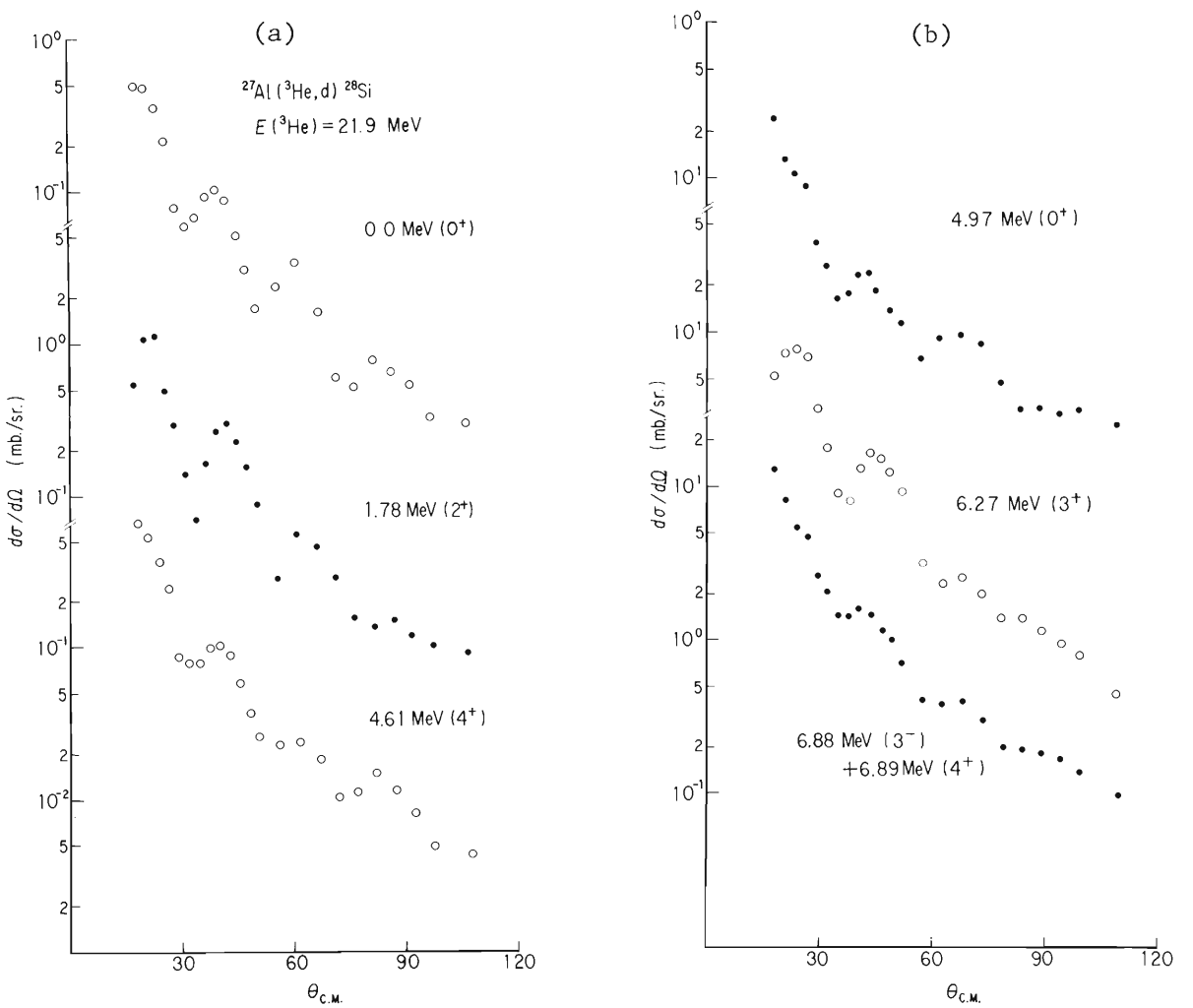

Fig. 2. Angular distributions of the ^{27}Al (^{3}He, d) ^{28}Si reaction for the low-lying states.

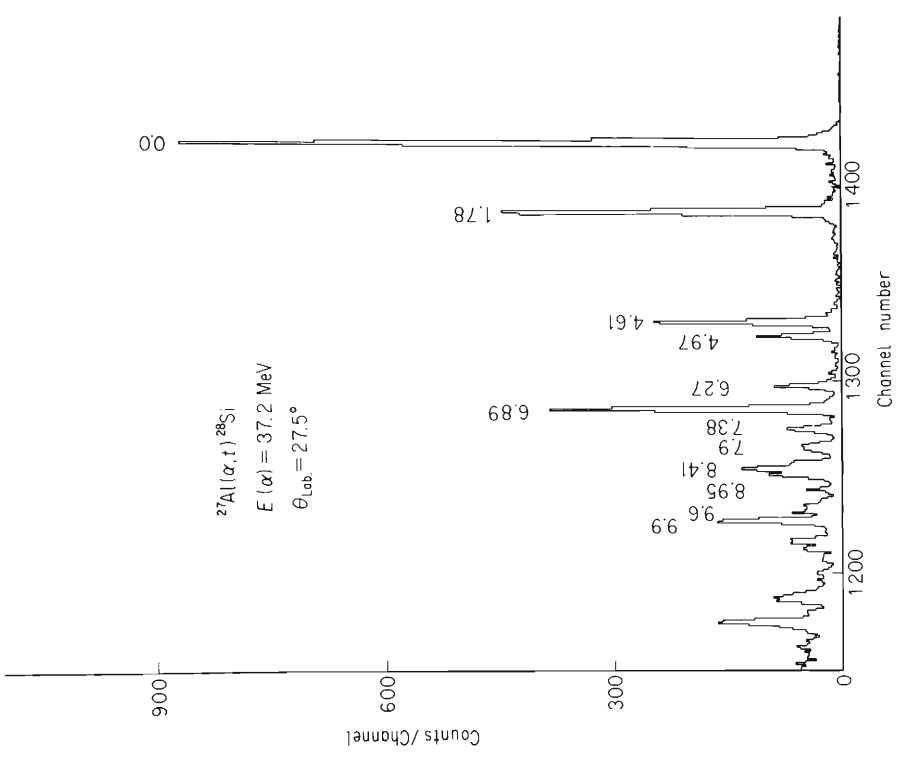

Fig. 3. A triton spectrum of the ^{27}Al (α,t) ^{28}Si and reaction at E (α) = 37.2 MeV $\theta_{lab.}$ = 27.5°

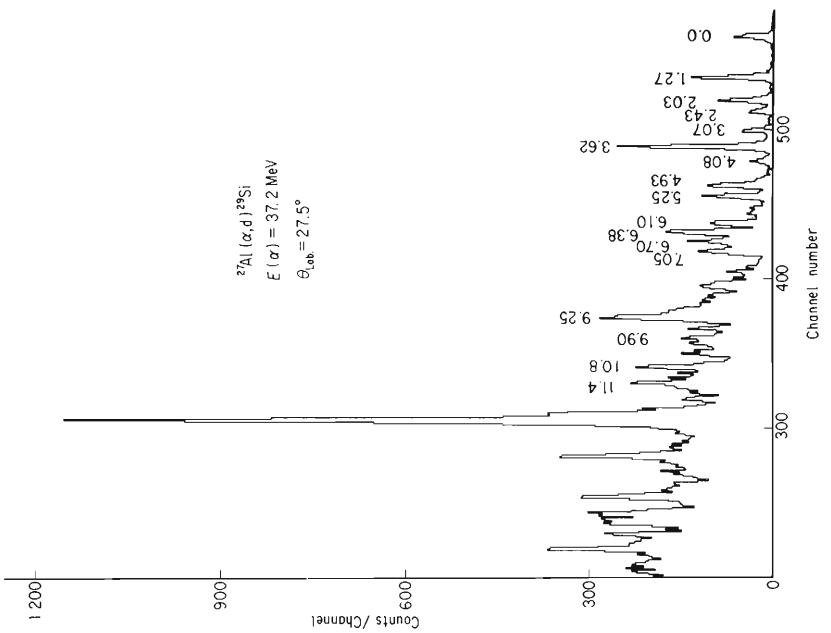

Fig. 5. A deuteron spectrum of the ^{27}Al (α, d) ^{29}Si reaction at E (α) = 37.2 MeV and $\theta_{lab.}$ = 27.5°

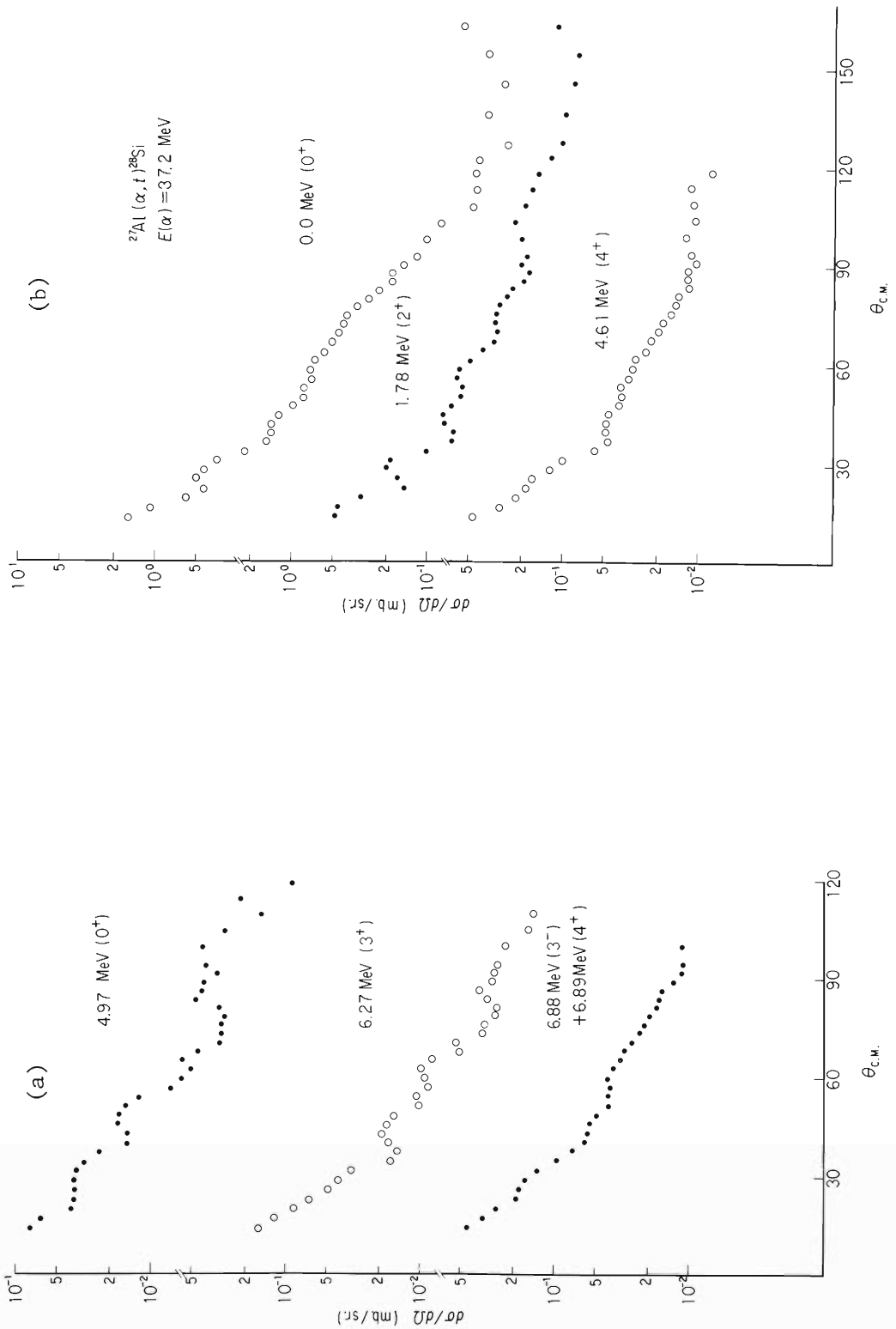

Fig. 4. Angular distributions of the ^{27}Al (α, t) ^{28}Si reaction for the low-lying states.

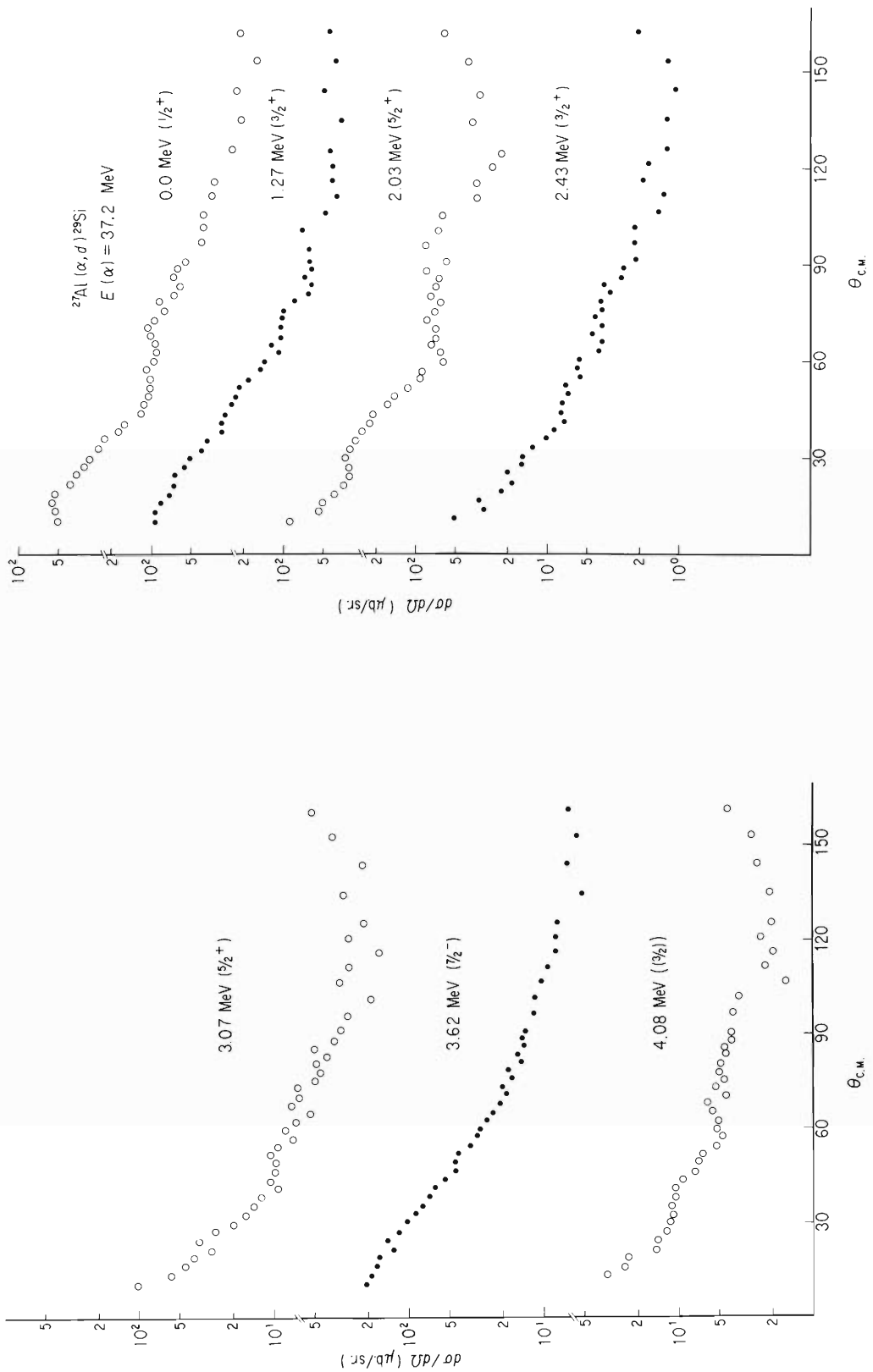

Fig. 6. Angular distributions of the ^{27}Al (α, d) ^{29}Si reaction for the low-lying states.

References

1) N. Nakanishi, S. Takeda, T. Wada, Y. Awaya, and K. Matsuda: IPCR Cyclotron Progr. Rep., 2, 74 (1968).
2) R.W. Barnard and G.D. Jones: Nucl. Phys., A108, 641 (1968).

4-5. Elastic and Inelastic Proton Scattering by Mo Isotopes

T. Wada, K. Matsuda, Y. Awaya,
N. Nakanishi, and S. Takeda

Elastic and inelastic scattering of proton by $^{92\sim100}$Mo were measured at E_p = 14.5 MeV. All the Mo targets were self-supporting foil and enriched to about 97%. The thickness was determined from the energy loss of alpha particles from ThC' and also from the normalization to the Rutherford scattering cross section of 16 MeV alpha particles at forward angles.

The scattering angle of proton was from 20 to 165° at intervals of 5°. Fig. 1 shows the angular distribution of elastic scattering. The solid curves are not theoretical. Figs. 2 and 3 show the angular distribution of proton which excited the 2^+ and 3^- levels. The solid lines give the results of preliminary DWBA calculation using complex form factors. β is the deformation parameter.

The excitation energy of levels was determined from the pulse height of the proton groups scattered from ^{16}O and ^{12}C and some new levels were found. Fig. 4 shows the energy levels of Mo isotopes. The left column for each isotope indicates the present result and the right the previous one.

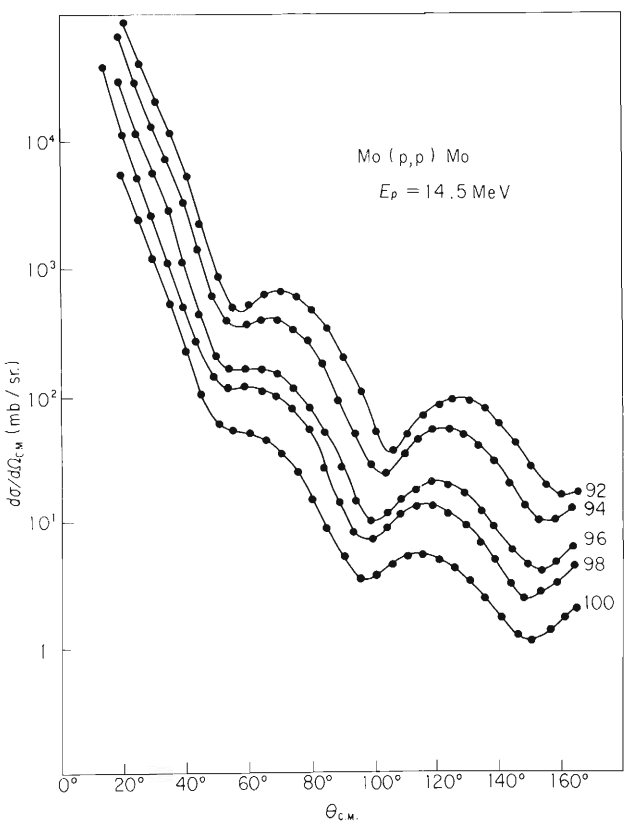

Fig. 1. Angular distribution of elastic scattering from Mo isotopes. The normalization are 1/2, 1/4, 1/8, and 1/16 from ^{94}Mo to ^{100}Mo. The solid lines are only for eyes guide.

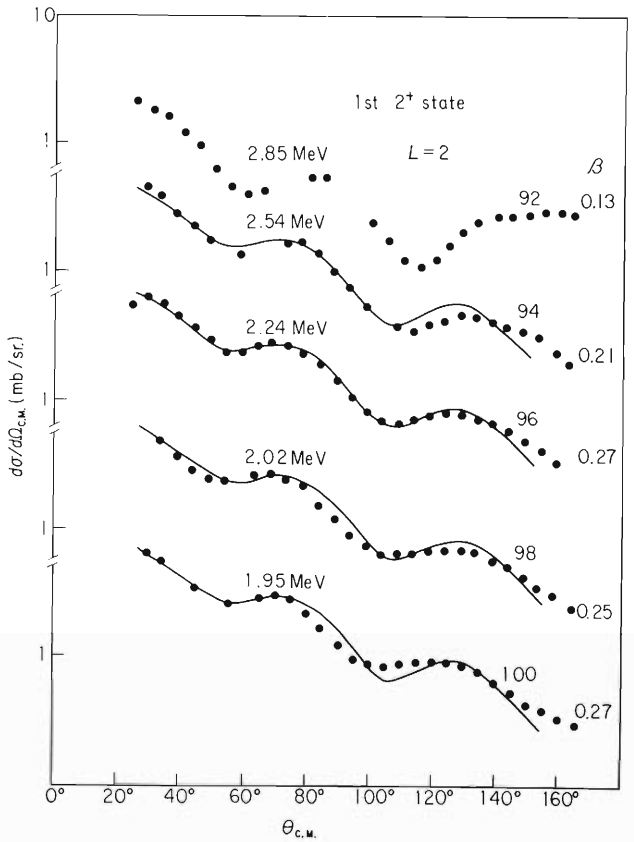

Fig. 2. Angular distribution of inelastic scattering from the first 2^+ levels of each Mo isotope. The solid lines are the results of preliminary DWBA calculation.

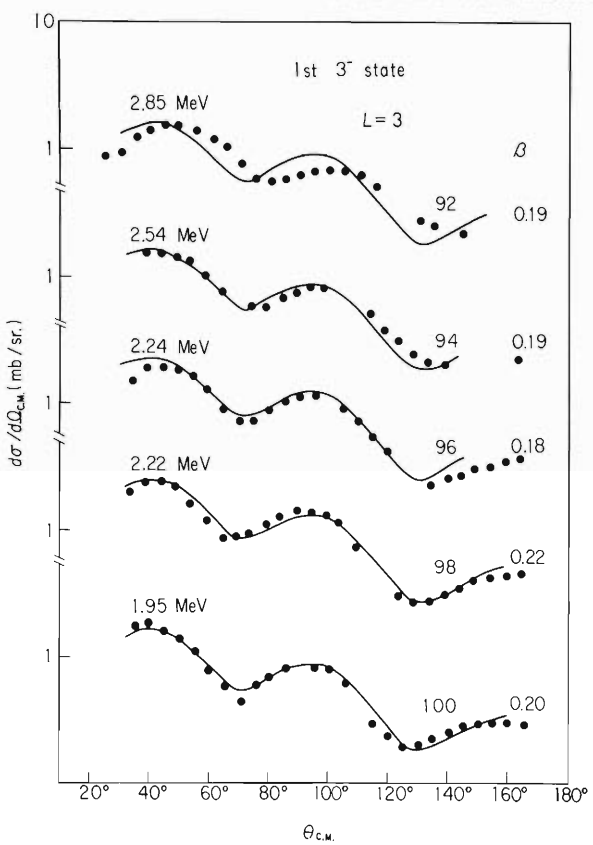

Fig. 3. Angular distribution of inelastic scattering from the first 3^- level of each Mo isotope. The solid lines are the results of the preliminary DWBA calculation.

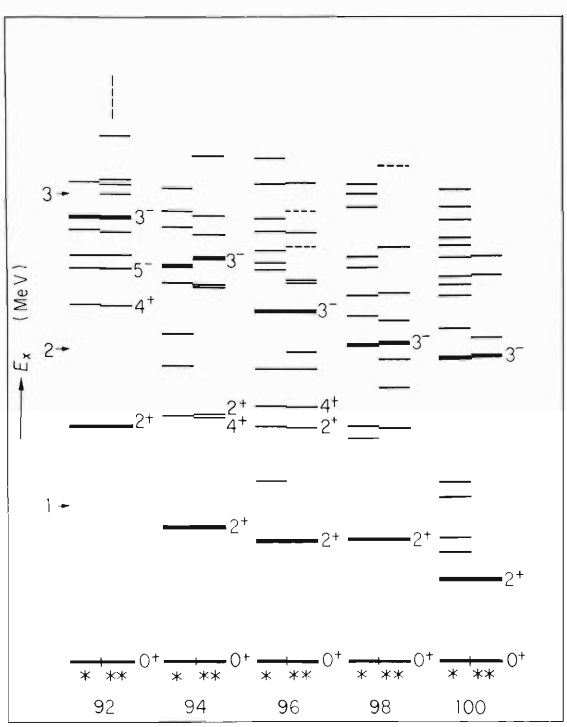

Fig. 4. Excited states of Mo isotopes. "**" means "present" and "*" previous.

4-6. Inelastic Proton Scattering from ^{98}Mo and ^{100}Mo

Y. Awaya, T. Wada, K. Matsuda,
N. Nakanishi, and S. Takeda

This is a precise report about a part of work presented in 4-5. The excited states in ^{98}Mo were mainly studied by the ^{97}Mo(d,p) reaction,[1] the decay of ^{98}Nb,[2,3] and that of ^{98m}Nb.[3] As to those in ^{100}Mo, the informations were limitted to only a few states.[4] The experiment of inelastic deuteron scattering from ^{98}Mo and ^{100}Mo was made[5] but as the angular distributions were not obtained, the precise study of inelastic proton scattering would be required.

The ^{98}Mo and ^{100}Mo targets were made of the self-supporting metallic foils isotopically enriched to 98.3 and 95.9 % obtained from the Oak Ridge National Laboratory. The thickness of them were estimated to be 0.80 and 1.08 mg/cm^2 for ^{98}Mo and ^{100}Mo, respectively, from both of the energy loss of ThC's alpha particles and the Rutherford scattering of about 16 MeV alpha particles at forward angles.

The proton beam was obtained from the IPCR Cyclotron and was momentum analyzed. The conditions of beam handling were reported previously.[6] The incident energy of protons were 14.69 and 14.67 MeV for ^{98}Mo and ^{100}Mo, respectively. The scattered protons were detected by two surface barrier silicon detectors with depletion layer of 2 mm placed making an angle of 30° apart from each other with the target. The spectra were recorded on the 1600 channel pulse height analyzer (Victoreen SCIPP 1600 type).

The spectra of scattered protons from ^{98}Mo and ^{100}Mo are shown in Figs. 1 and 2. The sixteen and twenty two states were assigned to ^{98}Mo and ^{100}Mo definitely and thirteen and fifteen angular distributions of inelastically scattered protons as well as those for elastic scattering were obtained for them, respectively. The unresolved peaks were separated by using the χ^2-fit code.* The level schemes for ^{98}Mo and ^{100}Mo observed in this work are shown in Fig. 3.

The optical model analysis of elastic scattering data was made by using the automatic search code "SEARCH".[7] The angular distributions of elastic scattering and the calculated curves are shown in Fig. 4. The optical parameters are shown in Table 1. The angular distributions of inelastic scattering are shown in Figs. 5 to 8. They were analyzed by the DWBA calculation using the code "INS-DWBA 2".** The one phonon excitation process was adopted and the real interaction was used. The calculations using the complex interaction are now in progress so the results of analysis presented here are the preliminary ones. The parameters of set A are used in the calculations. Some calculated curves were fitted to the experimental data and the assignments of transferred angular momentum, L, were able to make. The calculated curves are also shown in Figs.5 to 8 for the case where the fit was obtained. The deformation parameters, β_L, are listed in Table 2.

The behavior of level structure for ^{98}Mo and ^{100}Mo up to about 2 MeV seems to resemble each other as shown in Figs. 3, 5 and 6. There are two strongly excited states in each case, those are the first 2^+ and 3^- states, and the weakly excited two states appear at the excitation energy of almost twice as high as the first 2^+ state.

* The program was coded by one of the authors, T. Wada.

** Coded by Drs. M. Kawai, K. Kubo, and H. Yamaura.

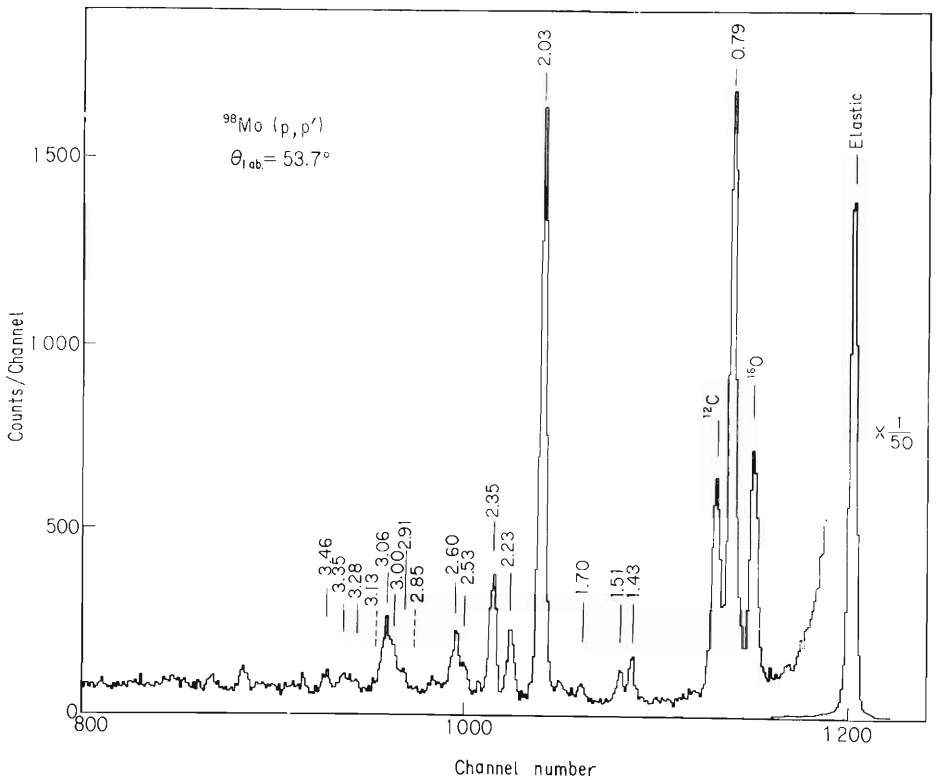

Fig. 1. The spectrum of scattered protons from ^{98}Mo.

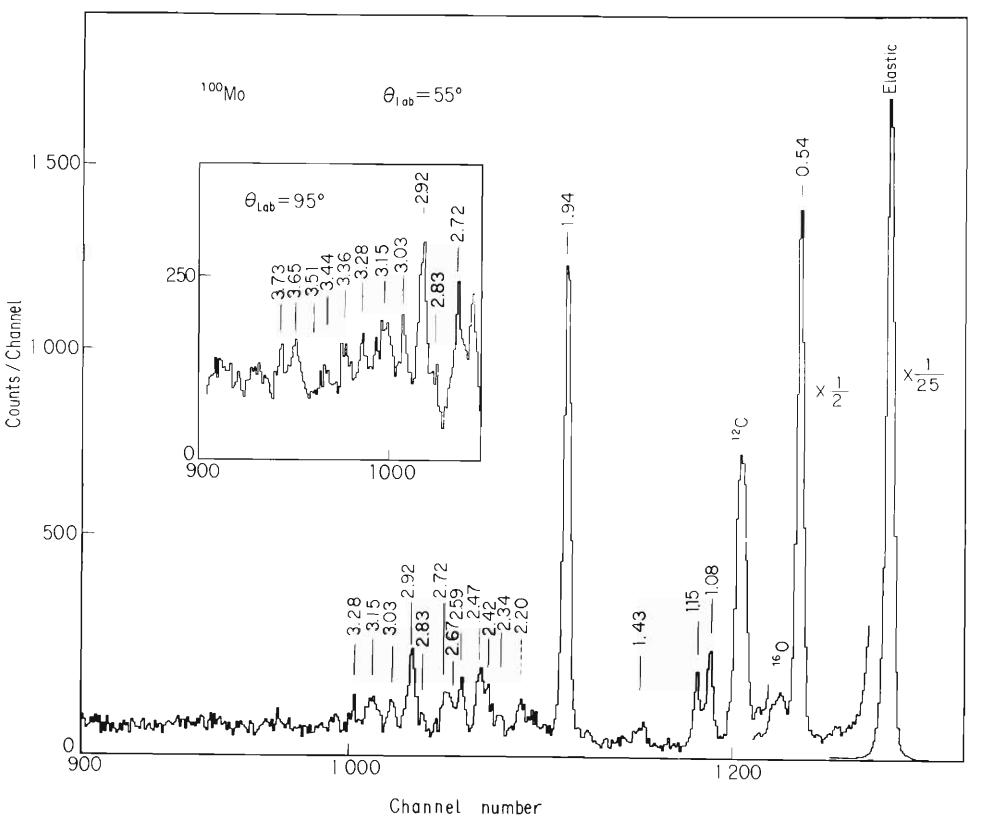

Fig. 2. The spectrum of scattered protons from ^{100}Mo.

Table 1. Optical parameters.

	V	W	$V_{\ell s}$	$r_0, r_{\ell s}$	r_I	$a_0, a_{\ell s}$	a_0	r_c
A	55.16	9.50	7.68	1.18	1.28	0.740	0.702	1.25
B	55.14	5.48	8.23	1.18	1.43	0.650	0.813	1.25

V, W, and $V_{\ell s}$ are in MeV.
r_0, r_I, $r_{\ell s}$, a_0, a_I, $a_{\ell s}$, and r_c are in fm.
Set A and B are the best fit parameters to ^{100}Mo and ^{98}Mo.
The form of optical potential is $-Vf(r,r_0,a_0) + 4i\, a_I W \frac{d}{dr} f(r,r_I,a_I)$
$+ 2(\frac{\hbar^2}{m\pi C}) V_{\ell s} \frac{1}{r} \frac{d}{dr} f(r,r_{\ell s}, a_{\ell s}) \cdot (\ell \cdot s) + V_c$, $f(r, r', a')$
$= [1 + \exp\{(r - r'A^{1/3})/a\}]^{-1}$ where V_c is the Coulomb potential for uniformly charged sphere with a radius of $r_c A^{1/3}$.

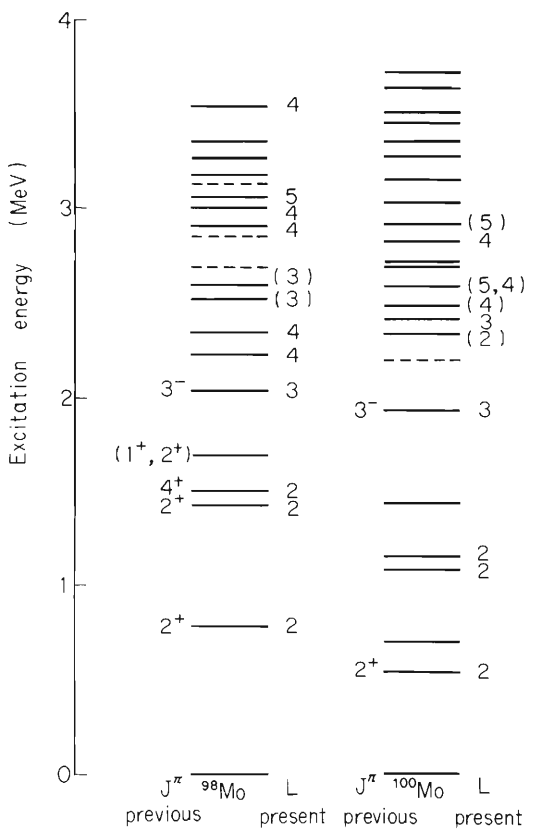

Fig. 3. The excited states for ^{98}Mo and ^{100}Mo observed in this experiment.

These weakly excited states seem to be the members of two phonon state and there is a possibility that the third member of the two phonon state exists despite unresolved. The 1.43 and 1.51 MeV states in ^{98}Mo were assigned to have spin-parities of 2^+ and 4^+ from the study of ^{98}Nb and ^{98m}Nb decay.[3] Then the spin-parities of the 1.08 and 1.15 MeV states in ^{100}Mo may be 2^+ and 4^+, respectively, because of the similarity of patterns of angular distributions. In the present DWBA calculation, the curve for L = 2 seems to fit to experimental data for both states in each nucleus, but as the one phonon excitation form factors are used, this difference is explicable. The more weakly excited level was observed in both nuclei at about the middle position between the two-phonon like state and the first 3^- state. If we dare to say, this might be the three phonon state. In the study of ^{98}Nb decay,[3] the 1.76 MeV state was found and its spin-parity was assigned to be $(1,2^+)$. The one exception is the 0.70 MeV state in ^{100}Mo. But in the studies of ^{97}Mo(d,p) reaction[1] and ^{98}Nb decay,[3] the 0^+ state was observed at 0.74 MeV. From the analogy of this, the 0.70 MeV state in ^{100}Mo may have the spin-parity of 0^+. We regret that the peak for the 0.74 MeV 0^+ state of ^{98}Mo was masked behind that for the strongly excited 2^+ state. These 0^+ or 0^+-like state heightens our interest, as except for them these two nuclei seem to have a typical vibrational character.

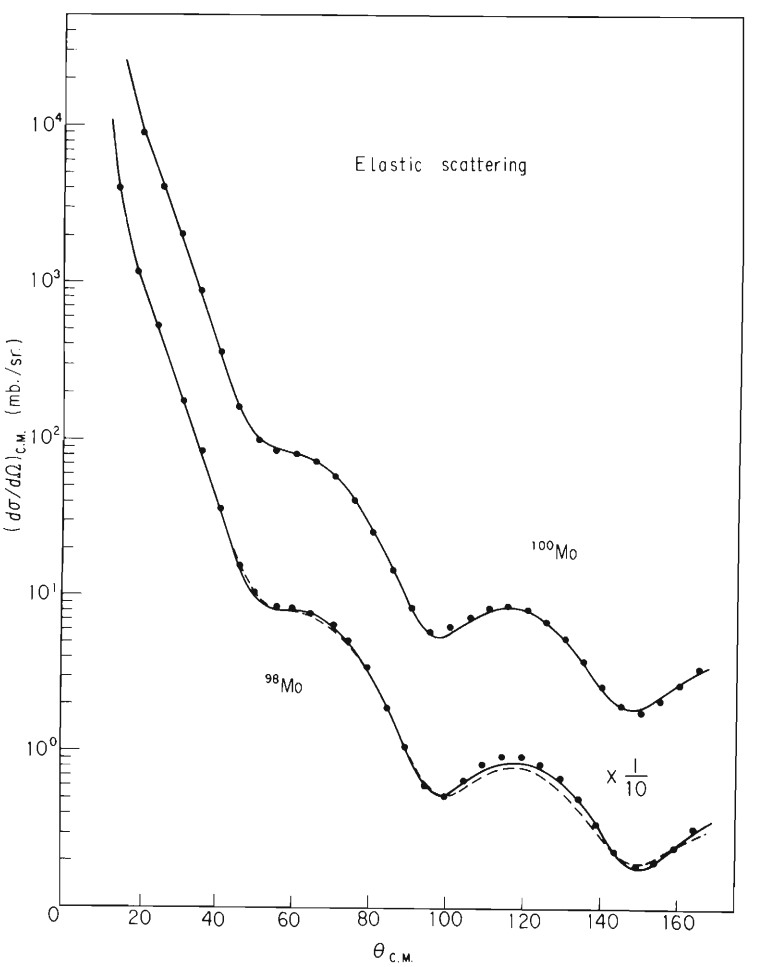

Fig. 4. The angular distributions of elastically scattered protons from ^{98}Mo and ^{100}Mo. The calculated curves are also shown. The curves drawn with solid line for ^{100}Mo and broken one for ^{98}Mo were obtained by using the parameters of set A. The solid curve for ^{98}Mo was obtained using the parameters of set B.

Above the first 3^- state, there are many weakly excited states in both nuclei and the similarity between them is not clear. In the ^{97}Mo(d,p) reaction, the states in ^{98}Mo above 2.2 MeV were more strongly excited than the levels up to 2.03 MeV as a whole. So the states above the first 3^- state in both nuclei may be mainly caused by the shell configurations.

Table 2. Excited states in ^{98}Mo and ^{100}Mo.

^{98}Mo			^{100}Mo		
Level (MeV)	L	β_L	Level (MeV)	L	β_L
0.79	2	0.24	0.54	2	0.26
1.43	(2)	0.07	0.70		
1.51	(2)	0.05	1.08	(2)	0.08
1.70			1.15	(2)	0.06
2.03	3	0.27	1.43		
2.23	4	0.09	1.94	3	0.25
2.35	4	0.11	(2.20)		
2.53	(3)	0.06	2.34	(2)	0.05
2.60	(3)	0.11	2.42	3	0.08
(2.69)			2.47	(4)	0.07
(2.85)			2.59	(5,4)	
2.91	4	0.05	2.67		
3.00	4	0.08	2.72		
3.06	5	0.11	2.83	4	0.05
(3.13)			2.92	(5)	0.12
3.28			3.03		
3.35			3.15*		
3.46	4	0.05	3.28		
			3.36		
			3.44		
			3.51		
			3.65		
			3.72		

* There is a probability that the peak is unresolved.

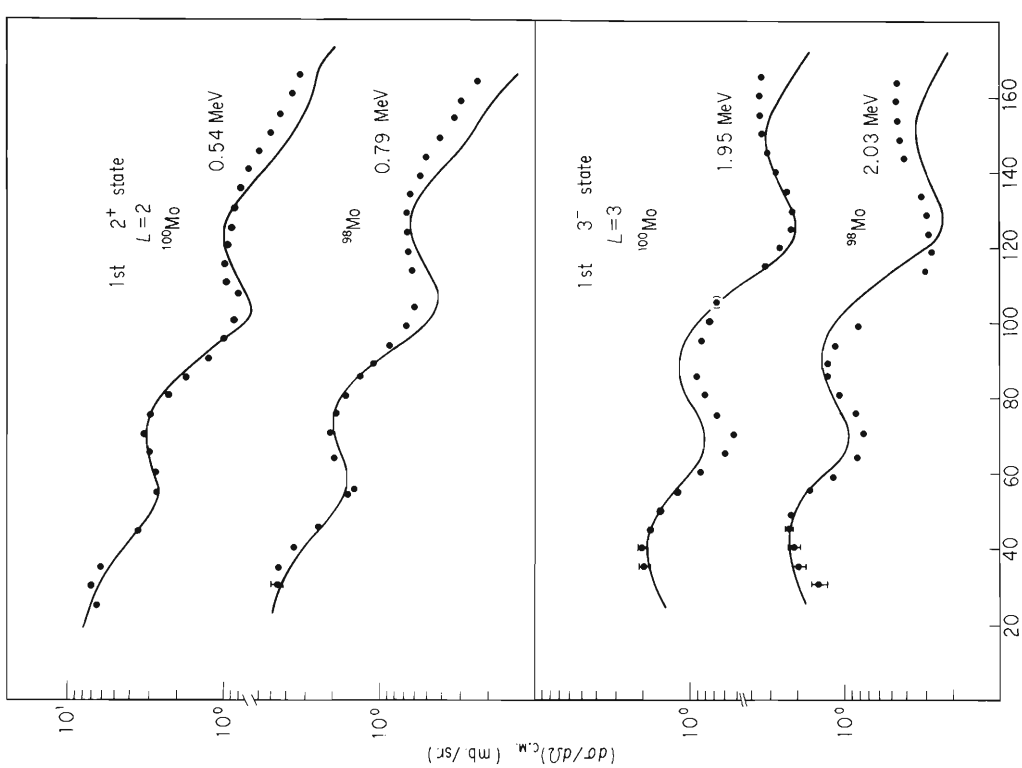

Fig. 5. The angular distributions for the first 2^+ and 3^- states in 98Mo and 100Mo. The calculated curves for L = 2 and L = 3 are also shown.

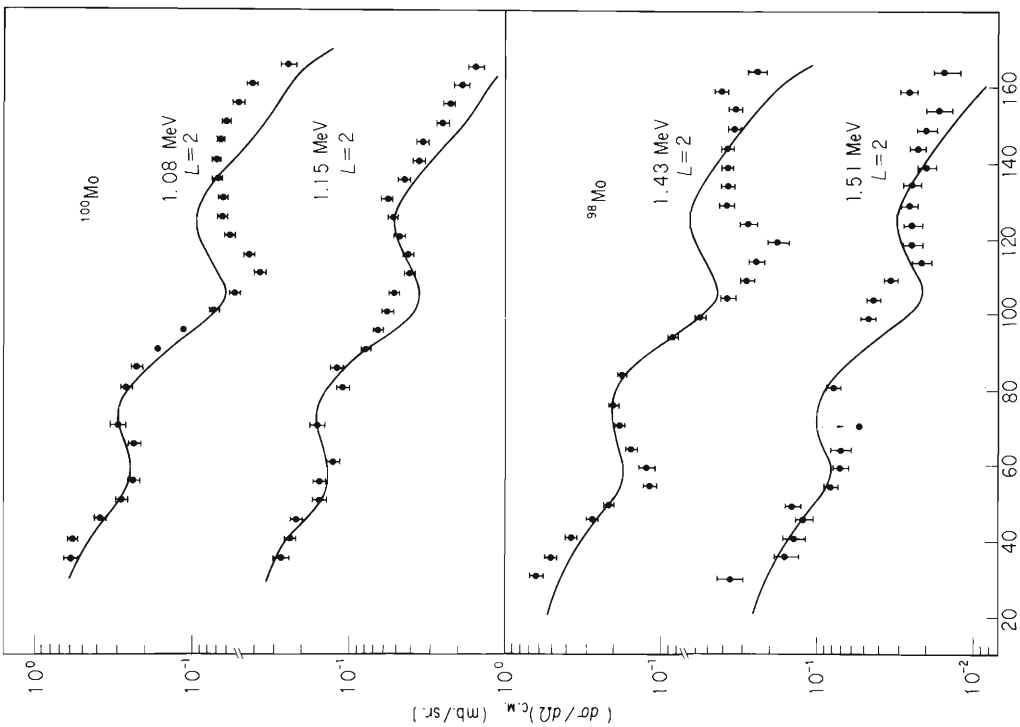

Fig. 6. The angular distributions for the two-phonon like states in 98Mo and 100Mo. The DWBA calculated curves for the one phonon excitation process are shown tentatively.

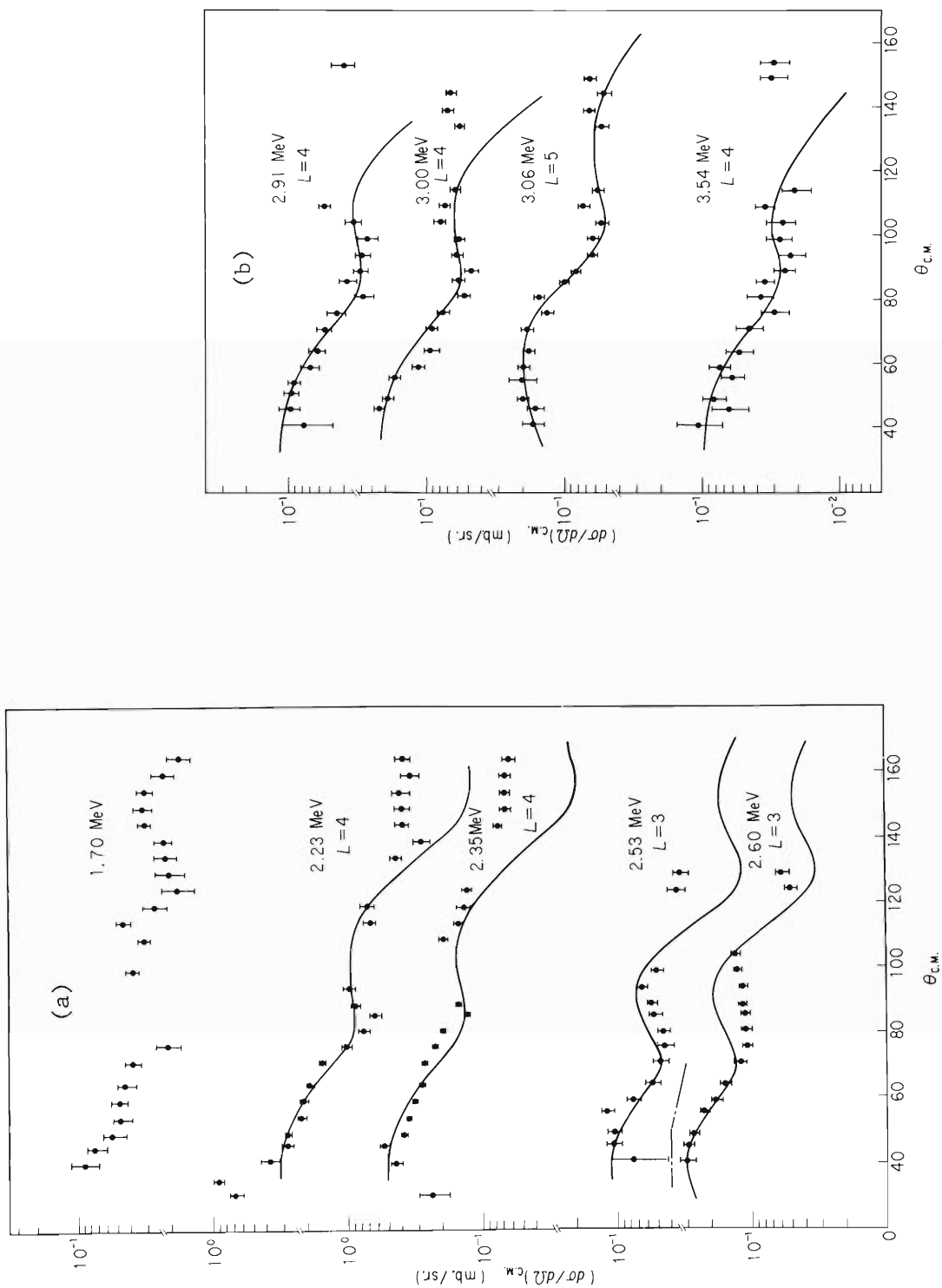

Fig. 7. Angular distributions for the states in ^{98}Mo other than those already shown. The calculated curves are also shown for some states.

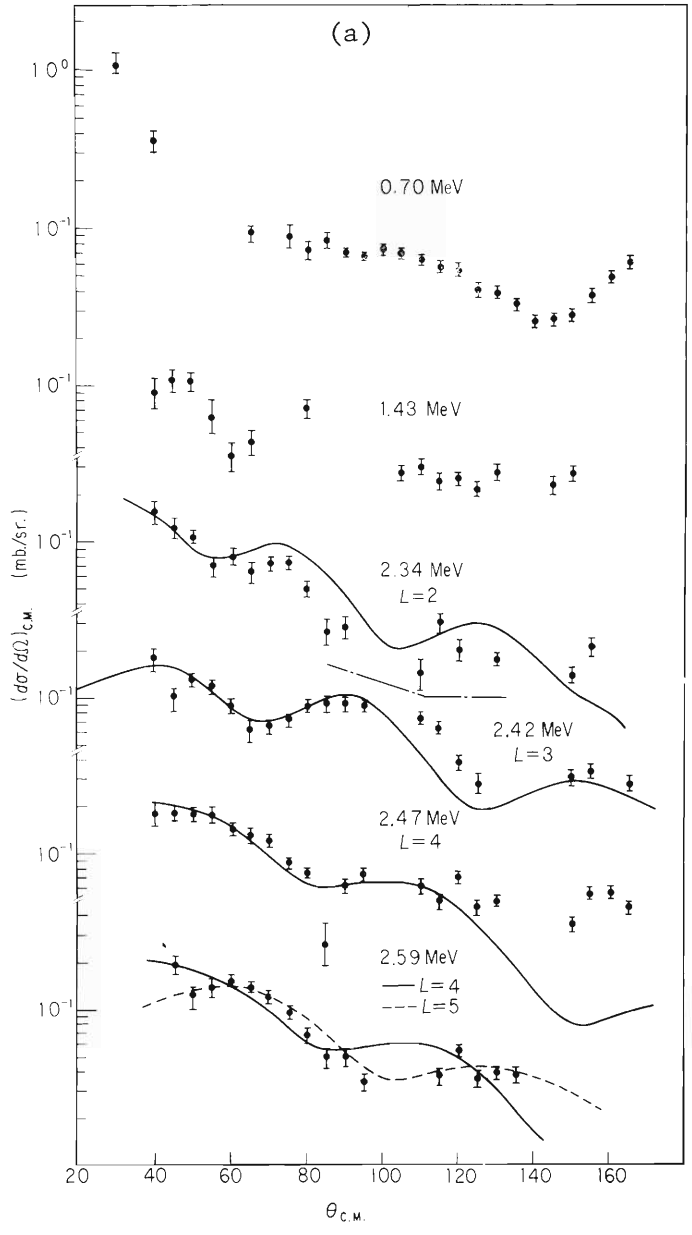

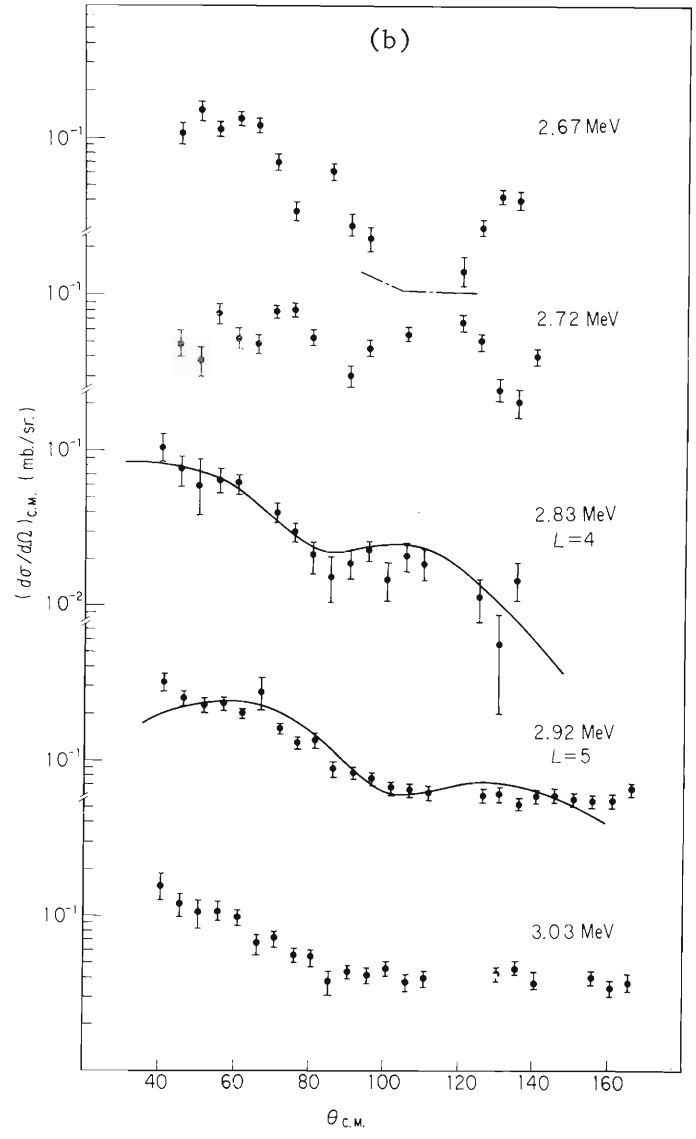

Fig. 8. Angular distributions for the states in ^{100}Mo other than those already shown. The calculated curves are also shown for some states.

References

1) K.R. Evans et al.: Phys. Rev., 165, 1327 (1968).
2) S.C. Gujarathi and S.K. Mukherjee: Nucl. Phys., 85, 288 (1966) and references cited there.
3) K. Hubenthal et al.: ibid., A128, 577 (1969).
4) C.M. Lederer et al.: "Table of Isotopes", John Wiley and Sons, N.Y., p. 236 (1967).
5) Y.S. Kim and B.L. Cohen: Phys. Rev., 142, 788 (1966).
6) Matsuda et al.: J. Phys. Soc. Japan, 25, 1207 (1968).
7) T. Wada: IPCR Cyclotron Progr. Rep., 2, 87 (1968).

4-7. Effect of Interaction Range and Spread of Projectile on the Cross Section in Case of ^{12}C (^{3}He, p) ^{14}N

S. Yamaji

Following the expression of two-nucleon transfer reaction,*1) the calculation of cross section of reaction $^{54}Fe(t,p)\ ^{56}Fe$[2] was done to test the computing code. It agreed with the result given in Reference 2.

In order to investigate the difference between "cluster" and "micro" concerning the inducing interaction and to see the effects of the variation of interaction range ξ and of the spread of projectile ^{3}He on the differential cross section, the reaction $^{12}C(^{3}He,p)^{14}N$ leaving the residual nucleus ^{14}N the excited 0^{+} state was treated. The incident energy of projectile ^{3}He was 25.4 MeV. The meanings of the terms "cluster" and "micro" are given in Reference 1.

The interaction range ξ is taken to be 0.4, 0.8, 1.6, and 3.2 fm and the spread η

Table 1. Optical parameters.

		V	W	r_{0R}	a_R	r_{0I}	a_I
Scattering state	^{3}He — ^{12}C	172.0	9.7	1.225	0.7249	1.482	0.96
	p — ^{14}N	44.8	6.0	1.25	0.65	1.25	0.65
Bound state	p — ^{12}C or n — ^{12}C	42.2	—	1.25	0.65	—	—

The potential is expressed by

$$V(r) = -\frac{V}{1+e^{x}} - \frac{4We^{x'}}{(1+e^{x'})^{2}} + V_{coulomb},$$

where

$$x = \frac{r - r_{0R} A^{1/3}}{a_R}, \qquad x' = \frac{r - r_{0I} A^{1/3}}{a_I}$$

In the case of p — ^{12}C, the Coulomb interaction was neglected and the depth of potential V was obtained by giving the binding energy 6.25 MeV.

* The following corrections should be done in Reference 1:

(a) $\delta \rightarrow \frac{1}{\sqrt{2}}\delta$ in the expression of Ω_b.

(b) $(\frac{a\nu\eta^2}{2C'^2})^{3/4} \longrightarrow (\frac{a\nu\eta^2}{2C^2})^{3/4}$ in the expression of Cn for "finite-range", in the case of "micro", but the correction is not necessary in the case of "cluster".

(c) $\beta^4 \rightarrow B^2$ in the expression of Cn for "zero-range" and "micro".

of projectile 0.1, 0.2, 0.4 fm^{-1}. The oscillator parameter ν is fixed at 0.43168 fm^{-2} calculated from the equation $\hbar\omega = 41/A^{1/3}$, where A is the mass number of target nucleus. The optical parameters are given in Table 1.

As can be seen from Fig. 1, the difference between $C_n^{(m)}$ and $C_n^{(c)}$ is not very large, where $C_n^{(m)}$ and $C_n^{(c)}$ are the overlap integrals of the projectile corresponding to "micro" and "cluster", respectively. In the limiting case of long-range interaction, $C \approx C'$, $D \approx D'$, and $C_n^{(m)} \approx C_n^{(c)}$. While in the case of short-range limit, $C \gg C'$ and $D \ll D'$ because of the large value of $\beta = 1/\xi$. But the inclinations of $C_n^{(m)}$ and of $C_n^{(c)}$ are similar. For example, in this (^{3}He,p) case, $C_n^{(m)} \propto (1-\frac{4\nu}{\nu+8\eta^2})^n$ and $C_n^{(c)} \propto (1-\frac{2\nu}{\nu+6\eta^2})^n$.

The absolute value of Cn depends strongly on the range parameter, while the behavior of Cn depends on the spread of projectile as the node n increases. So, when we discuss the absolute value of cross section, the choice of range parameter is important.

The form factors are shown in Figs. 2(a) and (b) and the corresponding cross sections in Figs. 3(a) and (b). As the difference between "cluster" and "micro" is similar to that of Fig. 4, only the case of "cluster" is shown in Figs. 2 and 3.

The spread of the projectile ^{3}He is determined uniquely by electron scattering experiments. The value η is equal to 0.242 fm^{-2}. But as the wave function of the projectile ^{3}He is assumed to be of Gaussian form, it is not meaningless that the change of the cross section is examined as a small change of the spread η. Concerning the interaction range ξ and the strength V_{np}, different values have been used by many authors. To examine the relation between the range ξ and the strength V_{np}, the Schrödinger equation was solved under the condition that a neutron and a proton is bounded at 2.226 MeV in the Gaussian well $V_{np} \exp(-r_{np}^2/\xi^2)$. It corresponds to the state of deuteron. The result is given in Table 2. When the intrinsic state of the projectile ^{3}He is assumed to be of Gaussian type, it can be expressed as the product of the wave function describing the motion between the proton and the deuteron and the wave function of the internal motion of the deuteron. The latter is given by $\varphi_{000}(3\eta^2, r_{np})$, that is, a harmonic oscillator wave function. In Table 2 is shown the spread η which gives the best overlap integral between the eigenfunction in the well $V_{np} \exp(-r_{np}^2/\xi^2)$ and the wave function $\varphi_{000}(3\eta^2, r_{np})$ and the corresponding overlap integral. The values of η are nearly equal to those of electron scattering experiments. In Fig. 5 the absolute value of the cross section at 0^o is shown. Although it is consistent to use the strength V_{np} corresponding to the interaction range ξ given in Table 2, it was

Table 2. Relation between the strength and the interaction range.

$\xi = 1/\beta$	V_{np} (MeV)	η (fm^{-1})	Overlap integrals (%)
0.4	781	0.24	89
0.8	212	0.22	92
1.6	64	0.119	96
2.0	45	0.18	97
3.2	22	0.16	98

taken to be 45 MeV to compare the relative cross section except for the strength of the interaction according to the change of parameters ξ and η.

Nine oscillator terms were used to expand the Woods-Saxon eigenfunction ($1P_{1/2}$) for the nucleus ^{13}C and produced a good asymptotic behavior of the form factor out to 7 fm. Behavior of the form factor calculated by taking only five oscillators is compared with that of nine oscillators in Fig. 6.

The excited 0^+ state (2.31 MeV) of the nucleus ^{14}N was approximated to be $(P_{1/2})^2_0$ and the investigation of suitable parameter to the calculated cross section in the experiment was not carried out. So concluding remarks are as follows:

(a) The absolute value of cross section increases as the interaction range is increased.

(b) The angular pattern of differential cross section is sensitive to the spread of projectile.

(c) Calculations for both "micro" and "cluster" give nearly the same results. The main difference is the internal behavior of form factor.

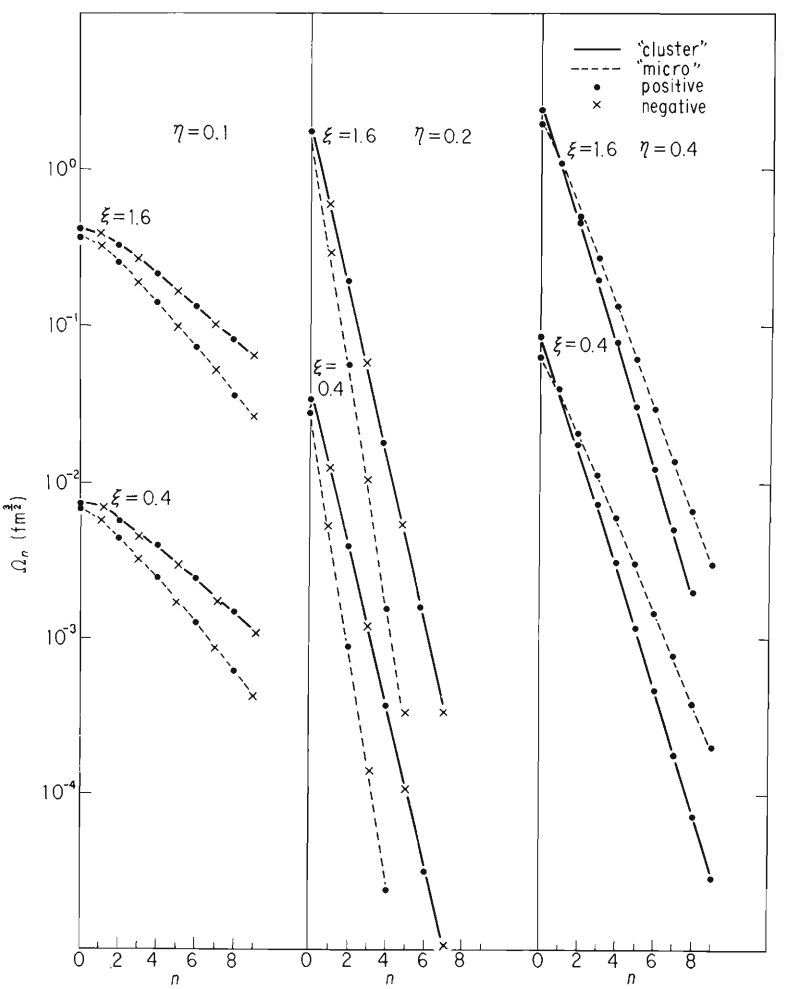

Fig. 1. Overlap integral of projectile.

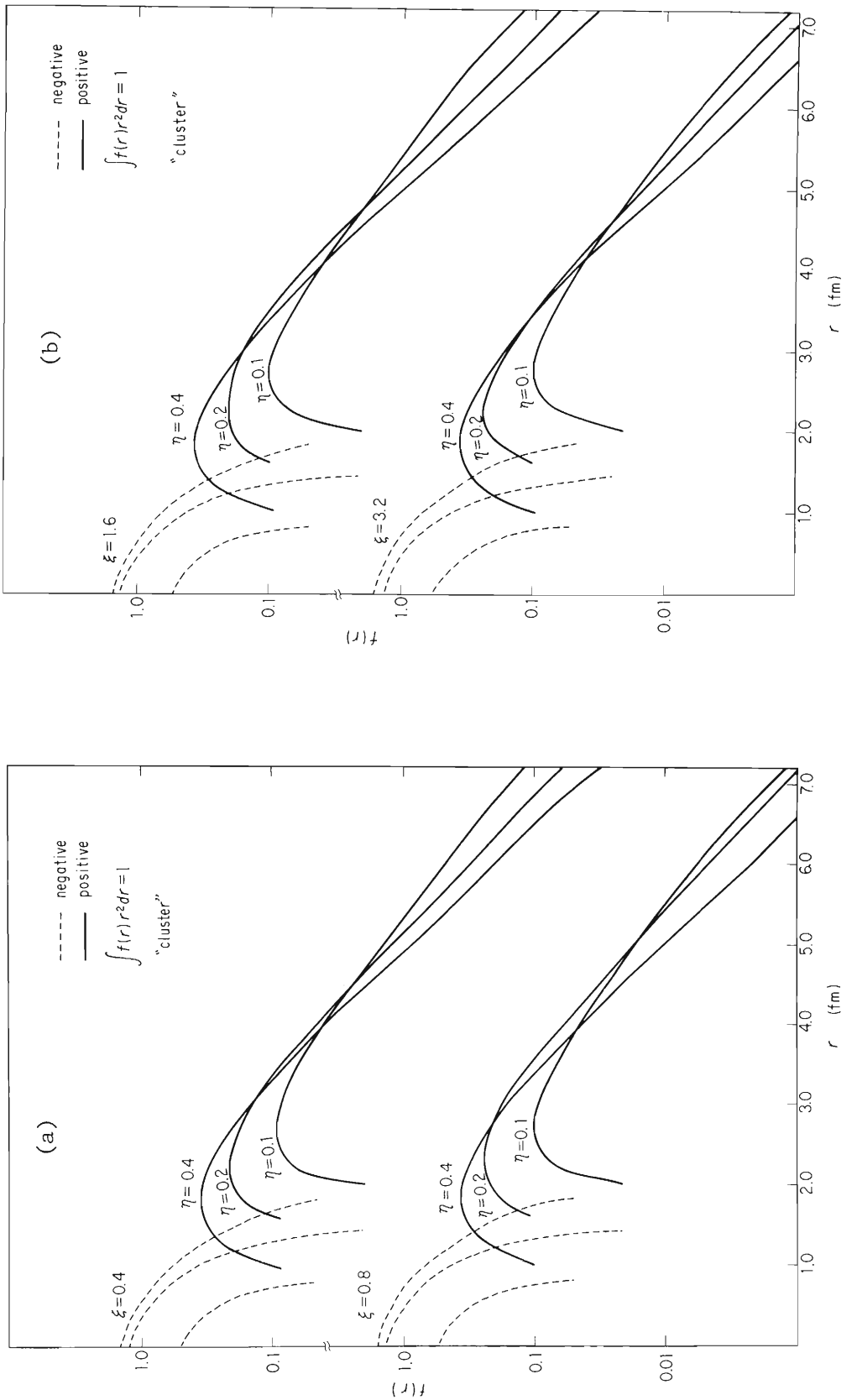

Fig. 2. Behavior of form factor.

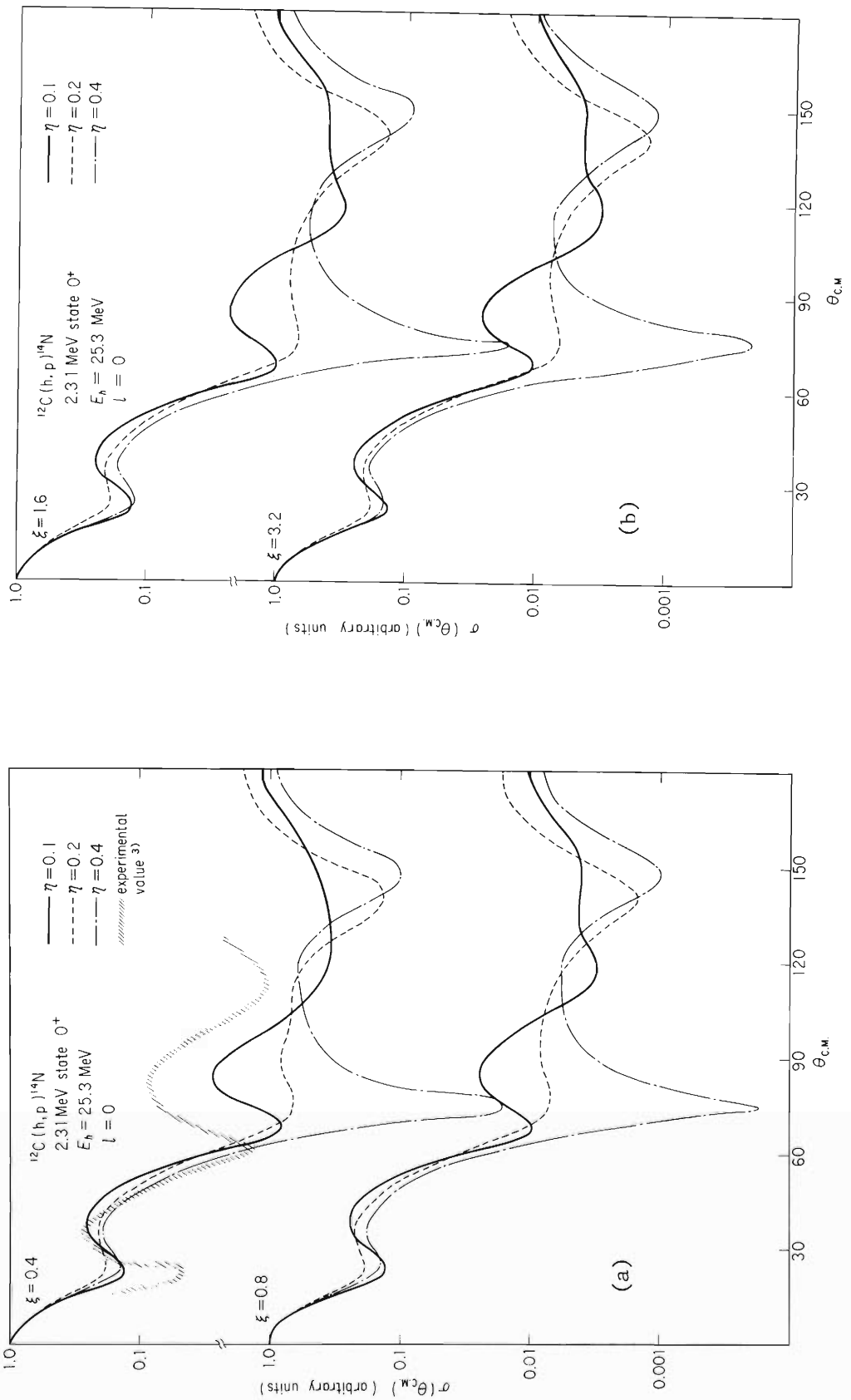

Fig. 3. Differential cross section.

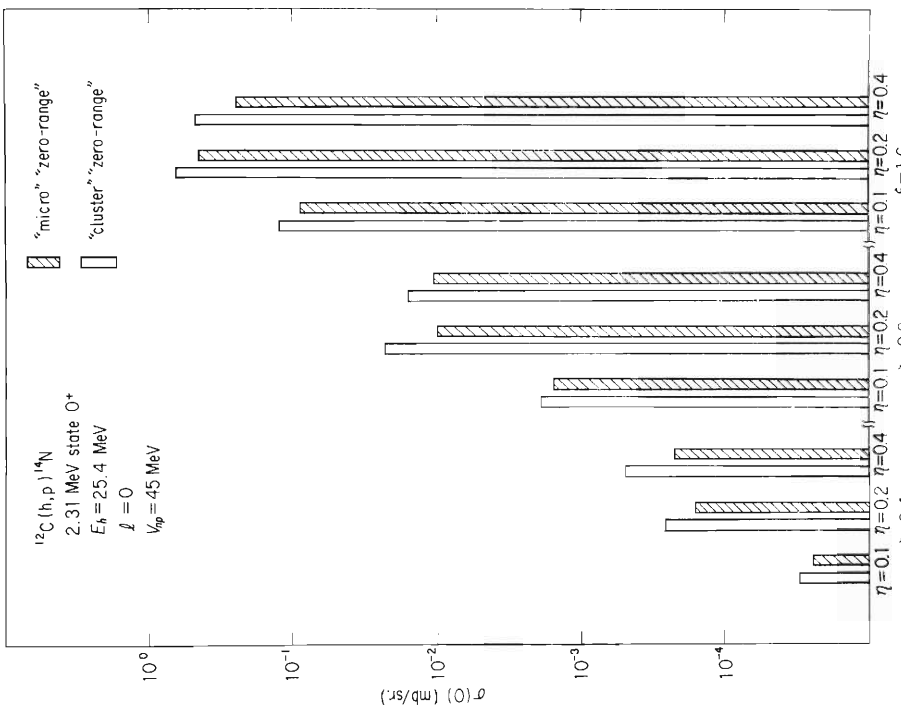

Fig. 5. Absolute value of differential cross section at 0 °.

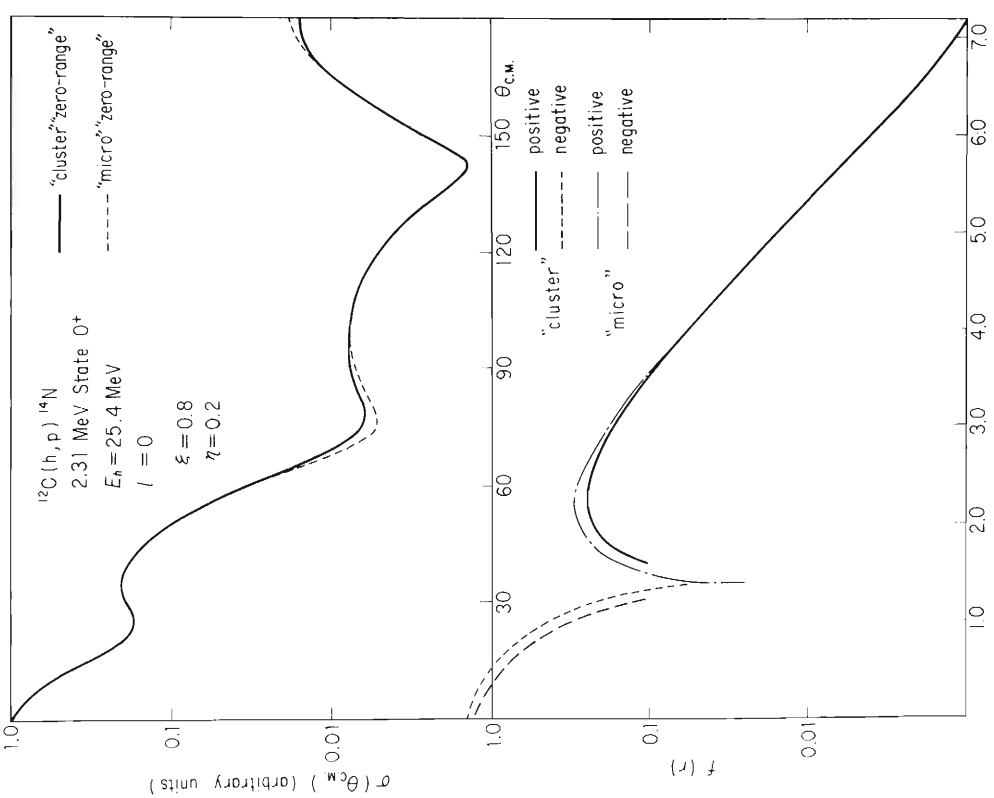

Fig. 4. Comparison between "micro" and "cluster".

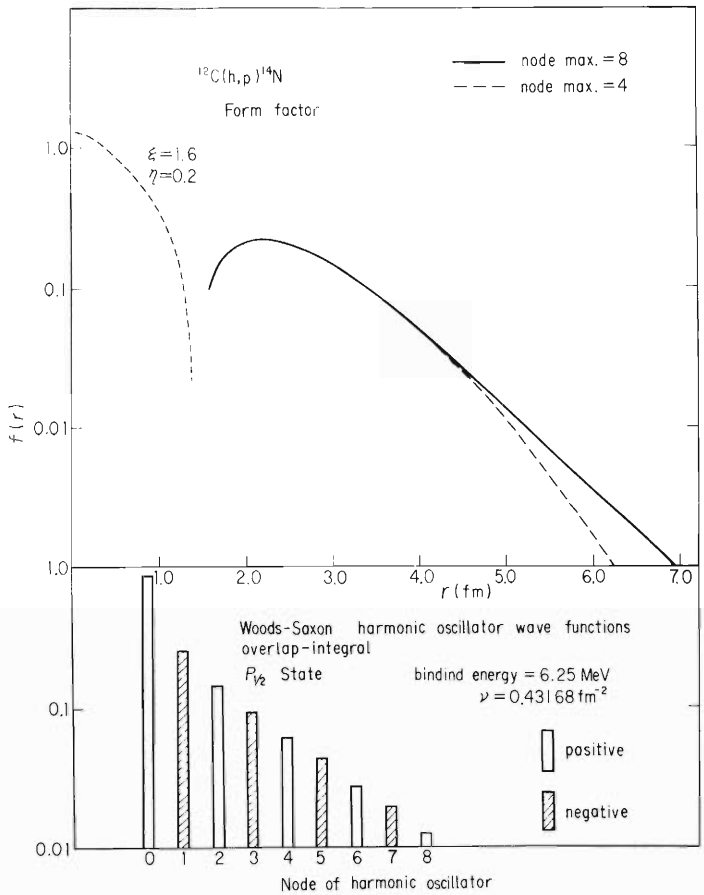

Fig. 6. Necessary number of oscillators to expand the Woods-Saxson eigenstate.

References

1) S. Yamaji: IPCR Cyclotron Progr. Rep. 2, 83 (1968).
2) R.M. Drisko and F. Rybicki: Phys. Rev. Letters, 16, 275 (1966).
3) K. Matsuda, N. Nakanishi, S. Takeda, and T. Wada: J. Phys. Soc. Japan, 25, 1207 (1960).

5. NUCLEAR PHYSICS
Nuclear Spectroscopy

5-1. Magnetic Core Polarization Effect in the $(h_{9/2}^2)^{8+}$ State of ^{210}Po

T. Katou, T. Inamura, A. Hashizume, Y. Tendow,
T. Yamazaki, and T. Nomura

The g-factor of the $(h_{9/2}^2)8^+$ state of ^{210}Po has been determined to be 0.925 ± 0.010 in the pulsed generation of the aligned state in the ^{208}Pb $(\alpha,2n)$ reaction.

Recently an 8^+ isomeric state of the $(h_{9/2}^2)$ configuration has been identified in ^{210}Po [1,2] (see the level structure in Fig. 1). Owing to its almost pure shell-model configuration, one can examine how long the core polarization of ^{208}Pb by $h_{9/2}$ proton persists from the one-particle state (^{209}Bi) to the two-particle state (^{210}Po). In this note we report on a g-factor measurement of the $(h_{9/2}^2)8^+$ state and discuss the magnetic core polarizability by two protons in order to elucidate the nature of the anomalous magnetic moment of the $(h_{9/2})$ state of ^{209}Bi. The experimental method was the same as that employed by Yamazaki and Mattias.[3]

A ^{208}Pb target of 30 mg/cm^2 thick metallic foil was bombarded by 25 MeV alpha particles from IPCR 160 cm Cyclotron. Gamma rays were detected with a $1\frac{1}{2}'' \times 1\frac{1}{2}''$ ϕ NaI (Tl) counter placed making an angle of 135 deg. with the beam direction. The time distributions of gamma rays were measured by the use of the natural beam bursts of 132 nsec interval. Delayed gamma ray spectra at this energy taken with a Ge(Li) detector ensured the use of a NaI(Tl) counter. The population of the 24 nsec 11^- state is negligible, and therefore, the delayed 245 keV and 1180 keV transitions are perturbed only through the 110 nsec 8^+ state and the 38 nsec 6^+ state. An external 10.93 ($\pm$ 0.5 %) kG magnetic field was applied up and down perpendicularly to the beam-detector plane. The time spectra and the normalized differences for the 245 keV peak are shown in Fig. 2, from which a Larmor frequency of 48.44 ± 0.04 MHz was obtained. The separation of the Larmor precessions at the 8^+ and 6^+ state was impossible; however, it is safely assumed that both states have the same g-factor, since they are of the same $h_{9/2}^2$ configuration. We thus obtain

$$g = 0.925 \pm 0.010$$

It is well known that the $h_{9/2}$ ground state of ^{209}Bi exhibits an extremely anomalous magnetic moment. A theoretical interpretation of this anomaly was given by Arima and Horie,[4] who took into account the particle ($j = \ell - 1/2$) - hole ($j = \ell + 1/2$) excitation of the ^{208}Pb core; however, they could account for only half of the observed anomaly in terms of such core polarization.

Table 1 summarizes the present results together with those of ^{209}Bi. The single-particle estimates, g_{sp}, with the free-nucleon g_s factor of 5.5856 is given in column 4 and $g_{exp} = g_{exp} - g_{sp}$ in column 5. If the same renormalization is associated with a state j, then

$$g(|j^2, J>) = g(|j>)$$

Table 1. Summary of anomalous magnetic moments in ^{209}Bi and ^{210}Po.

Nucleus	State	g_{exp}	g_{sp}	Δg_{exp}	$(\Delta g_s^{eff}/g_s^{free})_{exp}$
$^{209}_{83}Bi_{126}$	$h_{9/2}$	0.9067	0.5831	0.3236	0.6374
$^{210}_{84}Po_{126}$	$(h_{9/2}^2)\,8^+$	0.925±0.010	0.5831	0.342±0.010	0.6735

would hold. The nearly equal g_{exp} in both ^{209}Bi and ^{210}Po indicates the validity of the above shell-model additivity even for anomalous magnetic moments within two percent.

It was suggested by Arima* that the core polarization can be blocked out by the presence of particles in the $h_{9/2}$ orbit to such an extent as the $h_{9/2}$ orbit is involved in the core polarization. If the $(h_{11/2}^{-1}\ h_{9/2})\,1^+$ polarization is assumed to be fully responsible for the anomalous magnetic moment of ^{209}Bi, then we would expect

$$\frac{\Delta g\,(^{210}Po)}{\Delta g\,(^{209}Bi)} \approx \frac{8}{9} = 0.9$$

while

$$\frac{\Delta g_{exp}(^{210}Po)}{\Delta g_{exp}(^{209}Bi)} = 1.06 \pm 0.03.$$

This comparison implies that the $(h_{11/2}^{-1}\ h_{9/2})\,1^+$ excitation may not be the sole contribution to the anomalous magnetic moment of ^{209}Bi. The blocking effect was not obviously be confirmed.

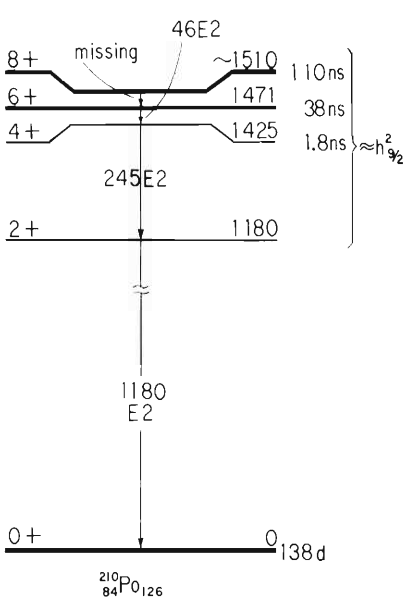

Fig. 1. The level structure of ^{210}Po.

* A. Arima: Private communication (1969).

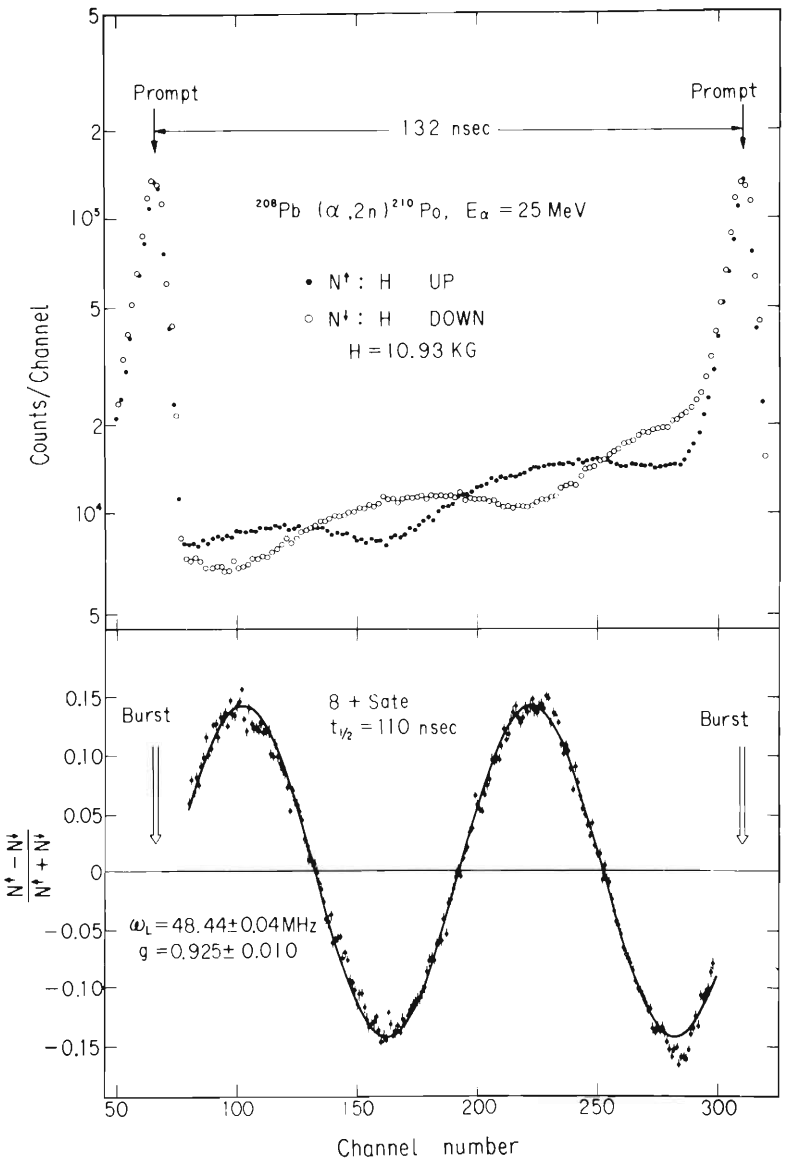

Fig. 2. The time spectra and the normalized differences for the 245 keV peak.

References

1) T. Yamazaki and G.T. Ewan: Phys. Letters, 24B, 278 (1967).
2) M. Ishihara, Y. Gono, K. Ishii, M. Sakai, and T. Yamazaki: Phys. Rev. Letters, 21, 1814 (1968).
3) T. Yamazaki and E. Matthias: Phys. Rev., 175, 1476 (1968).
4) A. Arima and H. Horie: Prog. Theor. Phys., 12, 623 (1954).

5-2. Systematics of Excited States of Even Cadmium Nuclei Investigated by (α, xnγ) and (^{12}C, xnγ) Reactions

A. Hashizume, T. Inamura, T. Katou,
Y. Tendow, T. Yamazaki, and T. Nomura

Gamma transitions followed by (α,xn), (^{3}He,xn) reactions on palladium isotopes and (^{12}C,xn) reactions on molybdenum isotopes were investigated for the purpose of studying the nuclear structure of neutron deficient even cadmium isotopes. Enriched palladium targets ^{102}Pd, ^{104}Pd, ^{106}Pd, and ^{110}Pd were bombarded with ^{4}He or ^{3}He particles with energies from 20 to 43 MeV and ^{92}Mo or ^{94}Mo was bombarded with ^{12}C having energies from 70 to 95 MeV accelerated by IPCR energy variable cyclotron. Gamma rays were observed with 4 mℓ and 23 mℓ Ge(Li) detectors at 90°. Excitation functions for (α,2n), (α,4n), (^{3}He,3n), and (^{12}C,4n) reactions were obtained from the area of photopeaks in gamma ray spectra taken at the step of 5 MeV of bombarding energy. The incident energies of heavy ions were also changed at the step of 5 MeV. In the case of reactions induced by heavy ions, the gamma rays resulting from radioactive decays were slightly recognized, so that the spectra after interruption of the beam were attentively studied and compared with those during the irradiation of the targets.

Typical energy spectra of gamma rays as well as excitation functions obtained from the area of photopeaks are shown in Figs. 1, 2, 3, and 4. The relative intensities of gamma rays assigned to the deexcitation in cadmium isotopes are shown in Table 1.

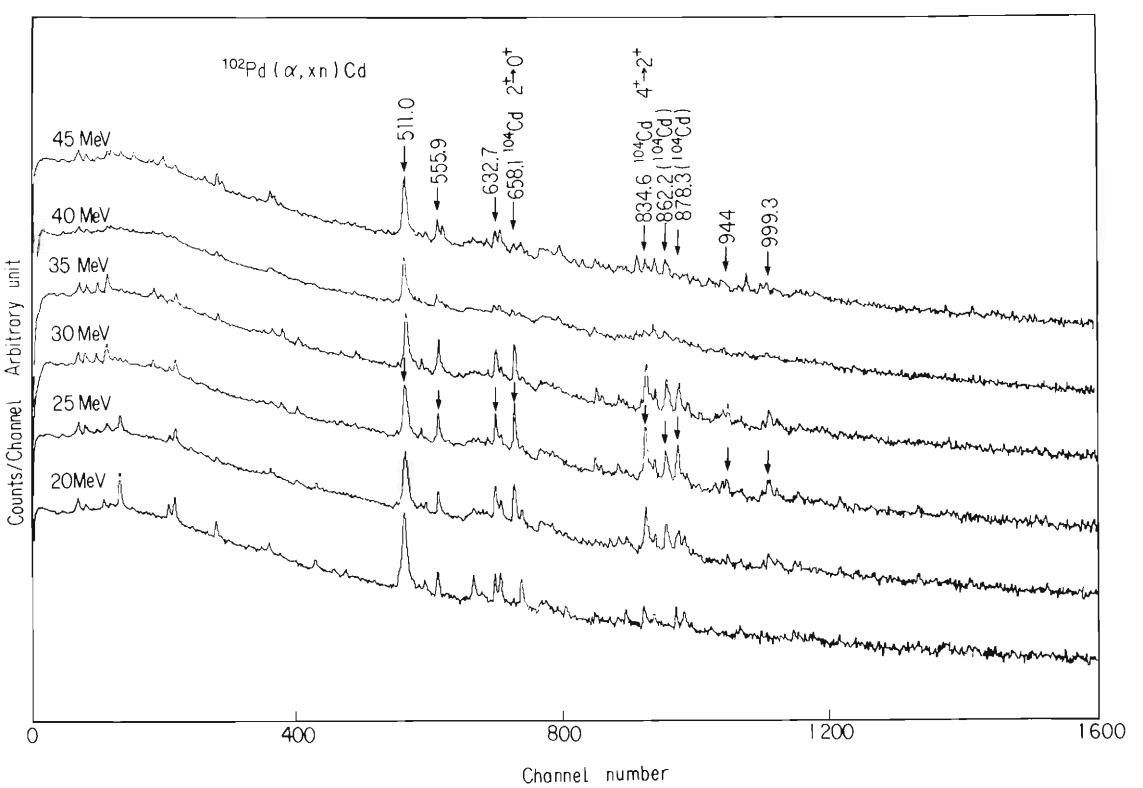

Fig. 1. Gamma rays spectra obtained ^{108}Pd (α, xn) Cd reactions.

Table 1. Relative intensities of gamma rays assigned to the deexcitation in cadmium isotopes.

$^{102}Pd(\alpha,2n)^{104}Cd$		$^{104}Pd(\alpha,2n)^{106}Cd$		$^{106}Pd(\alpha,2n)^{108}Cd$		$^{108}Pd(\alpha,2n)^{110}Cd$		$^{110}Pd(\alpha,2n)^{112}Cd$	
$E\gamma$	$I\gamma$	$E\gamma$	$I\gamma$	$E\gamma$	$I\gamma$	$E\gamma$	$I\gamma$	$E\gamma$	$I\gamma$
658.1 keV	100($2^+\rightarrow 0^+$)	633.0 keV	100($2^+\rightarrow 0^+$)	633.3 keV	100($2^+\rightarrow 0^+$)	658.1 keV	100($2^+\rightarrow 0^+$)	617.5 keV	100($2^+\rightarrow 0^+$)
834.6	83($4^+\rightarrow 2^+$)	861.8	95($4^+\rightarrow 2^+$)	872.0	83($4^+\rightarrow 2^+$)	884.8	80($4^+\rightarrow 2^+$)	797.6	63($4^+\rightarrow 2^+$)
862.2	52	998.5	31($6^+\rightarrow 4^+$)	1033	27($6^+\rightarrow 4^+$)	938.6	43($6^+\rightarrow 4^+$)	957.2	22($6^+\rightarrow 4^+$)
878.3	57	1010	19($8^+\rightarrow 6^+$)	1095	32	998.1	22($8^+\rightarrow 6^+$)		
999.3	14			1196	17($8^+\rightarrow 6^+$)				

$^{92}Mo(^{12}C,4n)^{100}Cd$		$^{94}Mo(^{12}C,4n)^{102}Cd$		$^{102}Pd(^{3}He,3n)^{102}Cd$		$^{104}Pd(^{3}He,3n)^{104}Cd$	
$E\gamma$	$I\gamma$	$E\gamma$	$I\gamma$	$E\gamma$	$I\gamma$	$E\gamma$	$I\gamma$
750.5 keV	100 RI?	719.7 keV	100($2^+\rightarrow 0^+$)	658.0 keV	12	658.2 keV	100($2^+\rightarrow 0^+$)
773.4	71 RI?	835.6	46($4^+\rightarrow 2^+$?)	719.5	100($2^+\rightarrow 0^+$)	834.9	108($4^+\rightarrow 2^+$)
798.6	49	848.3	37	836.2	50($4^+\rightarrow 2^+$)	847.5	34
857	69($2^+\rightarrow 0^+$?)	860.3	36	840	22	864.5	48
909.3	67	936	23	848	19	878.7	43
		970.9	26	862.7	20		

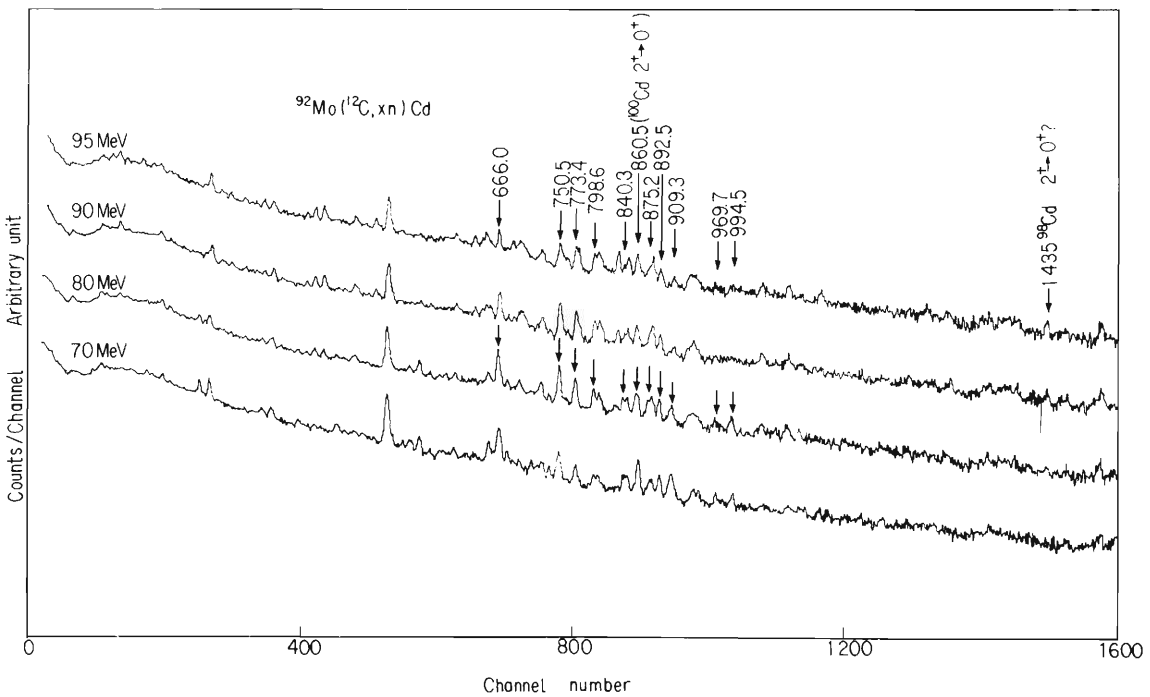

Fig. 2. Gamma rays spectra obtained ^{92}Mo (^{12}C, xn) Cd reactions.

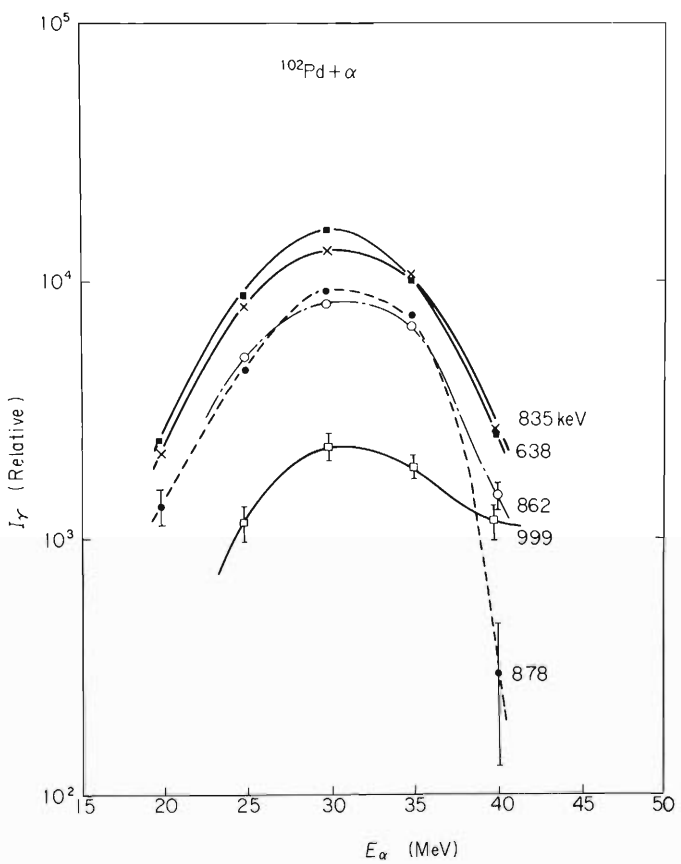

Fig. 3. Excitation curves for ^{102}Pd (α, 2n) ^{104}Cd reactions.

Assuming the cascade transitions from the high angular momentum states fed by compound states after emissions of neutrons, the level schemes in cadmium were obtained as shown in Fig. 5. It exhibits a very systematic behavior favoring some band structure. The ratios of the energies of 4^+, 6^+, and 8^+ states to that of 2^+ states are plotted (Fig. 6). The values of E(4)/E(2) change from 1.85 to 2.38, and those of E(6)/E(2) from 3.76 to 4.01, while E(8)/E(2) from 5.3 to 5.9. It has been argued by Ejiri[1] that the energy of the ground state band levels obeys a simple energy rule of the form $E(I) = aI(I+1) + bI$. This rule is able to compare with the experimental values as shown in Fig. 7. Energy levels of ^{108}Cd fit well to this rule, but those of ^{106}Cd and ^{110}Cd exhibit convex curve when E(I)/I is plotted against I. The 4^+ states could be interpreted in terms of one of the members caused by a quadrupole vibration of spherical nuclei, but the gamma rays from $2^{+'} \rightarrow 2^+$ transition were difficult to assign because of their weak intensities.

The delayed gamma rays were also searched using the bunched character of the beam from the cyclotron, but in even cadmium isotopes no delayed gamma rays were observed.

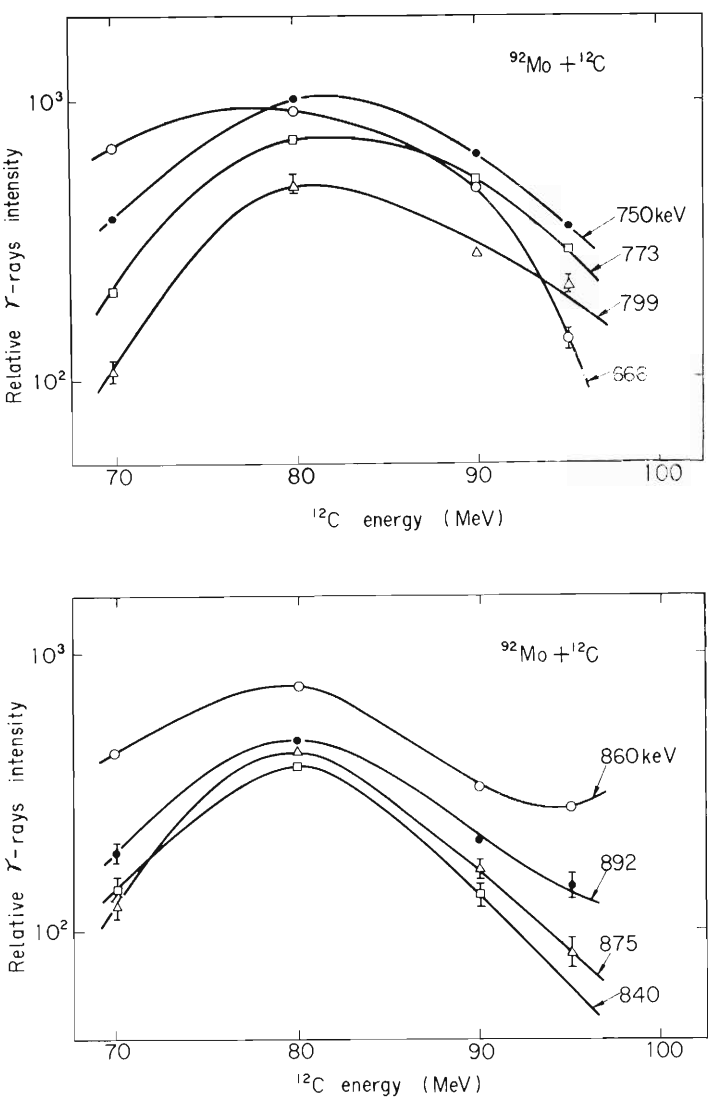

Fig. 4. Excitation curves for ^{92}Mo (^{12}C, 4n) ^{100}Cd reactions.

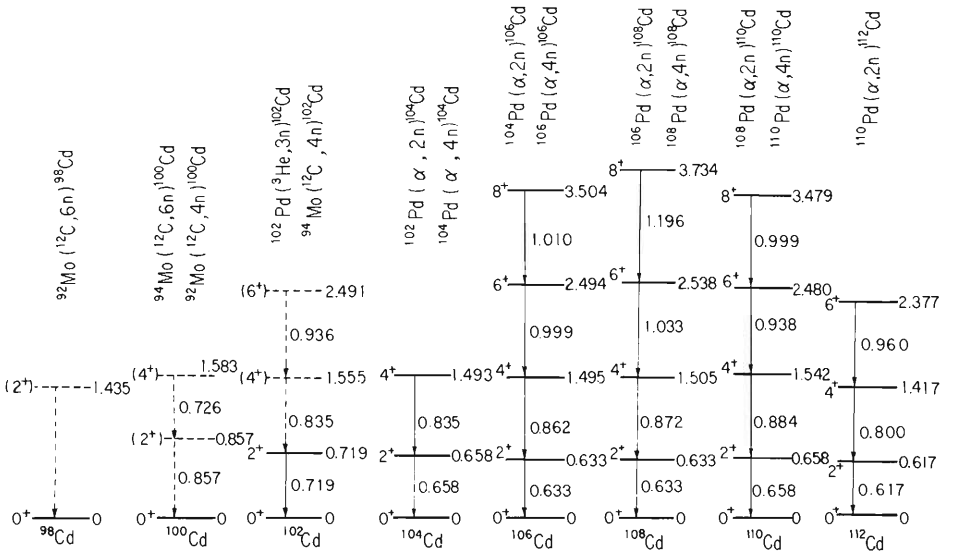

Fig. 5. Excited states observed in cadmium isotopes.

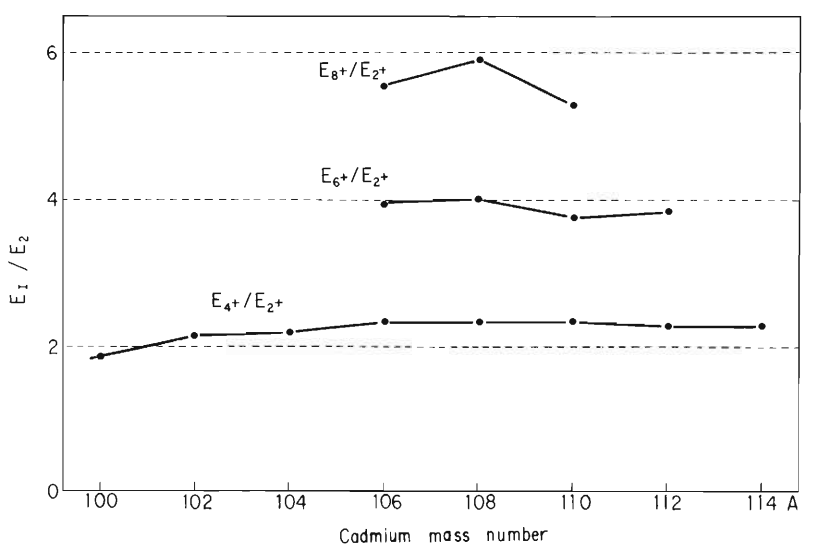

Fig. 6. Systematics of excited energy levels to first 2^+ states.

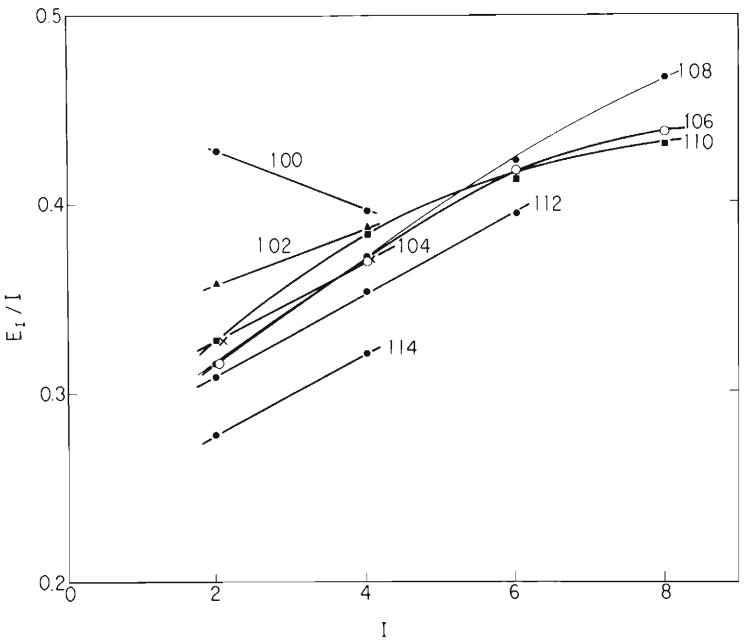

Fig. 7. Plot of E_1/I to I. The number on each curve is mass number.

Reference

1) H. Ejiri: INSJ - 101 (1966).

5-3. The Excited States in Neutron Deficient Even Tin Isotopes

T. Inamura, A. Hashizume, T. Katou,
Y. Tendow, T. Yamazaki, and T. Nomura

In-beam spectroscopy of gamma ray following a (H.I., Xn)-type reaction induced by heavy ions is a powerful method to study the properties of nuclei far from the stability line.

From an experimental point of view it is still open to question whether a nucleus with Z=N=50 will prove to be doubly magic. The excited states in neutron deficient even tin isotopes will give suggestive information to predict the nuclear structure of the Z=N=50 nucleus.

Even tin isotopes from A=108 to A=102 were produced by the following reactions using ^{12}C-beams from the IPCR 160 cm Cyclotron;

$^{100}Ru(^{12}C, 4n)^{108}Sn$, $^{98}Ru(^{12}C, 4n)^{106}Sn$,

$^{96}Ru(^{12}C, 4n)^{104}Sn$, $^{96}Ru(^{12}C, 6n)^{102}Sn$.

These targets ^{100}Ru, ^{98}Ru, and ^{96}Ru were enriched to 75.7, 54.6, and 98.1 % respectively and deposited uniformly on the 6 μ myler backing. Thickness of these targets was about 5 mg/cm^2. Gamma rays from these reactions were measured with an ORTEC 23 cm^3 coaxial Ge(Li) detector. Mass assignment of the residual nucleus was made by measurements of gamma ray yields with respect to bombarding energy in the range from 70 to 95 MeV in steps of 5 MeV; as a reference to settle (^{12}C, 4n) reaction were chosen the results of $^{106}Cd(\alpha, 2n)\ ^{108}Sn$ reaction performed by Yamazaki and Ewan.[1] Optimum bombarding energy for the (^{12}C, 4n) reaction was found to be about 80 MeV.

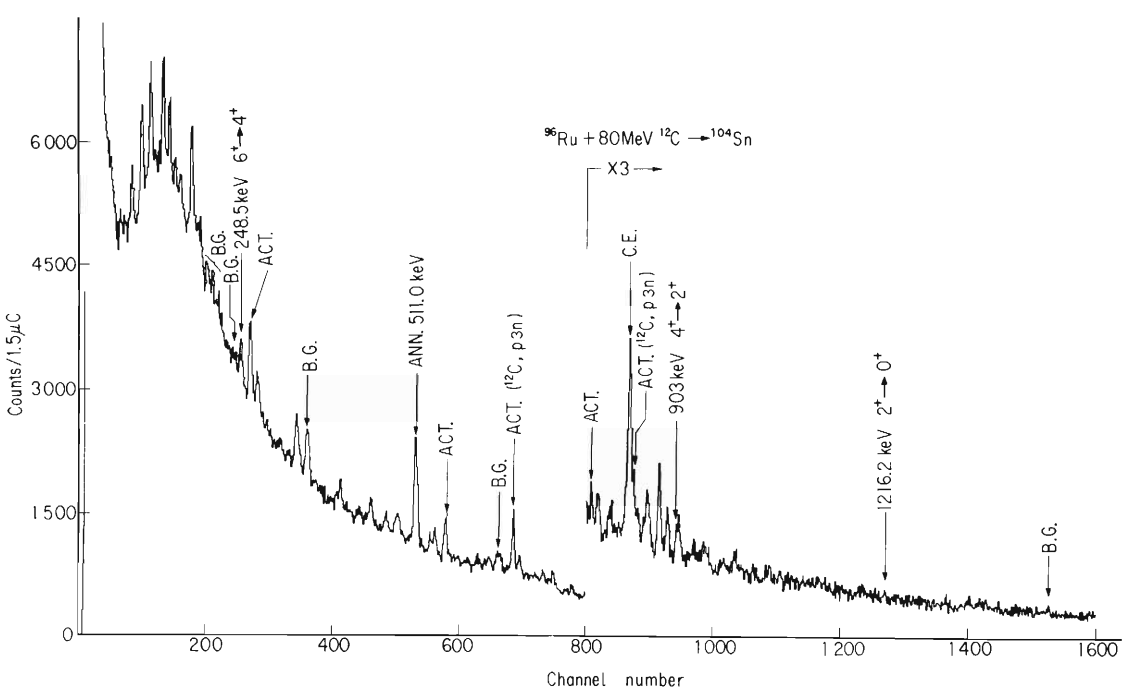

Fig. 1. Gamma ray spectrum observed in the case of ^{96}Ru+80 MeV ^{12}C.

A typical gamma ray spectrum is shown in Fig. 1. Unfortunately the gamma ray spectra were too complex to make definite assignments for all gamma rays observed. These complex spectra are due to other induced reactions, for instance, (^{12}C, p3n) reaction. It is noticeable that a predominant reaction is not (^{12}C, 4n) reaction, but (^{12}C, p3n) reaction for the Ru targets around the projectile energy of 80 MeV.

Transition assignments $2^+ \rightarrow 0^+$, $4^+ \rightarrow 2^+$, $6^+ \rightarrow 4^+$ for ^{108}Sn, ^{106}Sn, and ^{104}Sn were made in the order of intensity of respective gamma rays. The 1354 keV gamma ray appearing in the gamma ray spectra taken at 90 and 95 MeV incident energies for the ^{96}Ru target was assigned to the $2^+ \rightarrow 0^+$ transition in ^{102}Sn.

Fig. 2 shows a tentative level scheme of neutron deficient even tin isotopes from A=108 to A=102. From these results it may be said that the nucleus $^{100}_{50}Sn_{50}$ far from the stability line has the same properties as those of the doubly magic nuclei in the stable region. This supports a theoretical deduction that the Z=N=50 nucleus is doubly magic almost certainly because of the large spin orbit splitting between the $g_{7/2}$ and $g_{9/2}$ orbits.[2)]

The 6^+ state in tin isotopes with $N \leq 56$ is plausible because the $d_{5/2}$ orbit is very close to the $g_{7/2}$ orbit.

The level scheme proposed here is now being examined using the pulsed-beam method[1)] or e-γ coincidence technique.

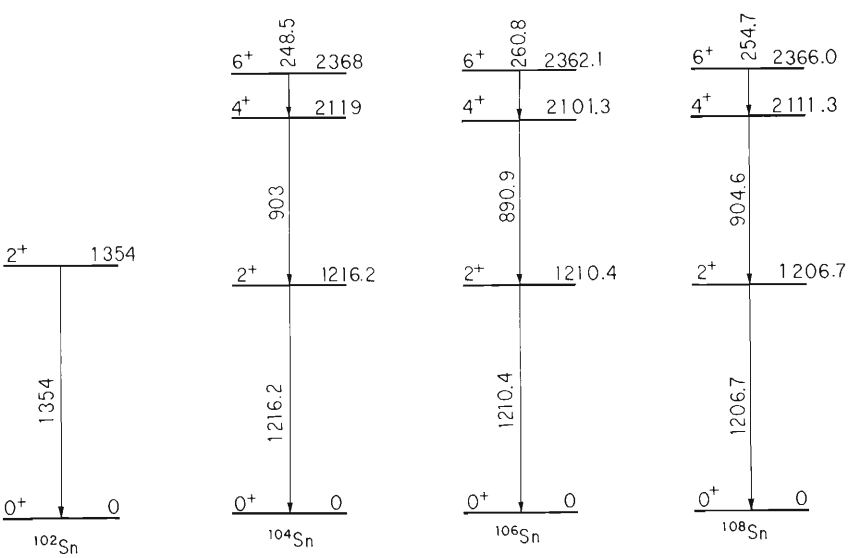

Fig. 2. A tentative level scheme of even tin isotopes from A=108 to A=102.

References

1) T. Yamazaki and G.T. Ewan: Nucl. Phys., A134, 81 (1969).
2) R.A. Sorensen: Arkiv. Fysik., 36, 585 (1966).

5-4. Decay of New Isotopes ^{100}Ag and ^{104}In

T. Inamura, A. Hashizume, T. Katou,
Y. Tendow, T. Yamazaki, and T. Nomura

In the course of in-beam spectroscopy of gamma rays following heavy-ion induced nuclear reactions, many gamma rays emitted by activities have been observed. Some gamma rays obtained by irradiation of ^{92}Mo and ^{96}Ru targets with ^{12}C-ions have been assigned to the decay of new isotopes ^{100}Ag and ^{104}In respectively on the basis of the following evidence.

Measurements were made with a Ge(Li) detector coupled to SCIPP 1600 or ND 4096 channel PHA. After irradiation of targets with 80 MeV ^{12}C-ions from the IPCR 160 cm Cyclotron, gamma ray spectra were taken repeatedly at suitable time intervals, and half-lives of the activities were determined. Excitation functions related to the activities have been obtained from measurements of yields of associated gamma rays with respect to irradiation energy. Mass assignment of the activities has been made on the basis of these excitation functions referring to the decay of ^{106}In, ^{108}In, and ^{102}Ag.

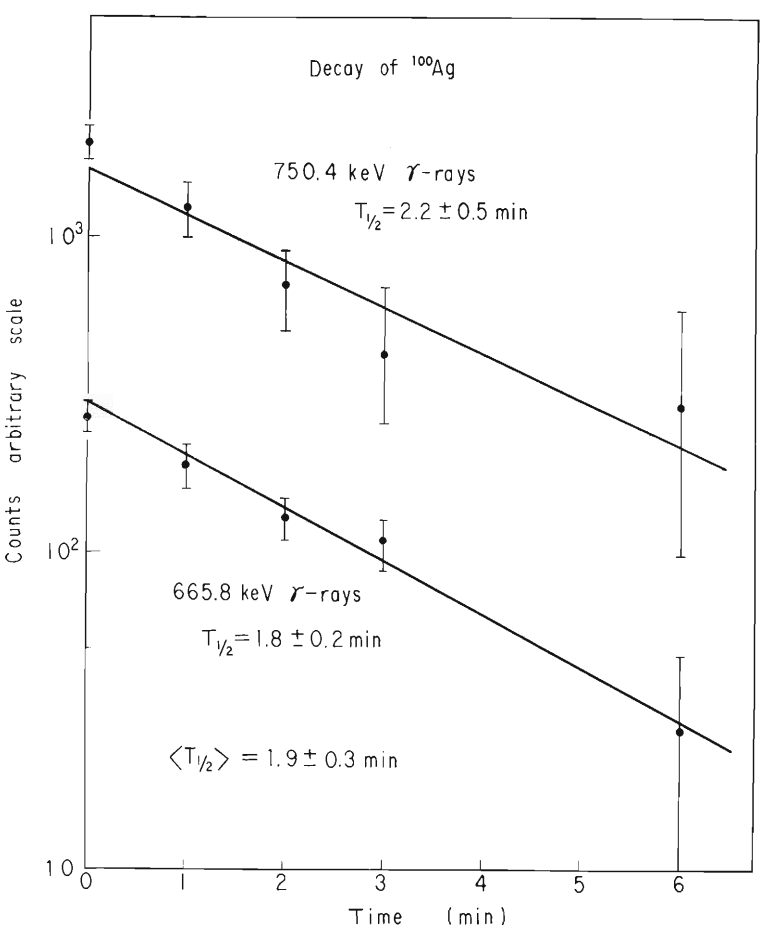

Fig. 1. Decay curves of the 665.8 and 750.4 keV gamma rays from ^{100}Ag.

Gamma rays resulted from the decay of these reference isotopes were observed by bombardment of enriched ^{98}Ru, ^{100}Ru, and ^{94}Mo targets, and their half-lives were confirmed to be consistent with those already known.[1] Moreover, the in-beam gamma ray spectra showed most prominent photopeaks due to these activities.* These results lead to the conclusion that the Ru(or Mo) (^{12}C, p3n) In(or Ag) reaction is more predominant than the Ru(or Mo) (^{12}C, 4n) Sn(or Cd) reaction around the incident energy of 80 MeV. Similar tendency seems to be held in the case of cadmium targets. Effects from the decay of the (^{12}C, 4n) reaction products were negligible.

Targets of interest were made by depositing ^{92}Mo and ^{96}Ru enriched metallic powder on a 6 μ myler film to ~ 5 mg/cm^2 thickness; their enrichment was 98 %. Activities in the myler backing and in the environment were checked and found to be negligible.

(1) $^{92}Mo(^{12}C, p3n)^{100}Ag \xrightarrow{\beta^+} {}^{100}Pd$

Prominent gamma rays of 665.8 and 750.4 keV obtained from the ^{92}Mo target irradiated with 80 MeV ^{12}C-ions showed that they had the same excitation function compatible with that of the (^{12}C, p3n) reaction. These two gamma rays have the same

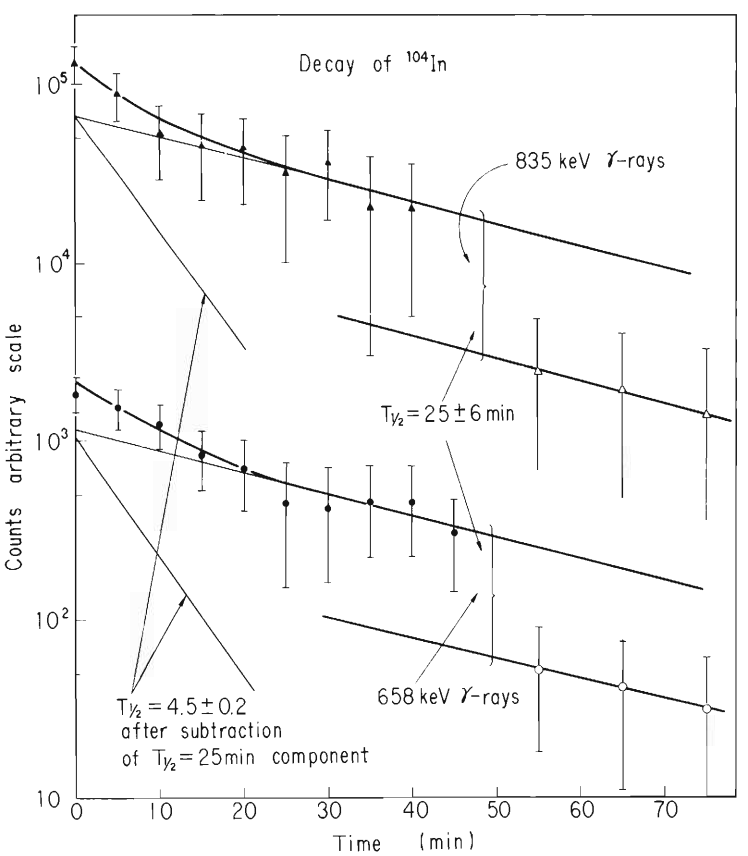

Fig. 2. Decay curves of the 658 and 835 keV gamma rays from ^{104}In. Closed circles (triangles) indicate that counting measurements were done for 200 sec at 5 min intervals, and open ones for 400 sec at 10 min intervals.

* See, for instance, this progress report 5-3.

decay curve within the limit of experimental error, as shown in Fig. 1. These facts prove that the 665.8 and 750.4 keV gamma rays were resulted from the decay of ^{100}Ag. The half-life of ^{100}Ag has been found to be $T_{1/2} = 1.9 \pm 0.3$ min. The 665.8 and 750.4 keV gamma rays have been assigned to the $2^+ \longrightarrow 0^+$ and $4^+ \longrightarrow 2^+$ transitions in the daughter nucleus ^{100}Pd, respectively, taking account of their intensities. A basic decay scheme of ^{100}Ag is presented in Fig. 3(a).

(2) ^{96}Ru(^{12}C, p3n)^{104}In $\xrightarrow{\beta^+}$ ^{104}Cd

Two gamma rays of 658 and 835 keV emitted by the activity of ^{104}In have been found in the same manner as in the case of ^{100}Ag. In addition, these gamma rays are exactly in agreement with the $2^+ \rightarrow 0^+$ and $4^+ \rightarrow 2^+$ transitions in ^{104}Cd that have been revealed by the ^{102}Pd(α, 2n)^{104}Cd reaction performed in our laboratory.[2] Fig. 2 shows the decay curves of these gamma rays. It is evident that there are two components having different half-lives. The long-lived component decays with a half-life of $T_{1/2} = 25 \pm 6$ min. After subtraction of this component, the half-life of the short-lived one has been found to be $T_{1/2} = 4.5 \pm 0.2$ min. Thus, the decay of ^{104}In has been established primarily as shown in Fig. 3(b).

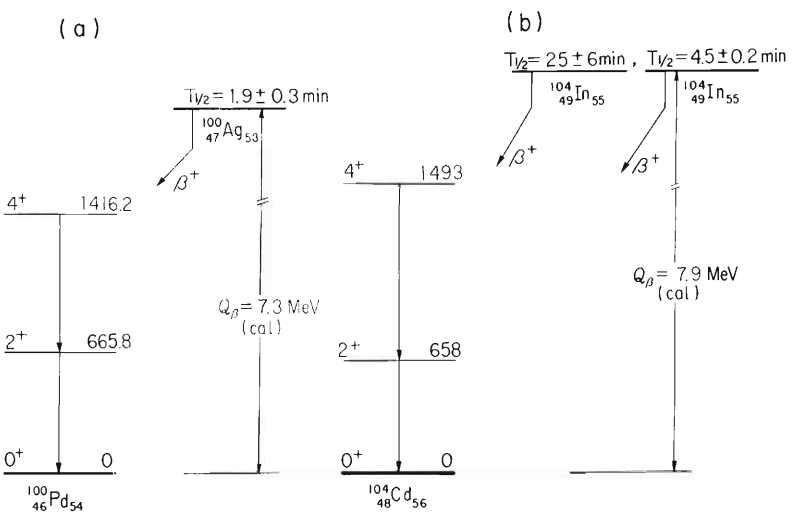

All energies are in keV.

Fig. 3. (a) Decay scheme of ^{100}Ag, (b) Decay scheme of ^{104}In.

References

1) C.M. Lederer et al. (Ed.): "Table of Isotopes", John Wiley & Sons, Inc., N. Y., (1967)
2) A. Hashizume et al.: "Contributions International Conference of Properties of Nuclear States" 3-4, Montreal (1969)

5-5. The Decay of ^{147}Gd and Energy Levels in ^{147}Eu

A. Hashizume, Y. Tendow, Y. Awaya, and T. Katou

This study is a part of the series to reveal the nuclear structure of odd nuclei of europium isotopes in the transition region just before the beginning of the deformation. The radioactive sources of ^{147}Gd were obtained by the reaction ^{147}Sm(^{3}He,3n)^{147}Gd using the helium particles of 35 or 38 MeV from the IPCR Cyclotron. The carrier free gadolinium activities were obtained by an ion exchange method consisting of three stages, i.e., separation, concentration, and purification. In the separation stage a column of Dia-ion SK#1, 14 mm in diameter and 50 cm in height, was used. The flow rate of eluent, composed of 0.5M NH_4B 20 % + HB 80 %,* was about 1.5 mℓ/min.

The gamma ray spectrum observed with a high resolution Compton-suppressed 23 mℓ coaxial type Ge(Li) detector is shown in Fig. 1. The energy calibration was made with ^{56}Co. The decay was followed for about 4 half-lives of ^{147}Gd and the photopeaks, attributed to the decay series ^{147}Gd $\rightarrow$ ^{147}Eu $\rightarrow$ ^{147}Sm, were selected. The gamma ray photopeaks resulting from the decay ^{146}Gd $\rightarrow$ ^{146}Eu $\rightarrow$ ^{146}Sm were also examined from the spectra of the radioactive sources made by the irradiation with 43 MeV ^{3}He-particles. The gamma ray energies and their intensities are shown in columns 1 and 2 of Table 1. To determine the transition types, the intensities of conversion electrons,[1),2)] used for the calculation of K conversion coefficients are shown in column 3. By assuming the M2 character of the 396 MeV transition, the mixing ratios of transitions were determined as shown in column 4.

It has been proved by gamma-gamma coincidence experiments that 229 keV gamma rays coincide with gamma rays whose energies are 310, 390, 550, 760, 900, 1130, 1330, and 1580 keV; 625 keV gamma rays coincide with 370, 520, 570, and 930 keV; 930 keV gamma rays coincide with 230, 400, and 625 keV gamma rays.[3),4),5)] As gamma rays were detected by NaI detectors, the above energies obtained by different authors were less precise and showed discrepancy of about 20 keV, but when comparing our data, as well as applying Ritz's rule, the existence of the levels at 229, 626, 996, 1358, 1554, and 1813 keV would be firmly confirmed and these levels were taken as the basis of the confirmation of another levels applying Ritz's rule. The 776 keV level was confirmed, on the one hand, from a cascade 547 keV and 229 keV transitions whose sum is 776 keV, and, on the other hand, 547 keV and 774 keV transitions became one of the members of the cascade transitions, e.g., (547, 1015; 1563), (547, 1037; 1584) or (777, 1015; 1792); the first and the second transitions indicate a cascade and the third their sum. After applying Ritz's rule and also taking into account the intensity of gamma rays, it seems reasonable to assign the levels to 1959, 1792, 1233, and 1122 keV. The conjectures to confirm 1068, 1037, 993, and 844 keV levels are based only on Ritz's rule and, consequently, the existence of these levels is only a suggestion. The proof should be made with Ge(Li) - Ge(Li) coincidence experiments. The spin assignment was made on the transition types made by K conversion coefficients. The measurement of conversion electrons by an air core spectrometer is now underway. The energy levels and gamma transitions suggested are shown in Fig. 2.

* We are indebted to Dr. H. Natsume and T. Sato for chemical separation methods.
HB: alpha-hydroxy-isobutyric acid.

Table 1.

E	I_γ	I_{ek}	Transition type	E	I_γ	I_{ek}	Transition type
167	0.72	1.4	E2	787	2.3	0.5	M2
193	0.52	1.3	M1 + (E2)	803	0.94		
209	0.29			808	1.3		
217	5.5			(818)	0.63		
230	210	220	M1 + E2	827	1.8		
241	4.4	4	M1 + E2	859	4.6	0.20	M1
250	1.2			875	0.7		
261	5.8	5	M1	892	22	0.60	M1 + E2
310	11	6	M1 + (E2)	909	1.4	0.04	M1 + E2
319	6.1	3	M1 + (E2)	928	53	1.9	M1 or E3
326	0.42			982	0.57		
346	5.9			1005	3.4		
370	53	13	(M1 + E2)	1015	0.4		
396	100	100	M2	1038	0.96		
485	8.9	1.3	M1 + (E2)	1068	17	0.1	E1
537	0.28			(1105)	0.03		
548	1.0	0.19		1122	2.3		
559	18	1.3~2.4	E2	1129	14	0.1	E1
574	0.56			1158	1.6		
610	4.3	0.25	E2	(1168)	0.21		
615	11	0.9	M1 or E3	(1182)	0.18		
625	11	1.6	M1 or E3	1233	2.68		
645	9			1303	0.20		
658	0.36			1322	1.9	0.01	E1
692	0.76	} 0.17		1387	0.15		
714	0.92			(1494)	0.03		
725	0.40			(1497)	0.04		
733	0.61	0.05	M1 or E3	1563	0.64		
754	4.9	0.4	M1 or E3	1584	1.3		
764	30	0.48	E1	1674	0.54		
776	22	1.2	M1	1792	0.05		
(780)	3.6			1959	0.10		

Transition type were determined, normalyzing 396 keV transition for M2, from α_K of each transition.

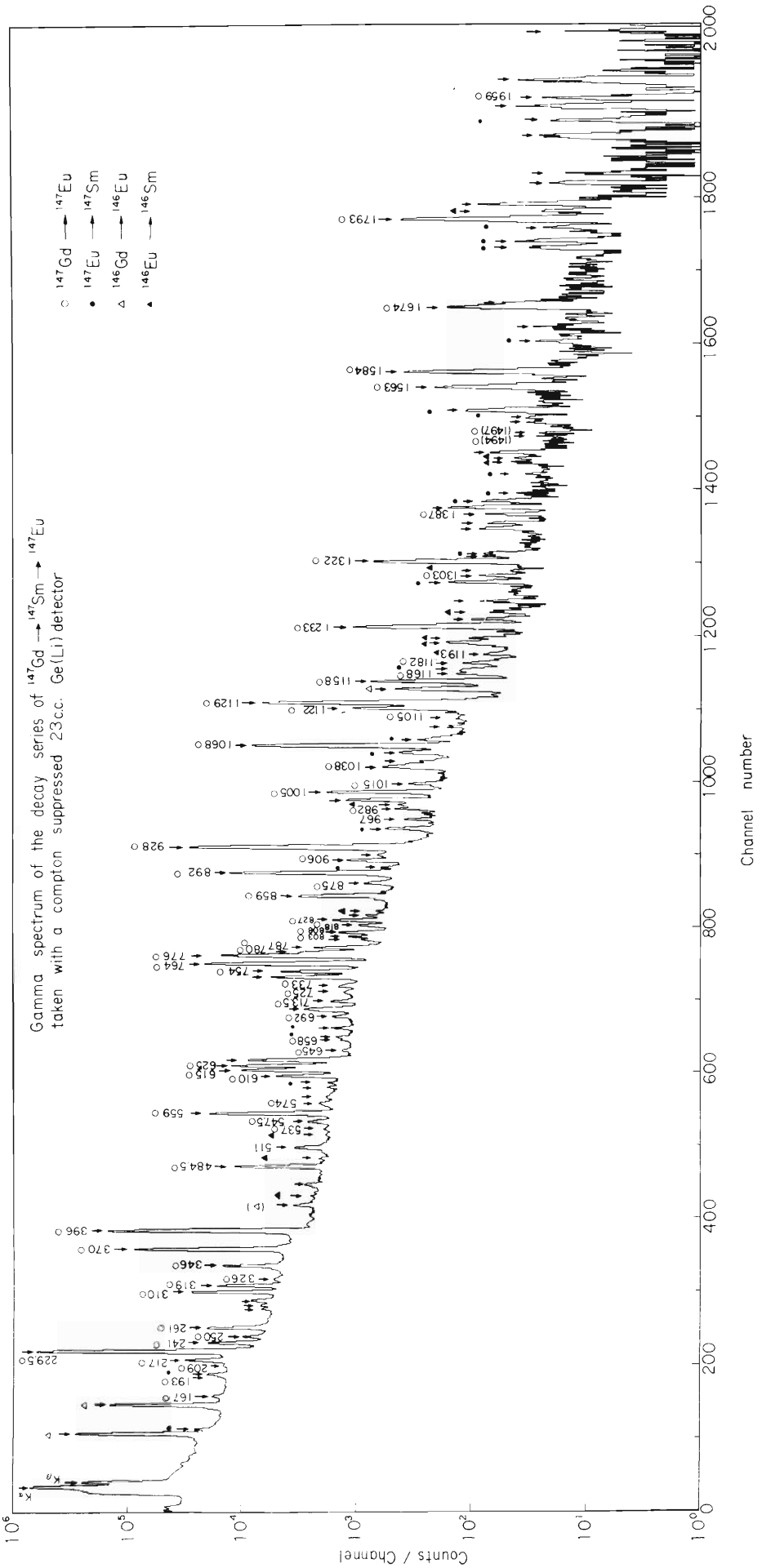

Fig. 1. Gamma spectrum of the decay series of $^{147}Gd \longrightarrow ^{147}Sm \longrightarrow ^{147}Eu$ taken with a Compton-suppressed 23 mℓ Ge (Li) detector.

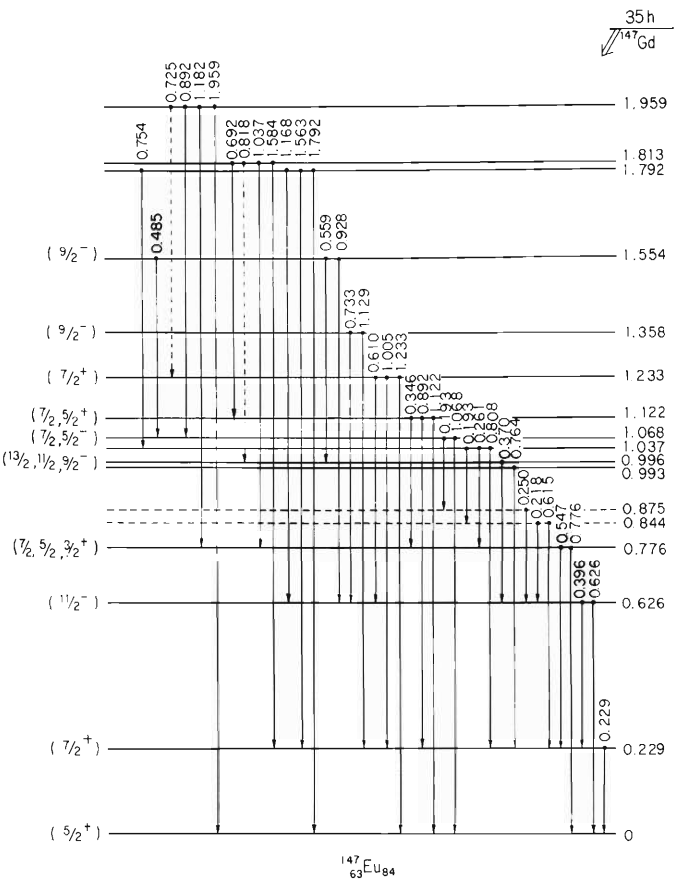

Fig. 2.

References

1) A.S. Danagulyan, N.A. Lebedev, and A.T. Strigachev: Izv. Akad. Nauk SSSR, Ser. Fiz., 27, 1392 (1963).
2) N.M. Anton'eva, A.A. Bashilov, B.S. Dzhelepov, and B.K. Preobrazhenskii: ibid., 22, 906 (1958).
3) E.E. Berlovich, O.V. Larinov, E.N. Tunimanova, and D.M. Khai: ibid., 25, 90 (1961).
4) E.E. Berlovich, V.N. Klement, L.V. Krasnov, and M.D. Nikitin: ibid., p.212.
5) A.A. Sorokin and K.P. Mitrofanov: ibid., p. 799.

5-6. Nuclide Analysis Using Nuclear Reactions

M. Okano, A. Hashizume, Y. Awaya,
Y. Tendow, T. Katou, and T. Hamada

In our study of nuclide analysis, we have established a method of obtaining C : O : N ratio in organic substance by measuring the energy spectrum of prompt gamma rays accompanying the (p, p'(γ)) reaction, in which a detector system consisting of a Ge(Li) detector and a split annular NaI(Tl) scintillator was employed as a pair- or anti-Compton spectrometer.[1)]

The spectrometer was also employed for activation analysis using high energy charged particles. In this case, it is essential to develop suitable techniques of target preparation and cooling for each sample, as well as to know mean energy and intensity of the bombarding particles.

To solve these problem, we have tried bombardments in which powdered samples were moulded into tablets, wrapped by appropriate metallic foils, and "stacked" with

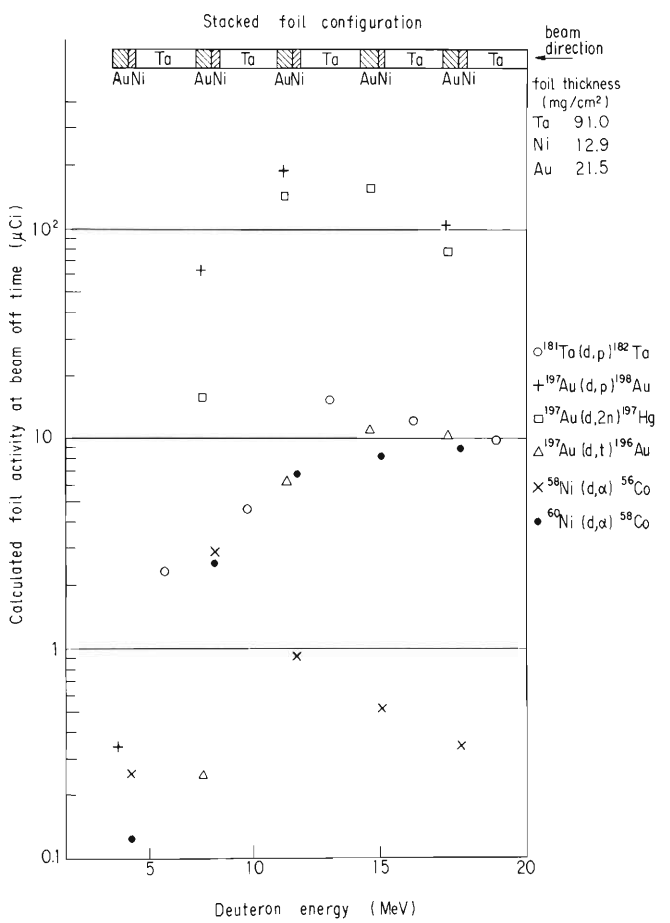

Fig. 1. Excitation functions for the deuteron-induced activities on the foils.

energy-checking foils on the front and back sides of the tablets. The energy-checking foil was a metallic foil or a combination of the foils the induced activity of which was already known as a function of particle energy. We have used so far Ta, Au, and Ni foils for deuteron bombardment and measured their excitation functions by using the above-mentioned spectrometer. The results are shown in Fig. 1. Au and Ni foils were found to be suitable for deuteron bombardment. Appropriate foils for other particles are under investigation.

Reference

1) M. Okano et al.: IPCR Cyclotron Progr. Rep., 2, 110 (1968).

6. NUCLEAR INSTRUMENTATION

6-1. Polarized Ion Source

S. Motonaga, M. Hemmi, H. Ono, Y. Yamazaki,
T. Fujisawa, S. Ikegami, and H. Kamitsubo

The fabrication of the components except the RF transition unit and the ionizer of ion source for polarized protons and deuterons was completed in 1968, and the results of bench test of each component were reported in the 1968 Progress Report.

Temporary assignment of higher priority to the development of the broad range nuclear reaction particle analyzer on the IPCR Cyclotron made it impossible to construct and test the full system of the source.

The RF transition unit and strong field ionizer are being designed in detail, and in order to obtain intense flux of atomic beam the investigation and measurements for atomic beam are now on the way.

(1) RF transition unit and ionizer

The atoms leaving the sextupole separation magnet enter the RF transition unit which is used to obtain high polarization. Because it is intended to apply the method used at Sacley, where the combination of the three transitions is used, the first of the three, that is, weak field transition unit is being designed. The transition probability of about 100 % is obtained and the adiabatic passage method proposed by Abragam and Winter is made use of.

Two level transitions do not require the cavity turned on ultra-high frequency for deuterons, as described by Glavish and Collins, while it is indispensable to use the cavity for protons. Such a thing is being considered.

The ionizer is also being designed to use a strong field, which makes it possible to obtain high polarization.

(2) Investigation of atomic beam

For investigation of lens properties with the sextupole magnet, some beam patterns were observed using the chemical reduction of yellow molybdenum oxide to blue oxide with less oxygen content. Thin layers of molybdenum oxide were produced by burning a molybdenum metal in an oxygen gas flame and depositing the vapor on a glass plate. Fig. 1 shows the beam patterns leaving the sextupole magnet with magnet off (left) and magnet on (right). The defined area of 10 mm in diameter can be seen.

The flux of the atomic hydrogen beam leaving the sextupole magnet was measured by a compression tube that is meant by an ionization gauge with an entrance channel of 10 mm diameter and 65 mm long, and flux measurements were carried out by observing the difference in pressure in the compression tube when the magnet was turned on and off.

A preliminary measurement of the atomic beam flux with different discharge power for dissociation as a function of the discharge tube pressure was carried out.

Fig. 2 shows an example of such a measurement with the uncoated discharge tube with a number of capillaries each of 0.15 mm in diameter and 2 mm in length. The increase in pressure in the compression tube due to incoming atomic beam, that is, the magnetic focusing effect is also shown in Fig. 3. From these observations the maximum intensity was found to be 1.3×10^{15} atoms/sec at present.

In order to produce higher intensity of the beam, some investigations and developments will be tried.

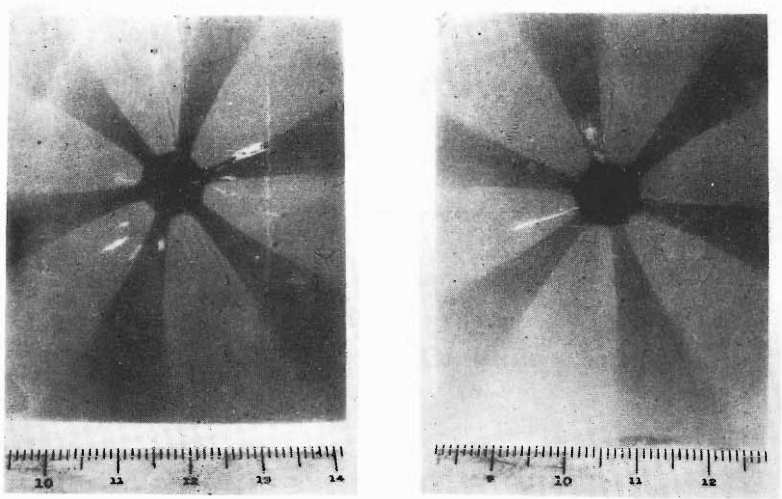

(Magnet off) (Magnet on)

Fig. 1. Beam patterns: magnet off (left), magnet on (right).

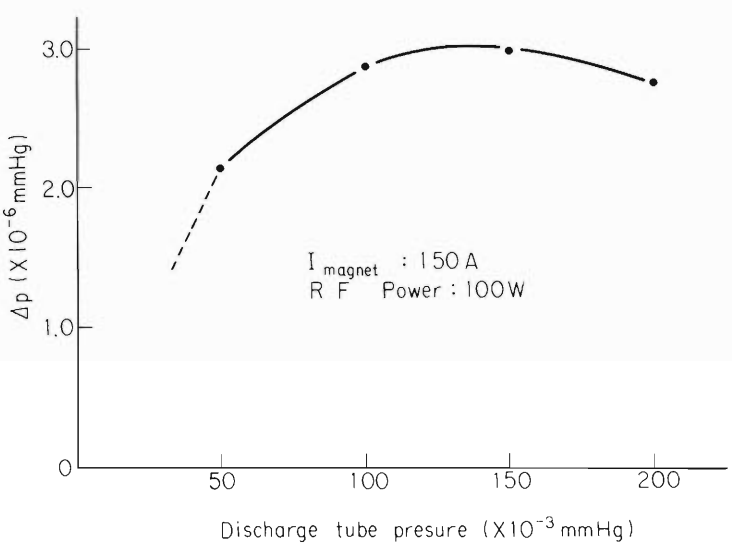

Fig. 2. Intensity of separated atomic beam as a function of pressure in the discharge tube.

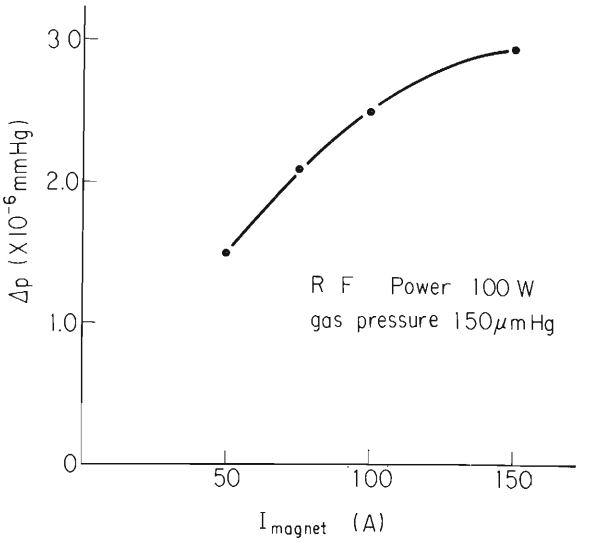

Fig. 3. Focusing effect of sextupole magnet.

6-2. The Ion Optical Properties of Particle Analyzer Determined by Floating Wire Technique

S. Motonaga, N. Nakanishi, K. Matsuda, M. Hemmi,
H. Ono, and Y. Awaya

The ion optical properties of a particle analyzer are determined by the well-known technique using a floating wire to simulate particle trajectories in a magnetic field. The resolution in momentum $\Delta p/p$ can be achieved in the order of 10^{-4} by this technique employed presently.

The particle analyzer system associated with the IPCR 160 cm cyclotron[1] is designed to achieve the following requirements, (i) remarkable dispersion factor, (ii) small vertical magnification, (iii) linearity of focusing line, (iv) resolution in mementum of $\Delta p/p \leq 5 \times 10^{-4}$ and (v) luminosity of 3×10^{-3} ster. Fig. 1 shows the complete set-up of the particle analyzer system schematically. It is composed of two magnets which have a homogeneous magnetic field and curved pole boundaries.

Some techniques would be used in the testing and the alignment of the magnetic analyzer system, one of which is the well-known floating wire technique.

The following optical properties are obtained from the measurement using the floating wire technique, (i) the focusing point and distance to the focus point from an exit boundary, (ii) the angle between outgoing ray and a focusing line, (iii) the dispersion projected on the horizontal focusing line and the momentum resolution.

The experimental arrangement is shown schematically in Fig. 2. The floating wire is anchored at one side of the magnet system, the target position in the scattering chamber, the other end being stretched over a pulley and kept under tension T by a weight G. Total length of the wire is about 8 m. To find image points of the magnetic lenses, the position of the wire is observed at two points with two reading microscopes.

(1) Pulley

As mentioned above, the stability required for the tension T in the wire is of the order of $\Delta T/T \leq 10^{-4}$. The tension on the copper wire was 150 g.

Thus the friction in the pulley must be less than 15 mg. To achieve this requirement a special pulley was constructed. The pulley is made of an aluminum disk of 20cm in diameter and fitted at the center, and a 2 mm diameter axle goes through to other bearings fitted into a supporting frame.

The factors governing the amount of friction are friction of the bearing and smoothness of the V-groove in the pulley. To obtain the friction due to the bearing, the pulley was at first loaded with the same weights on both sides and next the added weight with which the pulley began to rotate was measured. The added weight is of the order of milligrams. The result as shown in Fig. 3 was obtained. This curve indicates the sensitivity of $\Delta T/T \simeq 2 \times 10^{-4}$ for the loaded weight of 150 g.

Many different kinds and sizes of wires were tested, and the most suitable one was found to be a copper wire of 0.1 mm in diameter. In order to reduce the error due to stiffness of wire, the wire was annealed with heavy current.

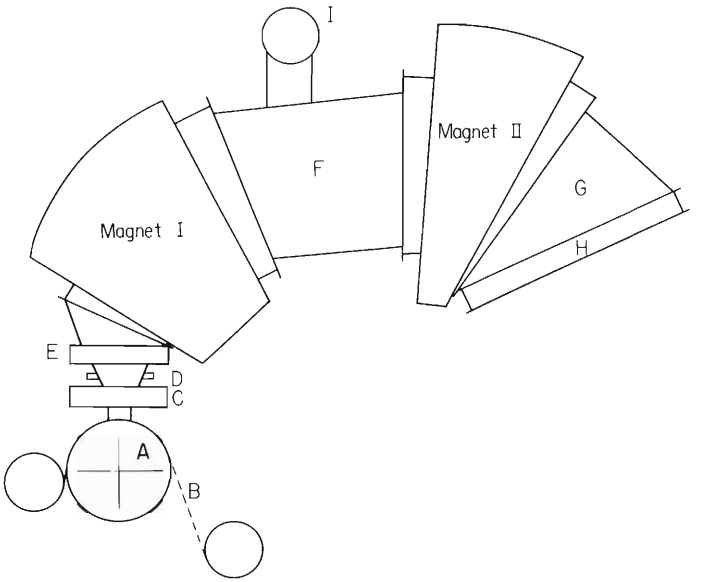

Magnet I Radius of curvature: 110 cm,
Deflection angle: 78.5°

Magnet II Radius of curvature: 110 cm,
Deflection angle: 38.5°

A : Scattering chamber, B : Sliding membrane,
C : Slit box, D : Pneumatic valve
E : Baffle box, F : Connecting vacuum chamber,
G : Detector chamber, H : Detector array,
I : Vacuum pump.

Fig. 1. Complete set up of the reaction particle analyzer.

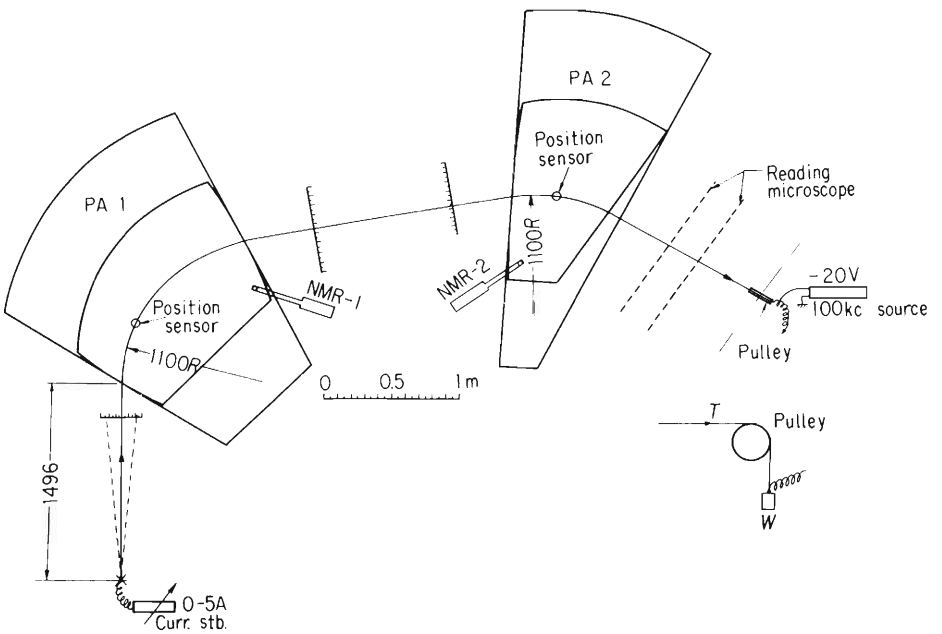

Fig. 2. Schematic view of set up for floating wire experiment.

(2) Determination of wire position

Two kinds of apparatuses are used for observation of the wire position. One is a measuring microscope of 40 magnifications, which is used to determine the position of the wire corresponding to the out-going ray of particles. Accuracy of wire position is in the order of 0.1 %, because the wire size is 0.1 mm in diameter, and uncertain small vibrations are induced on the wire. The other is a "non-conducting position sensor" which is operated by electrically sensing capacitance changes between the floating wire and a pair of metallic plates, and the sensor is used to determine the radius of curvature in the magnetic field. A block diagram of the sensor system is shown in Fig. 4 and the sensitivity for the position of the wire is also shown in Fig. 4. With this apparatus, the wire position can be determined with an accuracy of 0.05 mm.

(3) Experiment and result

The experimental set-up is shown in Fig. 2. The current i applied to the wire is regulated to $\Delta i/i \leq 2 \times 10^{-5}$ and magnetic field is stabilized to $\Delta B/B \leq 10^{-4}$. As this particle analyzer system is composed of two magnets, it is necessary to adjust the magnetic strengths to a difference less than 10^{-4} in this experiment.

The focusing line and the dispersion were determined by varying the floating wire current and moving the pulley position. The typical results are given in Fig. 5.
A focusing line could be fitted with maximum error of 4 cm in the image distance. The following parameters for the analyzer system were given.

(a) The focusing distance along the central ray is 132 cm $\pm$ 2 cm.
(b) The angle between outgoing ray and focusing line is 35°.
(c) The dispersion projected on the horizontal focusing line is 3 mm/5 $\times 10^{-4}$ relative momentum changes.
(d) The momentum resolution of $\Delta p/p$ is 5×10^{-4}.

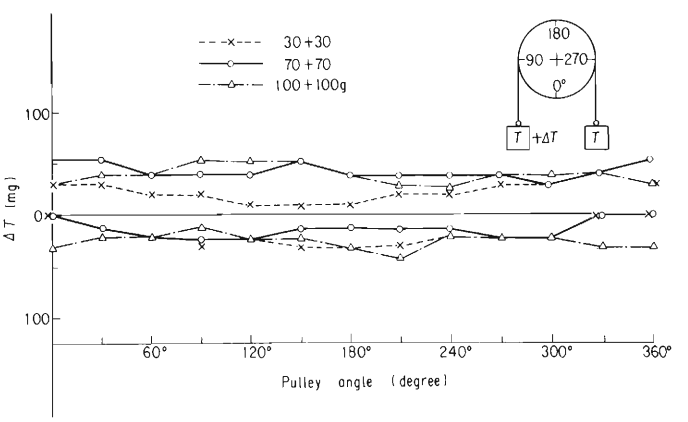

Fig. 3. Set up for test of friction measurement. The wire was stretched over the pulley and the weight for starting the rotation of the pulley ΔT was measured.

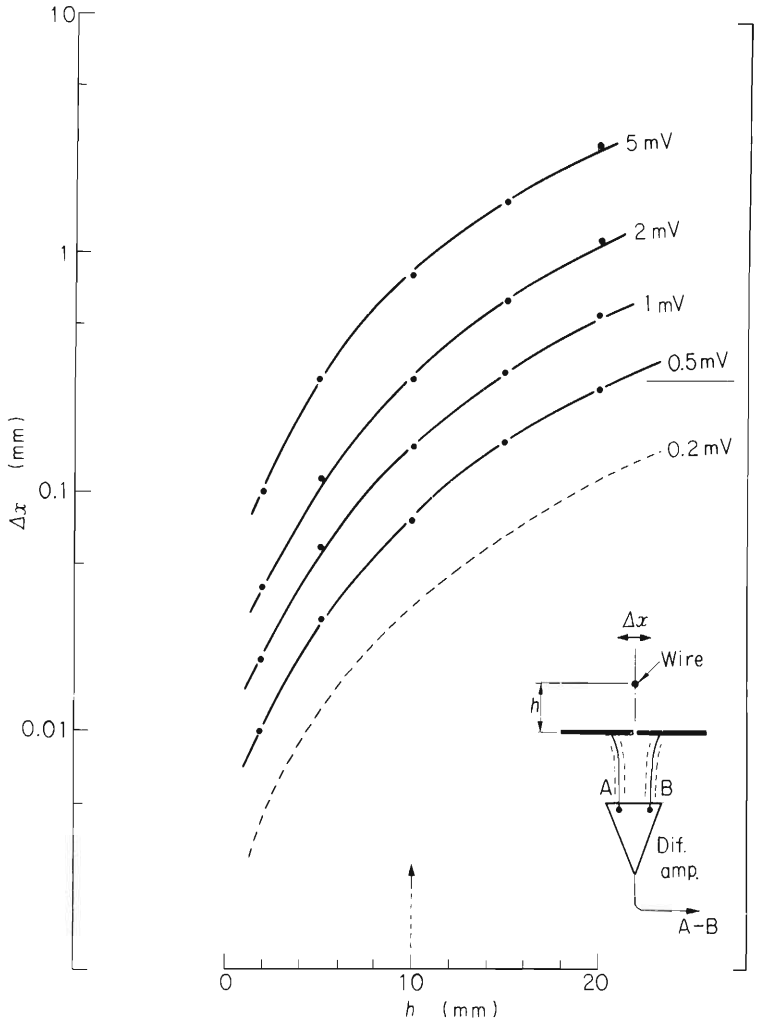

Fig. 4. Block diagram of wire position sensor and the sensitivity for the wire position.

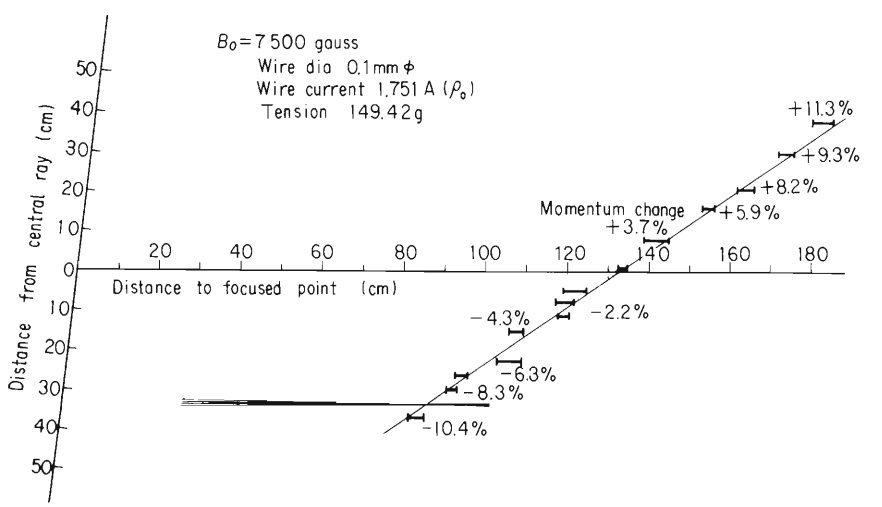

Fig. 5. Image plane and dispersion determined at $B_0 = 7500$ gauss.

Reference

1) N. Nakanishi and K. Matsuda: Nucl Instr. and Methods, 57, 245 (1967).

6-3. RI Irradiation System

A. Hashizume, T. Katou, and A. Shimamura

In order to produce radioisotopes having high specific activities, the targets are placed in the vacuum chamber of the cyclotron, and are bombarded by deflected beam.[1] The beam position and its profile depend on the operating conditions of the cyclotron. Despite the beam position is verified by exposing a photosensitive paper to the beam before every activation, its intensity distribution in vertical and holizontal directions is not well-defined by this method. It is sometimes important for obtaining high activities with limited quantity of enriched isotopes to know this distribution; the radioactive sources for a high resolution electron spectrometer could be prepared from the enriched isotopes after chemical separation.

Tantalum foils of 0.01 mm in thickness were bombarded with 11 MeV protons, 32 to 50 MeV alpha particles and 27 MeV ^{3}He. When tantalum was bombarded with alpha particles of 32 MeV, for example, the main part of the induced reaction would be $^{181}Ta(\alpha, 3n)^{182}Re$. Tantalum foils were chosen for their rigidness and for the long half-lives of radioactivities produced, which reduce the decay correction to a minimum. The activated foils were cut in mesh and their relative intensities of gamma activities were measured with a well-type scintillation counter to avoid the change of geometrical efficiencies.

Fig. 1 shows an example of a relative intensity distribution of ^{3}He-particles at the target position of the RI production system. The activation was carried out for 13 min with mean intensity of about 6.5μA. From the figure, if we assume the target area to be 10 mm $\times$ 50 mm, 99% of incident beam will enter into the target. If we assume it to be 4 mm $\times$ 40 mm, 70% of incident beam will be expected.

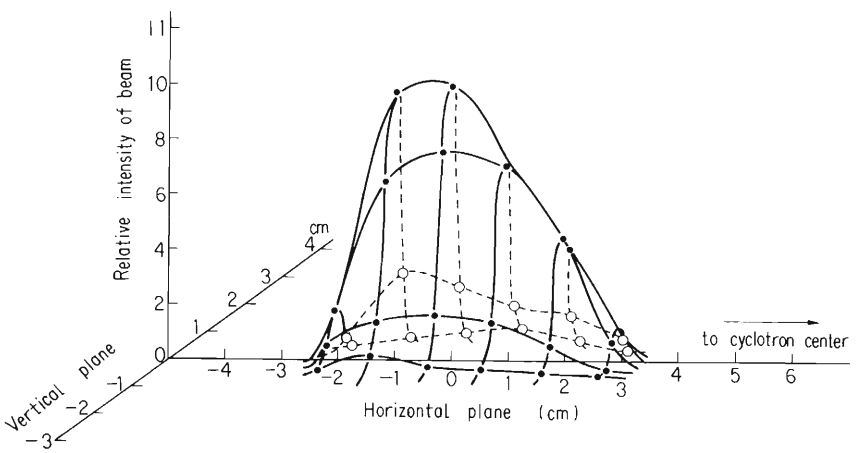

^{3}He : 26 MeV, f : 8.976 Mc/sec, V_{Dee} : 65 kV
Deflector: parallel 752, inclination 25 (to inward).

Fig. 1. The distribution of a beam intensity at RI target.

Another important point is the stability of a beam. In monitoring the target by a television camera, it was found that the beam position moves several millimeter toward outer or inner direction which depends on the operating conditions of the cyclotron like RF voltages or frequencies etc.

The radioactive source produced can be removed together with its base from the target stem and can be placed in a polyethylene reticule by means of remote control. After being placed in a container made of lead, the source passing through the tunnel, made of concrete wall, is carried in the hot-cell situated at the next room of the cyclotron. The total dose for handling the radioactivity is about 10 mrad.

Reference

1) A. Hashizume and A. Shimamura: IPCR Cyclotron Progr. Rep., 1, 73 (1967).

6-4. Installation of a Rotating Target Holder

A. Shimamura and T. Nozaki

A rotating target holder has been installed. It is useful for the simultaneous bombardment of a number of samples under equal conditions and for the RI production from target substances of low heat resistivity. Also, this equipment has been found to have a promising feature for use in the fast-neutron therapy as the target for neutron generation by the Li + d reaction. With the present equipment, the bombarded target, which usually contains high level activities, is put in a lead container for transportation by completely automatized operations.

A photo of the rotating target holder is shown in Fig. 1. Fig. 2 shows the layout of its main parts. For the bombardment, the equipment is connected to the beam outlet of Course II[1] next to the slit box. In order to effect the equal bombardment, each of the samples is attached on a side surface of a hexagonal pillar (1 in Fig. 2), which is caused to rotate at 10 r.p.m. The body of the pillar is made of duralumin, whereas aluminium plates, in which no high-level activities of long lives are induced by the bombardments, are used as the target-loading material. The aluminium plate is of $100 \times 30 \times 4$ mm dimension and is slid into a ditch dug in the pillar, as shown in Fig. 3. In order to minimize the bombardment of the other parts than the target substance, a kick rotation system using an eccentric cam has been adopted; the resting period is twice as long as the moving time. The cooling during the bombardment is effected by pure water streaming through the inside of the pillar and its shaft at a rate of about 10 ℓ/min. The pillar is electrically insulated, and thus the beam flux can be measured by a current integrator. An O-ring vacuum tight system is used to effect the bombardment in a vacuum chamber (5 in Fig. 2). The chamber has two transparent windows for the monitor of the rotation and the observation of the targets during the bombardment.

When the bombardment is finished, a three-way electromagnetic valve is operated to stop the cooling water and to drive away its remainder by compressed air (5 kg/cm^2). Then another valve is opened to introduce air into the bombardment chamber; its down-side iron door (8 in Fig. 2) opens spontaneously. The hexagonal pillar is then driven downward into the adapted-sized hole in the lead container (7 in Fig. 2), which has been set at the due position. The pillar is then screwed off from its shaft. Use is made of limit switches, pilot lumps and zoom television camera.

By the use of this rotating target holder, lithium metal targets were found to withstand to a bombardment with 10 MeV - 15 μA protons. The present equipment, however, has the following defects: (1) a major part of its total mass is in its upper half, and therefore it is apt to tumble when slightly inclined, (2) the electrical insulation system for the beam measurement is not satisfactory, (3) the vacuum tightness is not always complete, and thus a foil is necessary for separating the bombardment chamber from the cyclotron beam duct, and (4) the inside surface of the lead container is inclined to the contamination by activities in the target substance.

We intend to improve the equipment in order to make the followings possible: (1) the ordinary rotation of the hexagonal pillar with selected velocities in addition to the kick rotation, (2) the bombardment of given surfaces of the pillar for selected durations of time, (3) the use of a cylinder in addition to hexagonal pillar, (4) the reducing of the mass of the equipment, (5) the glancing bombardment by the insertion of an oblique duct between the equipment and the cyclotron beam duct, and (6) the detachment of the pillar

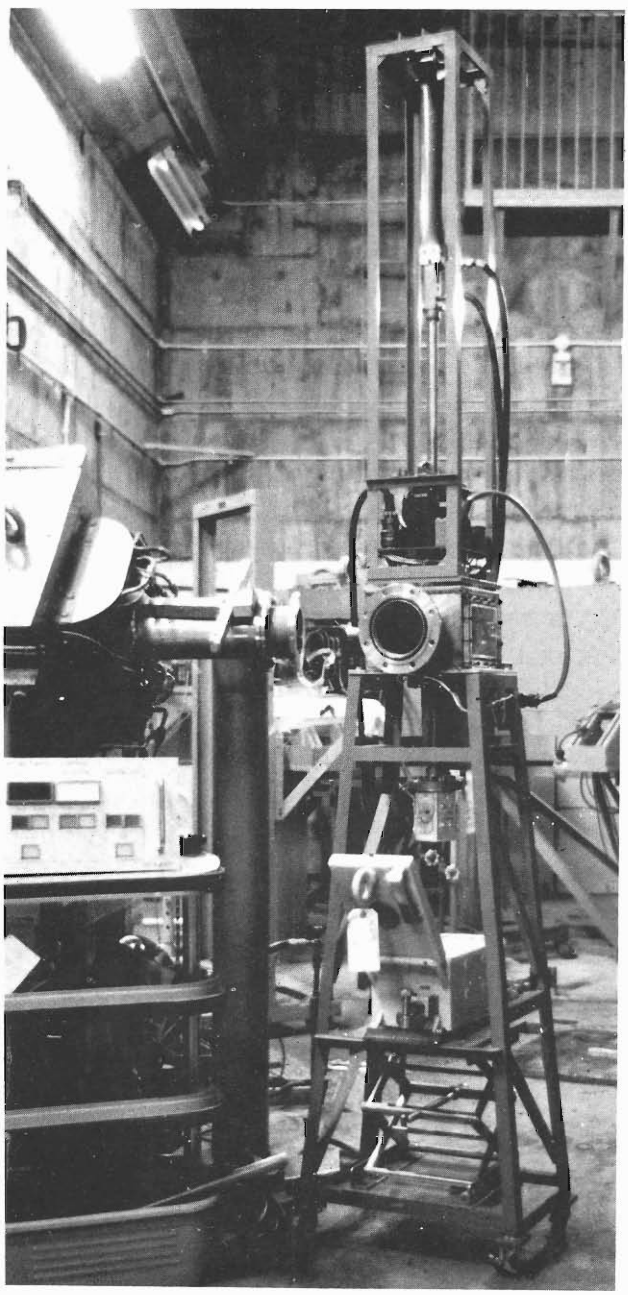

Fig. 1.

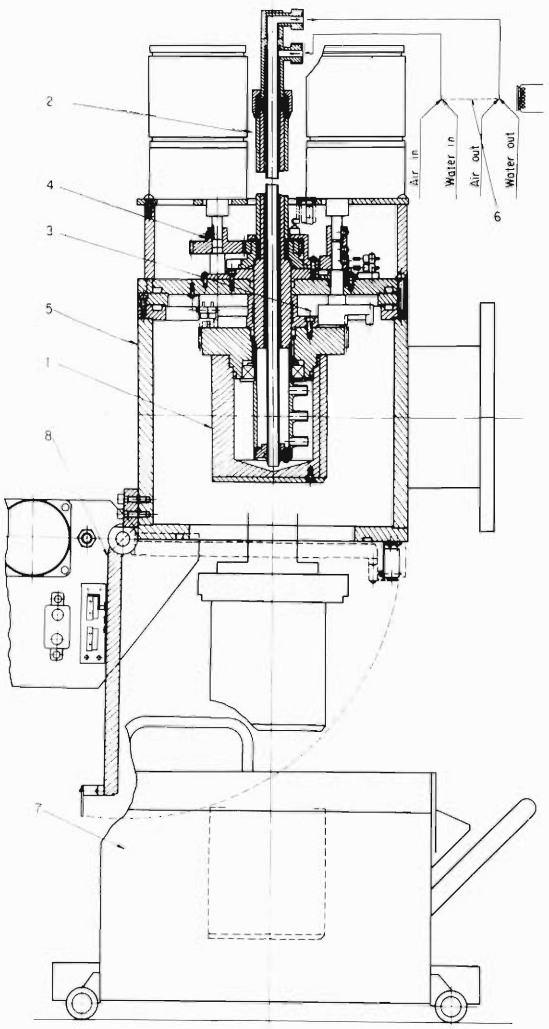

1: Hexagonal pillar,
2: Screwed shaft,
3: Can for the kick rotation,
4: Gear for the vertical operation of the shaft,
5: Bombardment box,
6: Electromagnetic three-way valve,
7: Lead container,
8: Downside door (of the bombardment box).

Fig. 2

or cylinder from its shaft at the bombardment position to be received in an enveloping sheet and put into the lead container.

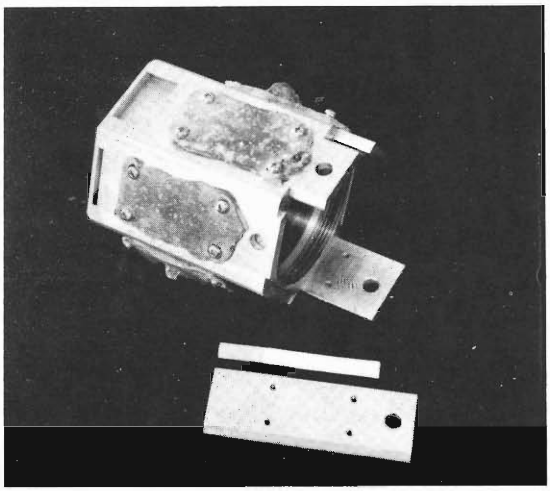

Fig. 3.

Reference

1) S. Motonaga et al.: IPCR Cyclotron Progr. Rep., 1, 12 (1967).

6-5. Nuclear Instrumentation under Construction

Several projects for constructing new instruments are now under way. These are a nuclear reaction particle analyzer, an on-line electron spectrometer and a pulsed beam bunch selector. The former two have already been in installation, however, not yet been completed. The detailed reports for these three will be published in the next Progress Report. Here short descriptions will be given on the present stage of each.

(1) Reaction particle analyzer (see **3-3** Fig. 1)

The principle of optical design for this system has been published.[1] The test of floating wire method was reported in this Progress Report. The performance test with actual reaction particles (elastic scattering from gold) was tried and an imperfection of the optical properties was found. The focusing plane of image points is not linear and then the energy resolution is about 0.1 % in a certain region and about 0.2 % in the other region if nuclear emulsion plates were set on a straight line. The reason for this is that the use of carbon steel vacuum chambers in the region of free space is still doubtful and the replacement with stainless steel chambers is now under consideration. Another defect was found in the mechanism of the sliding membrane of the scattering chamber. The design to synchronize the movement of the membrane with that of the analyzer system was difficult because of the time-lag in the pulling system for the membrane. Now a new device for driving with two motors and for making automatic regulation of both movements is installed.

(2) On-linc electron spectrometer (see **3-3** Fig. 1)

A sector type double-focusing β-ray spectrometer was installed on the beam line in the large irradiation room. It is of Siegbahn type with $\alpha = 1/2$, $\beta = 3/8$, and $\rho_0 = 34.0$ cm, and made by the Hitachi Co., Ltd. The test with ^{137}Cs K, L, M lines show the resolution of 0.16 % (momentum) for the transmission of 4×10^{-3}. The spectrometer plane was set perpendicularly to the beam line as shown in Fig. 1. The test with the cyclotron beam will be commenced at the beginning of 1970.

(3) Pulsed beam bunch selectro (see **3-3** Fig. 1)

The micro-bunching of cyclotron beam is very useful for neclear experiments of short time duration from nano seconds to micro seconds. In the IPCR Cyclotron the magnetic moment of short isometric states has been measured by utilizing this bunching. For wider applications, such as isomeric transitions and time-of-flight measurements, the selection of bunches is very important. A pulsed electric deflection system is now under construction. This will be installed between the exit of the cyclotron chamber and the switching magnet, so that the selected bunches will be introduced at any parts of the branched courses in the irradiation room.

The deflector is 90 cm long and designed to have a peak voltage of 10 keV. The pulse duration is about 140 nsec with a considerable flatt top. The system can suppress the successive beam bunches from one bunch to ten bunches. The design and test of the electronic part is in progress.

(4) Data processor

A short comment will be given here on the present status of the data processing system. The main part is the Honeywell DDP-124 8 K computer as reported in a previous Progress Report. The system is used as a live time data processor to drive the line printer, the degital potter and the magtape unit. In this case the input data are recorded on paper tapes from PHA systems. The processor is also used as a spectrum analyzer for charged particles and gamma rays. Sometimes it is useful as a off-line computer for small-scale scientific calculations. Now, the problem of particle identification in the heavy ion reaction is very important in this laboratory and a supper multichannel analyzer is desired. An event recording system using magnetic tapes is under progress.

(the editor)

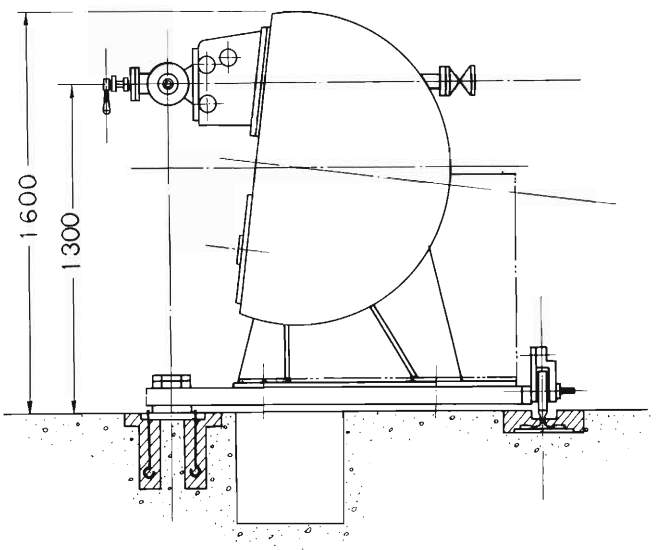

Fig. 1. Vertical view of the on-line electron spectrometer.

Reference

1) N. Nakanishi and K. Matsuda: Nucl. Instr. Methods, 57, 245 (1967).

7. RADIOCHEMISTRY

7-1. Charged Particle Activation Analysis for Carbon, Nitrogen, and Oxygen in Semiconductor Silicon

T. Nozaki, Y. Yatsurugi, and N. Akiyama

This work has been continued for about 3 years and most of our original aims have been achieved. The analytical processes and some results have already been reported, along with discussions concerning the interference reactions.[1~4] In this report, the following four further results are reported and discussed: (1) phase diagram of C-Si system in the extremely low carbon concentration range, (2) calibration curves for infra-red absorptiometry for carbon and oxygen in silicon, as standardized by activation analysis, (3) concentration ranges of carbon and oxygen in various commercial semiconductor silicons, and (4) equilibrium distribution coefficient of nitrogen between solid and liquid silicon. Also, we show a new technique devised in order to study the escape of carbon from the silicon matrix when it is fused.

(a) The analytical results described in the preceding report [2] offer enough information for us to draw the phase diagram shown in Fig. 1. The lowering of the melting point (ordinate of Fig. 1) was calculated by the well-known formula. The same technique as that described in Ref. 2) (i.e., combination of activation analysis with zone-melting or normal freezing) can surely be applied to the measurement of equilibrium conditions for minute impurities in high-purity matrices in general.

(b) Fig. 2 shows the infra-red absorbances vs. the carbon and oxygen contents of silicon as determined by the activation analysis. The IR method has been used for their determination, though there were some uncertainties in the absorption coefficients. Fortunately, fair agreements have been found between the absorption coefficients determined by the activation analysis and those measured by the ^{14}C-incorporation technique or by vacuum fusion. [5, 6] The IR method thus proved to give good results for carbon and oxygen concentrations over 400 p.p.b. in single-crystalline silicon. For lower concentrations, however, this method is less accurate and less reliable than the activation analysis, though its sensitivity reaches down to about 100 p.p.b. for both impurities.

(c) Table 1 shows carbon and oxygen concentrations in various commercial semiconductor silicons. The samples prepared by modern industrial techniques were found never to have a carbon concentration over the solubility in solid silicon at its melting point. The relatively high carbon and oxygen contents of the CZ samples can be explained as contaminations from the silica crucible and the graphite heating device used in the process.

(d) Determination of the equilibrium distribution coefficient of nitrogen involved some experimental difficulties because of its volatility. By modifying the technique

used for measuring the distribution coefficient of carbon, however, we determined it.[2] Molten zones were passed, at various velocities, though a silicon rod covered with a sufficient quantity of silicon nitride powder, and the resultant nitrogen distributions were measured for the zone-melted parts and the zone-end parts to give the effective distribution coefficients, from which the equilibrium distribution coefficient was then obtained by extrapolation to zero velocity. The coefficient was thus found to be about 5×10^{-4}.

Table 1. Carbon and oxygen concentrations in commercial semiconductor silicons.

	Carbon (10^{17} atoms/cm^3)	Oxygen (10^{17} atoms/cm^3)
Polycrystal	0.20 ~ 0.50	0.8 ~ 3.0
	(0.82)	(0.04)
Single crystal		
FZ in argon	0.15 ~ 0.35	0.05 ~ 0.20
FZ in vacuum	0.03 ~ 0.40	0.010 ~ 0.03
CZ	0.30 ~ 3.0	2 ~ 10
Dislocation free	0.40, 0.13	0.013, 0.019
(FZ)	0.016, 0.30	0.026, 0.10

Figures in the parentheses are exceptional values.

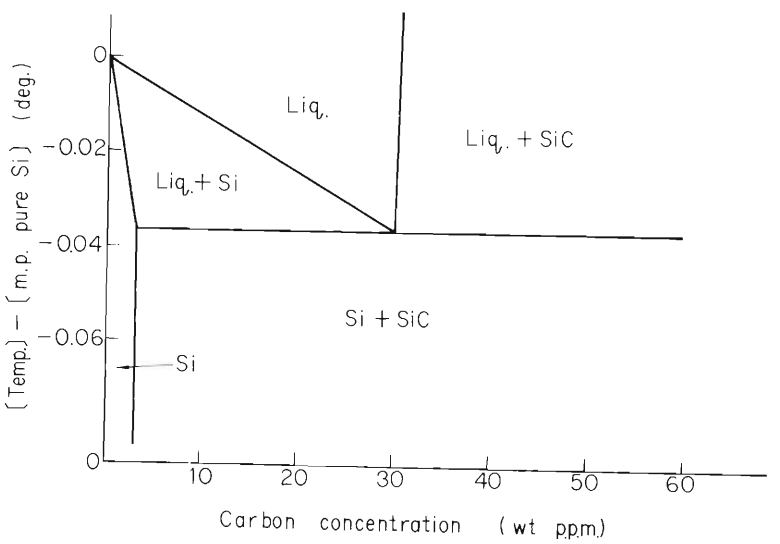

Fig. 1. Phase diagram of C-Si system at extremely low carbon concentration.

The analytical results so far obtained for carbon and oxygen suggest an escape of the carbon as carbon oxides from the silicon when it is fused. In order to get a proof of the escape and in order to get some semiquantitative information about it, we devised the following new technique : (1) bombard a silicon sample of known carbon and oxygen contents with ^{3}He-particles of high energy in order to produce ^{11}C in the sample by the fission of the silicon itself, [2~4] (2) fuse the sample by high-frequency heating in vacuum, and measure the ^{11}C activity thus evolved as ^{11}CO and $^{11}CO_2$ using radiogas chromatography, and (3) then measure the ^{11}C remaining in the silicon. The results demonstrate the escape of ^{11}CO, though this study is still in its beginning stage.

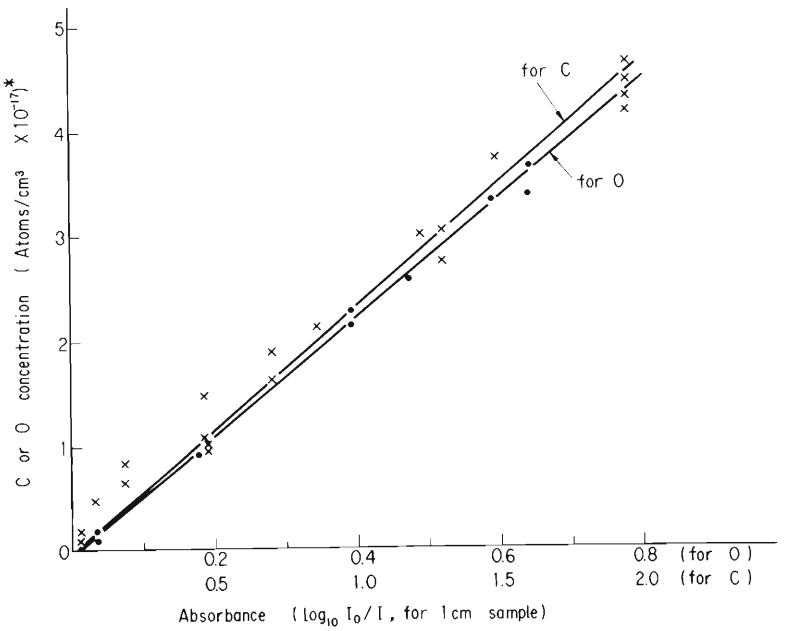

Room temperature, Double beam method,
Wave number : 608 cm^{-1} for C, 1110 cm^{-1} for O.

* 1×10^{17} atoms/cm^3: 0.855 wt. p.p.m. for C, 1.14 wt. p.p.m.for O.

Fig. 2. Infrared absorbances vs C and O concentrations.

References

1) T. Nozaki: ICPR Cyclotron Progr. Rep., 1, 66 (1967).
2) T. Nozaki, Y. Yatsurugi, and N. Akiyama: ibid., 2, 121 (1968).
3) T. Nozaki, Y. Yatsurugi,and N. Akiyama: "Modern Trends in Activation Analysis", Natl. Bur. Stand, USA, 2, 842 (1969).
4) T. Nozaki, Y. Yatsurugi, and N. Akiyama: J. Radioanalyt. Chem. (in press).
5) R. C. Newman and J. B. Willis: J. Phys. Chem. Solids, 26, 373 (1965).
6) W. Kaiser and P. H. Keck: J. Appl. Phys., 28, 882 (1957).

7-2. Charge Spectrometry of Recoil Atoms

M. Aratani and N. Saito

The relative abundances of differently-charged ^{206}Pb ions emitted from the surface of a silver plate with deposited ^{210}Po ($\sim 10\,\mu$Ci) were measured with the IPCR charge spectrometer.

The silver plate which constituted the ion source is shown in Fig. 1. The alpha ray spectrum of ^{210}Po in the silver plate reveals that the polonium atoms are distributed not on the surface but in the interior of the plate, and that the polonium atoms are most densely populated in the layer a little deeper below the surface than the recoil range of ^{206}Pb atoms in the silver plate. In other words, only a fraction of the recoiled ^{206}Pb atoms may travel to the surface of the plate. The charged ^{206}Pb atoms emitted from the surface were propelled in the presence of an electrostatic potential of 5000 V at maximum towards a slit which leads to an analyzer of the spectrometer. The pressure of the ion source chamber was kept at about $10^{-6} \sim 10^{-7}$ Torr. After passing through the analyzer, the ions were counted with a 16-stage Cu-Be electron multiplier.

One of the charge spectra of the recoil ^{206}Pb ions obtained in this experiment is shown in Fig. 2. The figure shows that singly-charged ions are most abundant. It also indicates that the abundances of multiply-charged ions tend to decrease as the ionic charge increases. However, an irregularity is seen with +5-charged ions. The shape of the spectrum is similar to that obtained by Gunter, Asaro, and Helmholz [1] for recoils from ^{226}Th alpha decay.

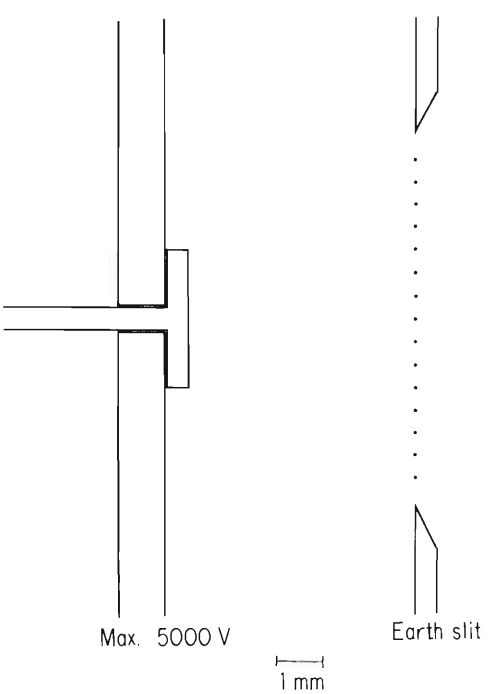

Electrodes : SUS-32 stainless steel
α-supporter : Ag

Fig. 1. α-emitter ion source.

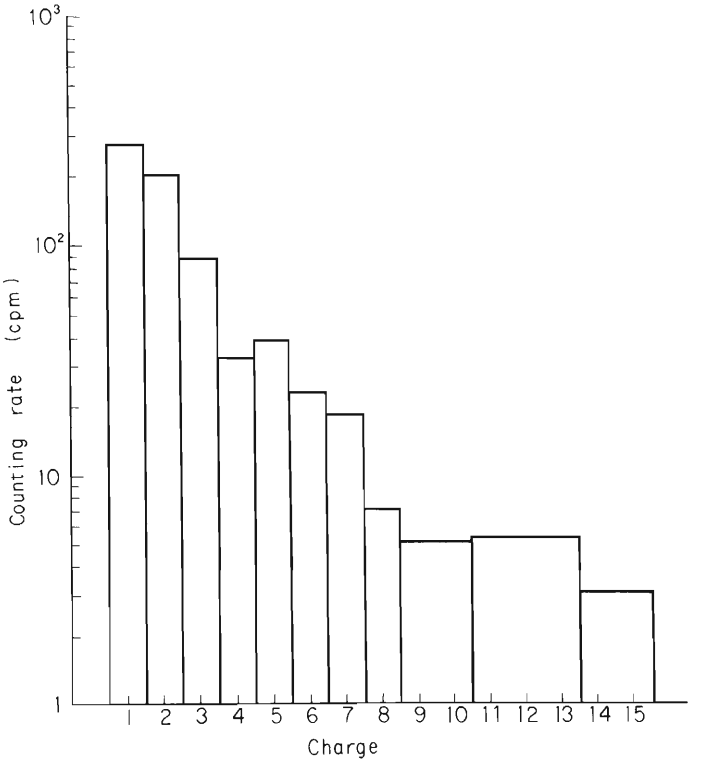

Acceleration voltage : 4000 V
Slit width : 8 mm × 8 mm
Vacuum : 2×10^{-7} Torr

Fig. 2. Charge spectrum of ion species from ^{210}Po-Ag ion source

---

Reference

1) K. Gunter, F. Asaro, and A. C. Helmholz: Phys. Rev. Letters, 16, 362 (1966).

7-3. Carbon-14 Labeling Reaction by Bombardment with Alpha Particles from Cyclotron

Y. G. Tanaka and T. Karasawa

The recoil labeling reactions on organic compounds by atomic pile have certainly a great advantage of labeling with short life nuclide, because large amont of nuclide is produced in a short time irradiation. On the contrary, it is less useful for labeling with carbon-14, a typical long life nuclide with a half life of 5730 years, for two reasons of necessity of long time irradiation for production of carbon-14 and large amount of radiation damage occurred during bombardment onto an organic target. Though carbon-14 labeled compounds are the most important tracers in biochemical research, the authors intended to study a new direct labeling reaction of organic compound with carbon-14.

Present investigation of a new labeling reaction with carbon 14 is carried out by bombardment with accelerated alpha particles onto a mixture of carbon-14 and an organic compound. A pyrex irradiation cell attached with 50 μm thickness alminum foil on both sides was filled with a methanol solution of urea-^{14}C. An irradiation was carried out with a beam of alpha particles after passing a thin aluminum window and an air layer. The reaction mixture was chilled with a cooling liquid to keep the temperature between 35^{o}C and 42^{o}C during the irradiation, and the beam intensity was 2.1$\sim$2.7 μA. The input charge into the solution was monitored by reading the integrated current from the copper plate in contact with the back side aluminum foil to the ground.

In the previous results with accelerated protons, we found that the specific activity and the total activity of produced methanol-^{14}C were proportional to charge input, when the energy of proton was constant, and to the concentration of carbon-14 in the sample before irradiation. In the present investigation, the sample was irradiated with alpha particle with stepwisely changed energies: 11.8, 16.7, 21.1, 24.6, 29.0, 34.6 MeV; total charge input was 12 millicoulombs each.

After irradiation, excess urea-^{14}C and gaseous by-products were separated from liquid substances by a vacuum frozen distillation. By-products, formaldehyde, was removed from methanol with sodium borohydride, glycol, by accurate distillation, carbon dioxide, with caustic soda. The purified methanol-^{14}C was identified by a Carry-Loenco radio gas chromatography with a carbowax 20M column. The activities of methanol-^{14}C were measured every 10 minutes by a Beckman LS 150 liquid scintillation counter, with scintillator Dolite PPO, POPOP toluene.

The results are given in Fig. 1.

In the energy range of the present investigation:

(a) Methanol was also labeled with carbon-14 when a mixture of urea-^{14}C and methanol was bombarded with accelerated alpha particles.

(b) The specific activity and the total activity of methanol-^{14}C increased proportionally with concentration of carbon-14 in methanol before irradiation.

(c) When the total charge input was constant, the specific activity and the total activity of methanol-^{14}C increased proportionally with increasing energy of alpha particles.

(d) Values of specific activities of methanol-^{14}C almost fitted on the extended lines of the values obtained by proton. This tendency was notable at total carbon-14 in methanol-^{14}C.

(e) The same samples were irradiated by gamma rays from cobalt-60, but a very small amount of methanol-^{14}C was obtained.

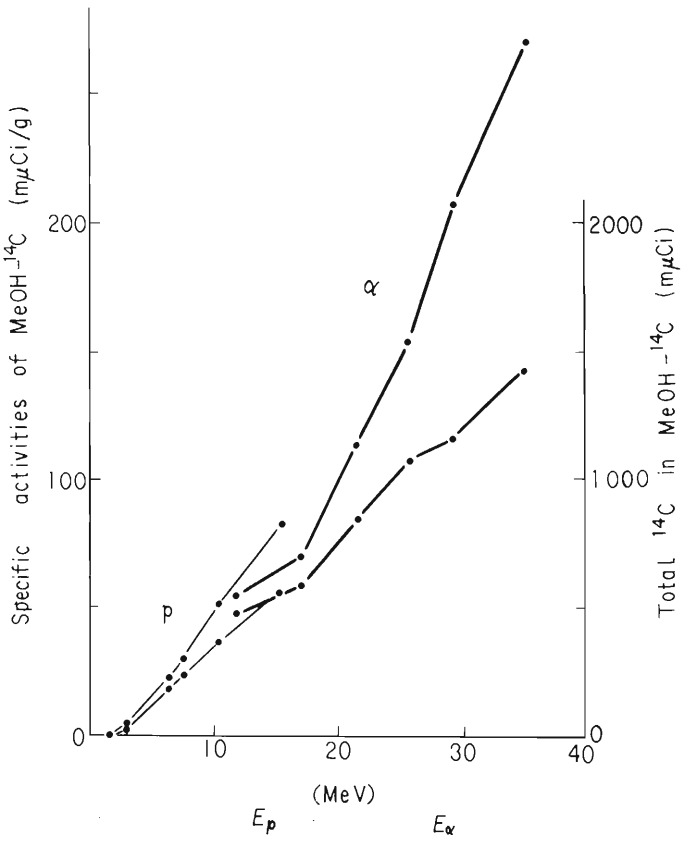

Fig. 1. Specific activities of methanol-^{14}C (left side lines) and total carbon-14 in methanol-^{14}C (right side lines) vs. energy of proton (E_p) and that of alpha particle (E_α) in MeV. Hair stroke lines mean results obtained by proton, and thick lines mean results obtained by alpha particles.

8. RADIATION CHEMISTRY

8-1. LET and Dose-Rate Effects in the Radiolysis of Aqueous Ferrous Sulfate Solutions
Interpretation of the Data

M. Matsui, H. Seki, T. Karasawa, and M. Imamura

(1) Experimental results

In this period we have investigated the dose-rate effect on the oxidation yield, $G(Fe^{3+})$, of Fricke solutions in more detail. Fig. 1 illustrates the variation of $G(Fe^{3+})$ with beam current of 13 MeV helium ions for 1 and 10 mM aerated Fricke solutions. It is seen that the yield is constant at lower beam current and decreases with increasing current. With increasing energy of particles the critical beam current becomes higher. At extremely high beam current, the yield seems to level off as seen from Fig. 1.

Fig. 1 also implies that the yield for 10 mM solution is always higher than that for 1 mM solution. Solutions saturated with oxygen gave practically the same yields as those for aerated ones.

The yields for nitrogen-saturated solutions irradiated with protons and helium ions are shown in Table 1. Calculated values in the last two columns will be explained later.

Table 1. $G(Fe^{3+})$ in nitrogen-saturated solution.

Particle	Energy (MeV)	Mean current (nA)	$G(Fe^{3+})$			
			1 mM	10 mM	calcd. by eq. III	calcd. by eq. IV
Proton	13.2	2	4.7	6.4	6.7	4.0
Helium ion	25.3	1	3.3	4.4	4.8	3.4
		0.2	3.9	4.5		
Helium ion	13.0	0.6	2.5	2.9	4.3	3.3

Stirring speed: 30 r.p.s.

(2) Interpretation

The reaction mechanism in aerated ferrous sulfate solution is believed to be well understood. The subsequent reactions are : [1]

$$Fe^{2+} + OH \longrightarrow Fe^{3+} + OH^- \quad (1)$$

$$H + O_2 \longrightarrow HO_2 \quad (2)$$

$$Fe^{2+} + HO_2 + H^+ \longrightarrow Fe^{3+} + H_2O_2 \quad (3)$$

$$Fe^{2+} + H_2O_2 \longrightarrow Fe^{3+} + OH + OH^- \quad (4)$$

The overall yield is then given by

$$G(Fe^{3+}) = G_{OH} + 3G_H + 2G_{H_2O_2}. \quad (I)$$

Helium ions of 13 MeV have an initial LET of 4.65 eV/Å for water. Using the initial yields of $G_H = 1.0$, $G_{OH} = 0.7$, and $G_{H_2O_2} = 1.2$ expected for this LET-value,[2] one can calculate $G(Fe^{3+}) = 6.2$, which is close to the experimental values obtained at the lowest beam current (Fig. 1).

At higher beam currents, several fast interspur reactions will predominate because of the increase in local concentrations of H and OH radicals. These reactions will compete with Reactions (1) and (2).

$$H + H \longrightarrow H_2 \quad (5)$$

$$OH + OH \longrightarrow H_2O_2 \quad (6)$$

$$H + OH \longrightarrow H_2O. \quad (7)$$

Reactions (5) ~ (7) have the rate constants in the order of $10^9 \sim 10^{10}$ $M^{-1}sec^{-1}$.[3,4] The rate constant of Reaction (2) being high ($\sim 10^{10}$ $M^{-1}sec^{-1}$),[3] the depletion of oxygen will soon take place in the reaction zone under a high beam current and reactions including HO_2 radicals would be neglected.

At extremely high beam current, therefore, only Reaction (4) proceeds in the bulk of the solution. Considering these competition reactions, we have finally obtained Eqn. (II) for the yield at extremely high beam current.

$$G(Fe^{3+}) = \frac{3}{2} G_{H_2O_2} + \frac{1}{2} G_{OH}. \quad (II)$$

The experimental results were found to be in fair agreement with the values calculated by Eqn. (II).

In the absence of oxygen, ferrous ions are oxidized by Reactions (1), (4), and (8),

$$Fe^{2+} + H + H^+ \longrightarrow Fe^{3+} + H_2 \quad (8)$$

with the yield given by

$$G(Fe^{3+}) = G_H + G_{OH} + 2G_{H_2O_2}. \quad (III)$$

However, as seen from Table 1, the experimental yields are lower than those calculated by Eqn. (III), which may be due to the competition of Reaction (8) with Reaction (5) and (7). For the extreme case, Eqn. (IV) instead of (III) should be applied and the yields calculated by Eqn. (IV) are listed in the last column of Table 1.

$$G(Fe^{3+}) = G_{OH} + 2G_{H_2O_2}. \quad (IV)$$

The present results and discussion were presented briefly at the International Conference on the Use of Cyclotrons in Chemistry, Metallurgy, and Biology held at

St. Catherine's College, Oxford, England, on 22 ~ 23, September, 1969 and will be published at length elsewhere.[5]

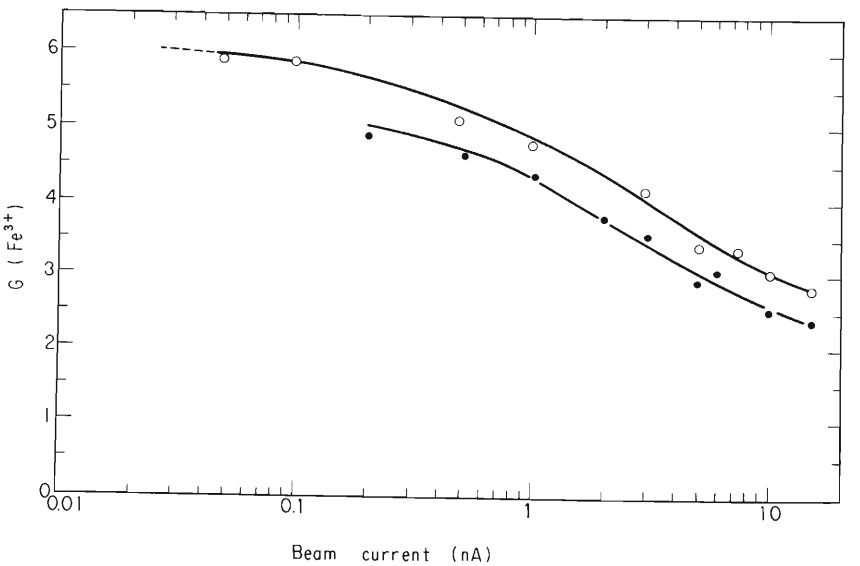

● : 1 mM, o : 10 mM aerated ferrous sulfate solution. Stirring speed : 36 r.p.s.

Fig. 1. G (Fe^{3+}) as a function of beam current of 13 MeV helium ions.

References

1) T. Rigg, G. Stein, and J. Weiss . Proc. Roy. Soc. (London), A 211, 375 (1952).
2) A. O. Allen : "The Radiation Chemistry of Water and Aqueous Solutions", van Nostrand, Princeton (1961).
3) J. P. Sweet and J. K. Thomas : J. Phys. Chem., 68, 1365 (1964).
4) H. Fricke and J. K. Thomas : Radiat. Res. Suppl., 4, 35 (1964).
5) M. Matsui, H. Seki, T. Karasawa, and M. Imamura : J. Nucl. Sci. Tech. (To be published).

8-2. LET Effect in the Radiolysis of Some Organic Liquids
Tetrahydrofuran, Anisole, and Methanol

M. Matsui, H. Seki, T. Karasawa, and M. Imamura

(1) Tetrahydrofuran

The yield of solvated electron produced in liquid tetrahydrofuran (THF) has been tried to determine for alpha radiolysis. In the gamma radiolysis of THF some aliphatic acid anhydrides were found to react with solvated electrons to produce CO quantitatively.[1] The similar technique has been applied to alpha radiolysis. The values of G (CO) were found lower than that for gamma radiolysis, which clearly indicates that the majority of solvated electrons are recombined in the alpha tracks. The preliminary value of G (CO) is ~ 0.1 for 23 MeV helium ions. The exact value of G (CO) has not yet been established in the course of investigation of the dose-rate and other effects on this system.

(2) Anisole

No LET effect study has been reported on the radiolysis of liquid anisole. The yields of products of the radiolysis of liquid anisole are tabulated in Table 1 for 10 MeV helium ions as well as for gamma rays. The increases in the yields of all products except CH_4 were observed with increasing LET. Further studies are in progress.

Table 1. Product yields for liquid anisole.

Product	G	
	Co-60 γ	10 MeV α
H_2	0.19	0.22
CH_4	0.14	0.05
C_2H_6	0.02	0.05
CO	0.01	0.04
C_2H_2	0.002	0.005

(3) Methanol

In the previous report[2] we reported the G-value for solvated electron produced in the radiolysis of liquid methanol with 30 MeV helium ions. The yield of solvated electron has also been determined for 14 MeV protons and the result is shown in Table 2 together with the more accurate value for 30 MeV helium ions. These results show a gradual decrease in G (e^-_{solv}) with increasing LET as illustrated in Fig. 1.

The isotopic composition of hydrogen gas from CH_3OD was also determined for 20 MeV helium ions and those for Co-60 gamma rays, 30 MeV helium ions and recoiled particles from the ^{10}B (n, α) ^7Li reactions were reported previously.[2] These results are plotted in Fig. 1 as a function of initial LET of radiation.

Table 2. Yields of solvated electron in methanol.

Radiation	G (e^-_{solv})
Co-60 γ	2.0
Proton, 14 MeV	1.6
Helium ion, 30 MeV	1.0
α , ^{7}Li-recoils	0.2

The increasing yield of H_2 with increasing LET may be explained by assuming following two types of recombination reaction in spurs and tracks.

$$CH_3OD^+ + e^- \longrightarrow H, D \quad (1)$$

$$CH_3OD_2^+ , CH_3ODH^+ + e^- \longrightarrow H, D. \quad (2)$$

In the gamma radiolysis the recombination takes place mainly via Reaction (2) to produce probably more D-atoms than H-atoms, giving the higher yield of HD than that of H_2. The ions, $CH_3OD_2^+$ and CH_3ODH^+, are formed by the ion-molecule reaction (Reaction (3)).

$$CH_3OD^+ + CH_3OD \longrightarrow CH_3OD_2^+ , CH_3ODH^+ \quad (3).$$

In the radiolysis by high-LET radiations, however, parent ions, CH_3OD^+, may have

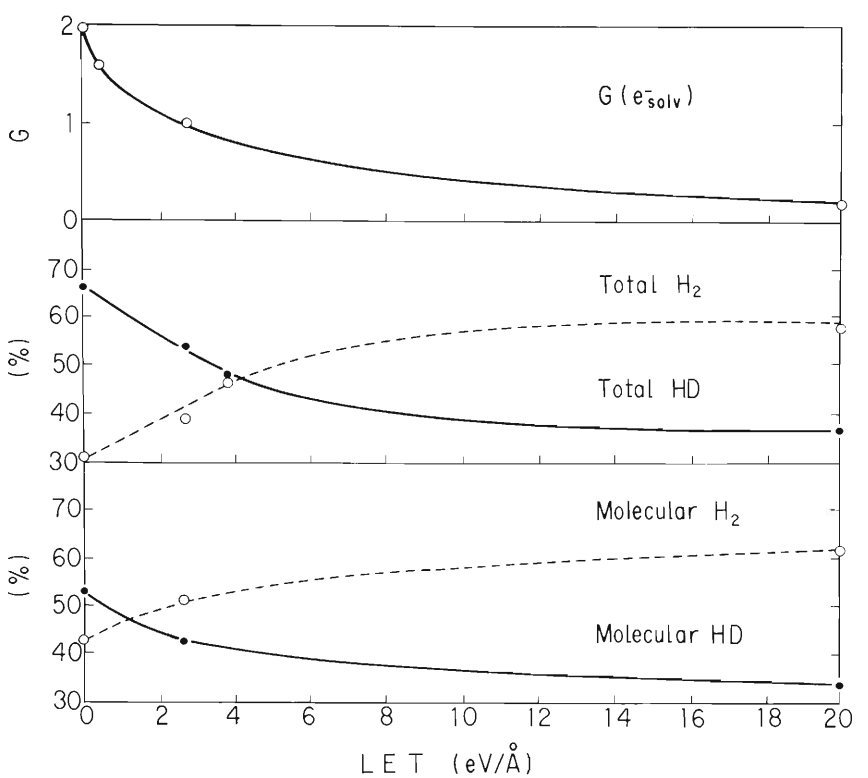

Fig. 1. Variations of G (e^-_{solv}) and isotopic composition of product hydrogen from CH_3OD with LET.

chances to recombine with electrons before occurrence of Reactions (3) and (2), and Reaction (1) is presumably of increasing importance in such dense ionization tracks of radiation. If the electrons recombine before solvation, no energy is dissipated by dipolar relaxation and the immediate recombination products are assumed to be H and D atoms with a statistical ratio of 3 : 1, resulting in the higher yield of H_2 than via Reaction (2).

Radiolysis study on alkaline methanol is being carried out, too.

References

1) M. Matsui and M. Imamura : Bull. Chem. Soc. Japan, 42, 3362 (1969).
2) M. Matsui, H. Seki, T. Karasawa, and M. Imamura : IPCR Cyclotron Progr. Rep., 2, 138 (1968).

8-3. The LET Effects on Bacterial Cells

A. Matsuyama, T. Karasawa, S. Kitayama, and R. Takeshita

In the study on the LET effects on bacterial cells, the solid-phase irradiation is now being carried out as well as the liquid-phase irradiation.[1,2] The bacterial strains of different radio-sensitivities to gamma rays, on one hand, such as the log-phase cells of Escherichia coli B_{S-1} and B/r and those of Micrococcus radiodurans R_1 and, on the other hand, dormant spores of a thymine-requiring mutant of Bacillus subtilis 168, thy^-, ind^-, leu^- (MY2Y1U2) have been used in this study.

Each 0.02 mℓ aliquot of these vegetative cell or spore suspensions was fed on a membrane filter (Millipore filter type HA, 8 mm in diameter) and a monolayer of bacteria obtained on a membrane filter was exposed to 4.8- and 13.5-MeV protons, 6.1-, 8.7-, 11.7- and 26-MeV alpha particles and 75-MeV C^{6+} ions from the cyclotron in air. A membrane filter loaded with bacterial cells was mounted on a target plate and fluctuated vertically and horizontally over the square area of 20 × 20 mm during irradiation. The absorption dose D in krad was calculated according to the following equation:

$$D = 2.5 \frac{L \cdot Q}{Z}$$

where L is a LET value in eV/A, Q is the charge input in nC and Z is the charge number of ionizing particles used. After irradiation, survivals were determined by the visible-colony counting method.

Examples of survival curves of four bacteria for ionizing particles of different LETs are illustrated in Fig. 1. The observed LET effects on the radiolethality revealed the decrease in an induction dose with M. radiodurans and the change in the RBE with all bacteria. As will be reported later, the survival curve of M. radiodurans has been found exponential at very higher LETs and this fact suggests the possibility of different mechanism for radiolethality in this bacterium caused by heavy ions. The RBE is represented in $1/D_{37}$ with two strains of E. coli and B. subtilis and the reciprocal of the dose is required for 1 % survival in the case of M. radiodurans (Figs. 2 and 3). Increase in the RBE was observed in the range of the LET between 2.7 eV/A and 8 eV/A for E. coli B/r, B. subtilis spore, and M. radiodurans, but not for E. coli B_{S-1}. Comparative radiosensitivities of these bacteria on solid- and liquid-phase irradiation are indicated in Table 1. It is notable that M. radiodurans is remarkably radioresistant even at higher LETs, while B. subtilis spore is not so resistant as E. coli B_{S-1} and B/r for heavy ions of high-LET.

Table 1. The D_{37} values.*

Bacteria	Solid-phase irrad.			Liquid-phase irrad. with 26 MeV α
	$^{60}Co\ \gamma$	6.1 MeV α	75 MeV C^{6+}	
E. coli B_{S-1}	1.01(1) (krad)	2.44(1) (krad)	4.98(1) (krad)	7.49(1) (nC)
E. coli B/r	6.45(6.4)	4.45(1.8)	11.6(2.3)	18.6(2.5)
M. radiodurans R_1		282(116)	278(56)	891(119)
B. subtilis 168 thy spore	42.9(43)	16.4(6.7)	23.1(4.6)	

* The figure in a parenthesis represents the ratio in D_{37} to E. coli B_{S-1}.

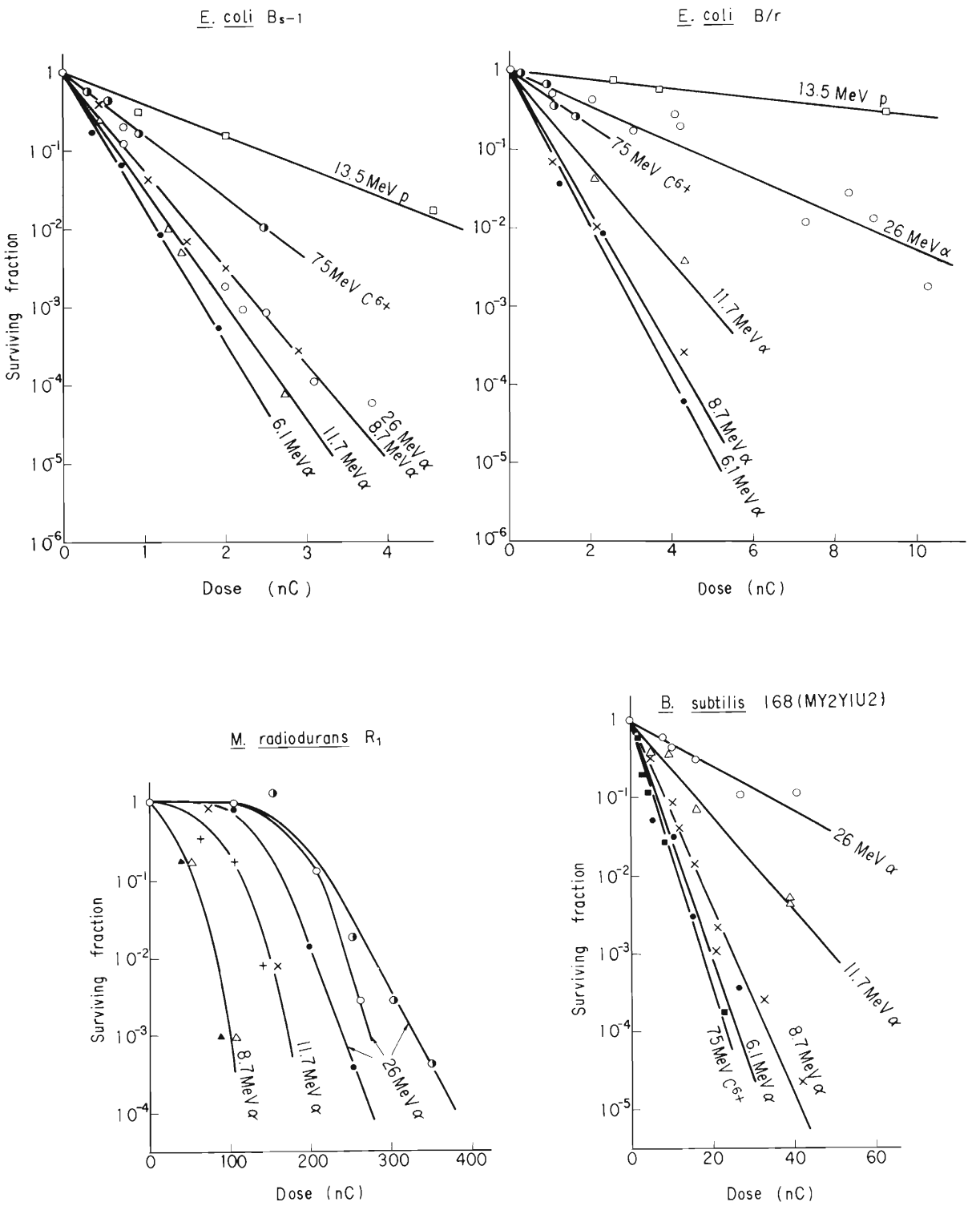

Fig. 1. Survival curves.

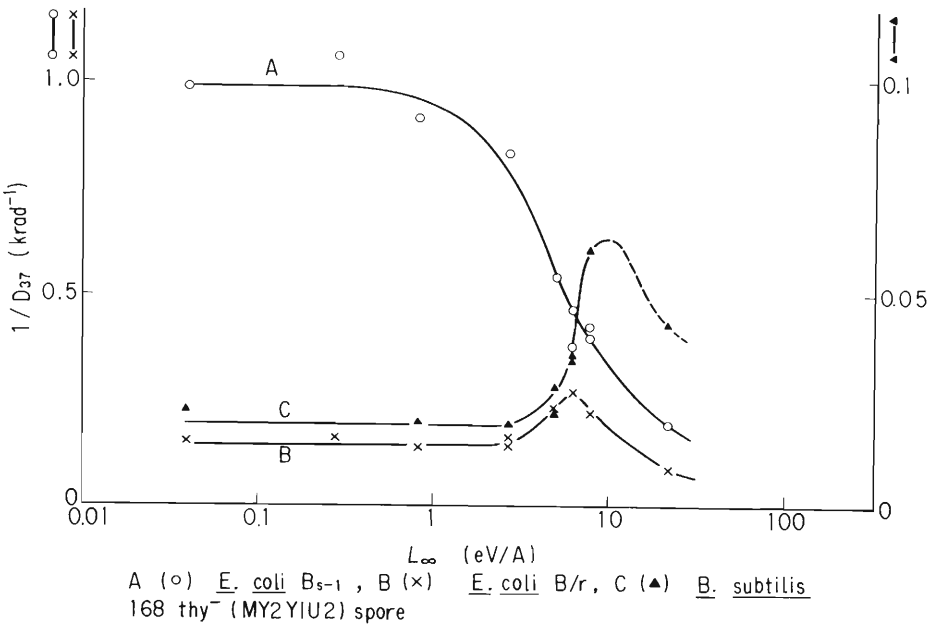

Fig. 2. Radiosensitivities of three bacterial strains versus L_∞.

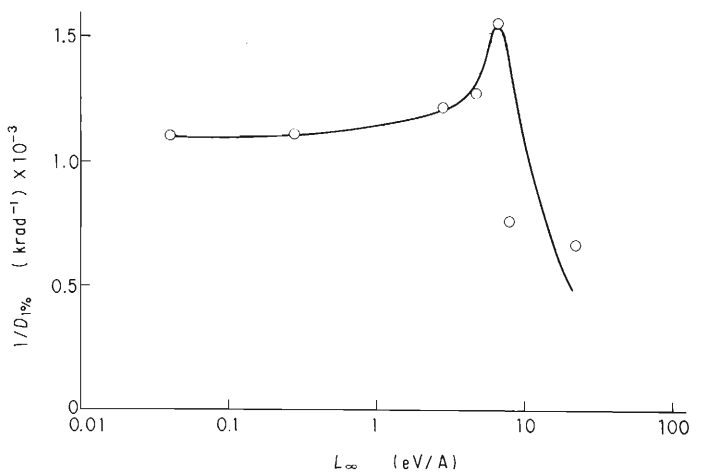

Fig. 3. Radiosensitivity of M. radiodurans R_1 versus L_∞.

References

1) A. Matsuyama, S. Kitayama, and T. Karasawa : IPCR Cyclotron Progr. Rep., 2, 141 (1968).
2) S. Kitayama, T. Karasawa, and A. Matsuyama : Agr. Biol. Chem., 33, 628 (1969).

9. SOLID STATE PHYSICS

9-1. Damage Rate of Cu_3Au by Proton Irradiation at Low Temperature

H. Sakairi, E. Yagi, T. Karasawa, and R. R. Hasiguti

The study of radiation damage deals usually, as its fundamental problem, with the displacement of atoms from crystalline lattice. But displacement events often accompany with replacements, which is an effective mechanism for transportation of collisional energy or momentum. Further, some collisions can cause only replacements, without displacements. Such collisions make no damage in pure metals but leave the disorder in ordered alloys.

Disordering of ordered Cu_3Au or ordering of disordered ones by irradiation was extensively studied about fifteen years ago. Most of those studies were carried out with reactor neutrons and the irradiation was almost done at room temperature, and a few at the liquid nitrogen temperature. So all of these studies dealt with replacements which are not only the result of collision events but that of thermal migration of point defects created by displacements of atoms.

We are carrying out the proton irradiation at liquid helium temperature to exclude an annealing effect from replacement processes. Yet, at present, so few experimental data are obtained at the liquid helium temperature that we describe here the results of the damage rate of Cu_3Au irradiated by heavy charged particles at liquid nitrogen temperature. A datum at liquid helium temperature is also presented, but the irradiation dose in its experiment was too small to derive the accurate value of damage rate.

(1) Experimental

The specimen was a ribbon, 4 mm wide and $30 \sim 40 \mu$m thick, and a part of it (8 mm long) was irradiated. The specimens were heat-treated for the strain removal and for the ordering. The specific resistivity of them was about $3 \mu\Omega$cm at liquid nitrogen temperature. That of perfectly ordered one was about $2 \mu\Omega$ cm, and that of completely disordered one was about $10 \mu\Omega$ cm,[1] so this specimen was believed to be well ordered, though not perfect.

To check the experimental accuracy, especially of the measurement of integrated dose, copper specimen, 2 mm wide and 50μm thick, was also irradiated.

Protons with energy of 14 MeV and 10 MeV were used for the irradiation. But, because of the energy loss in the widow of aluminum foil and in the specimen itself, the average proton energy in Cu_3Au dropped to 13 and 9 MeV. For Cu it was nearly the same because the Cu specimen was thicker than Cu_3Au specimen. Details of the target box and irradiation technique will be described elsewhere.

(2) Summarized discussions

(a) The increase of electrical resistivity of specimen by the irradiation at the liquid nitrogen temperature is shown in Fig. 1.

(b) Damage rate of Cu and Cu_3Au obtained by us were smaller than those obtained by others (Table 1). Reproducibility seemed satisfactory in our experiments, however, we are reexamining our apparatus and technique especially about the measurement of irradiation dose.

(c) The damage rate of Cu_3Au does not depend on the proton energy. It is shown that degree of disordering is not directly related to the number of displacement atoms, which must be inversely proportional to the energy of striking particle.

(d) The damage rate at liquid helium temperature was more than 10 times larger than that at liquid nitrogen temperature. It shows the existence of a large annealing stage between liquid helium and liquid nitrogen temperatures, perhaps at that of stage I of pure metals. We believed that annealing at that stage is caused by a migration of a crowd ion, which is created at the end of focusing collision chains. One dimensional thermal migration of this defect to the starting point of collision chain can effectively reorder the one dimensional replacement chain.

(e) The damage of Cu_3Au irradiated at liquid nitrogen temperature was reduced to 60 % by an annealing at room temperature. However, Brinkman et al. reported it was reduced to 75 % by an pulse annealing up to 130 °C.

(f) The annealing behaviors of specimens irradiated at liquid nitrogen temperature and at liquid helium temperature will be studied in detail in this laboratory.

Table 1.

Summary of the damage rate of Cu and Cu_3Au irradiated by protons.

Specimen	Irrad. Temp.	Proton energy (MeV)	Damage rate Ω cm/(p/cm^2)	Authors
Cu	Liq. N_2 T.	10	3.3×10^{-25}	Dworschak et al.[2]
			5.5×10^{-25}	
		9	2.5×10^{-25}	Present authors
Cu_3Au	Liq. N_2 T.	9	8.5×10^{-24}	Brinkman et al.[3]
		9	5.4×10^{-24}	Present authors
			6.4×10^{-24}	
		13	6.0×10^{-24}	Present authors
			5.8×10^{-24}	
			5.6×10^{-24}	
			6.6×10^{-24}	
	Liq. He T.	13	1×10^{-22}	Present authors

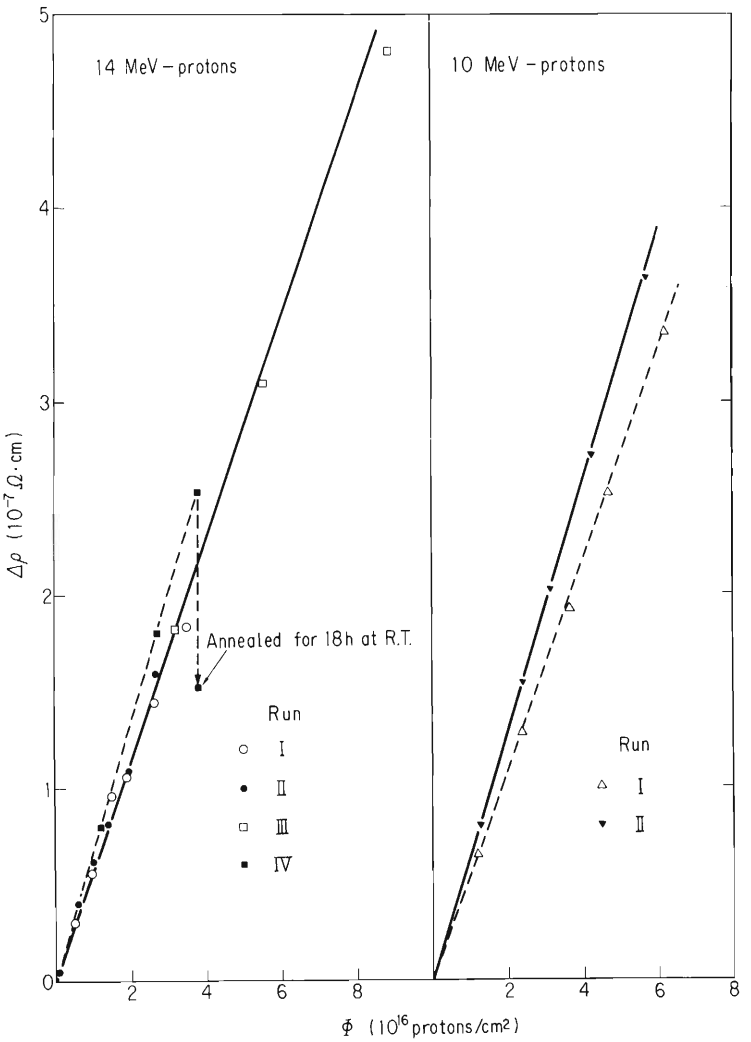

Fig. 1. Damage production curves of Cu_3Au irradiated by protons.

References

1) M. Hirabayashi and Y. Muto : Acta Met., 9, 497 (1961).
2) Dworschak, K. Herschbach, and J. S. Koehler : Phys. Rev., 133, A293 (1964).
3) J. A. Brinkman, C. E. Dixon, and C. J. Meechan : Acta Met., 2, 38 (1954).

9-2. Electron Microscopic Observation on the Helium Bubbles in Aluminum Irradiated by Alpha Particles

R. R. Hasiguti, M. Kobayashi, H. Sakairi, E. Yagi,
and T. Karasawa

The behavior of gas atoms produced by nuclear fission in reactor materials was widely investigated. The alpha particle irradiation by cyclotron makes a good simulative experiments of (n, α) reactions, because it avoids a strong residual radioactivity caused by reactor irradiation, which disturbs the detailed experimental analyses of samples.

In our laboratory, transmission electron microscopic observation of He bubbles in stainless steel and pure aluminum are continued. The stainless steel is representative of practical materials and the aluminum is of such a materials that fundamental physical properties, especially of lattice imperfections, have been fairly well understood.

In this report some of the results of the investigation of the relationship between bubbles and lattice imperfections in pure aluminum will be briefly described.

(1) Experimental

Three kinds of specimens, A, B, and C, as followings, are prepared.

A: cold-rolled,
B: annealed for two hours at 400 ° C in vac.,
C: annealed for two hours at 400 ° C in vac. and strained to 10 % in tension.

The thickness of specimen is 20 μm.

A stack of specimen foils was irradiated by 23 MeV alpha particles. They stopped in the foil laid just at their range. Total dose was $10^{15} \sim 10^{16}$ α/cm^2, which gave the density of about $10^{18} \sim 10^{19}$ He/cm^3 near the range of alpha particles.

The temperature of specimen rised to 150°~200° C during irradiation. Most specimens were annealed in vacuum for an hour at 300°, 400°or 500° C, before they were electropolished for a JEM-120 electron microscopic observation. Some specimens were not heat-treated before electropolishing.

(2) Results

In general, the higher the annealing temperature, the larger the size of bubbles and the fewer the number of bubbles.

(a) Interaction with dislocations

The formation of bubbles on dislocation lines was not observed in most specimens. A few examples of the dislocation-bubble contact were thought to be formed by the migration of dislocation to an already grown bubble (Figs. 1 and 2).

(b) Interaction with grain boundaries

Bubbles did not appear on grain boundaries at all in the specimens A. In other specimens bubbles on grain boundaries were observed only after heat-treatment at 300° C (Figs. 3 and 4). Also, in the heating experiment during the observation in the microscope, bubbles began to appear at 200° C and the most of them disappeared at 400° C.

(c) Interaction with precipitates

In most cases bubbles appeared at the surface of precipitates (Fig. 5). Especially many bubbles were seen there in the cold-rolled specimens as irradiated state. But few were observed in other specimens as irradiated state.

(3) Summarized discussions

(a) Results of observation mentioned above are summarized in Table 1. It is noted that bubbles are formed preferentially at the grain boundaries and precipitates while they are not found on the dislocation lines.

(b) But this shows only the absence of an interaction between large visible bubbles and dislocations. The existence of an interaction between small unvisible bubbles (or He atoms themselves) and dislocations is suggested by some facts as follows:

Table 1. Summary of the results of observation.

Specimen	Site	Annealing temperature			
		200° C	300° C	400° C	500° C
A	Matrix	++	+	+	+
	Boundary	−	−	−	−
	Precipitate	+	+	+	+
	Dislocation	−	−	−	−
B	Matrix	−	+	+	+
	Boundary	−	+	−	−
	Precipitate	−	+	+	+
	Dislocation	−	−	−	−
C	Matrix	−	+	+	+
	Boundary	++	+	−	−
	Precipitate	−	+	+	+
	Dislocation	−	−	−	−

++ : observed frequently, + : observed, − : not observed.

(i) The bubble formation at grain boundaries is remarkable in such specimens, into which the dislocations are previously introduced.

(ii) The bubble formation at grain boundary occurs near 200° C and they disappear above 300° C. This characteristic temperature range is a recrystallization one.

(iii) Observations mentioned above are about the relation between bubbles and the defects which exists in crystal before the irradiation. But the irradiation itself produces some defects. The role of such radiation-induced defects in the bubble formation is another problem, which is one of the present theme in our laboratory.

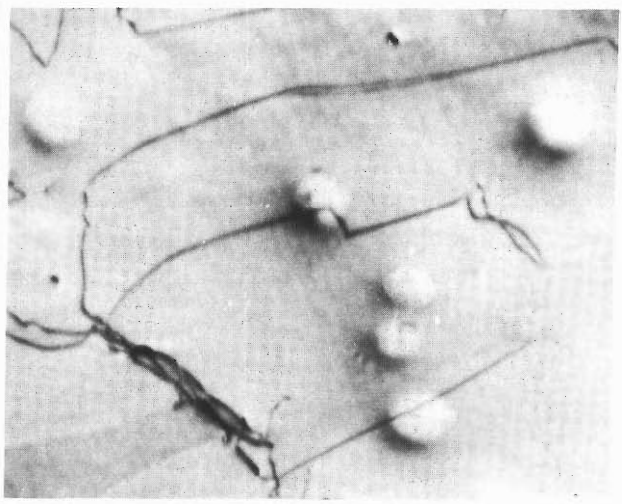

Fig. 1. Bubbles and dislocations in specimen C annealed at 500 °C. (×25000)

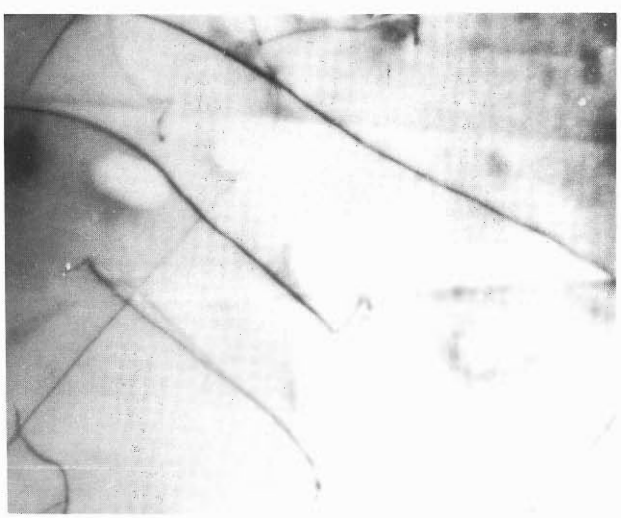

Fig. 2. Bubbles and dislocations in specimen C annealed at 500 °C. (×30000)

Fig. 3. Bubbles and grain boundaries in specimen A as irradiated. (×50000)

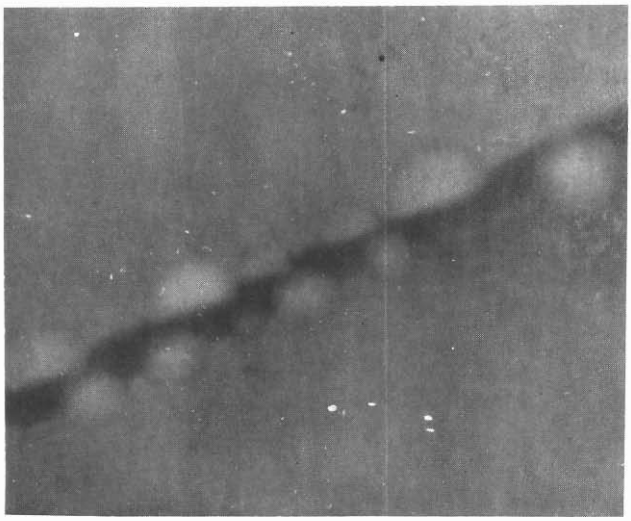

Fig. 4. Bubbles and grain boundaries in specimen C as irradiated. (×20000)

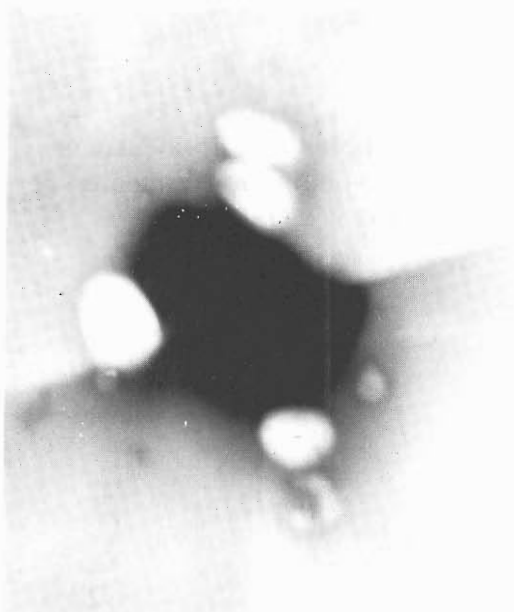

Fig. 5. Bubbles and presipitates in specimen C annealed at 300 °C. (×15000)

9-3. Mössbauer Effect of ^{61}Ni in Spinel Type Magnetic Oxides

H. Sekizawa, T. Okada, S. Okamoto, F. Ambe,
and A. Shimamura

(1) Introduction

Mössbauer effect is utilized extensively to investigate magnetism and magnetic substances. But most of the works were made by ^{57}Fe, which fulfils so many necessary requirements as a convenient nuclide for such experiments. Among the Mössbauer nuclides other than ^{57}Fe, ^{61}Ni occupies a special position. It is inferior to ^{57}Fe on many points, but it is the only known Mössbauer nuclide in the iron group elements except ^{57}Fe, and the informations obtained by it should be unique in the research of magnetism, especially in investigating magnetic substances containing Ni. An extensive study of magnetism by radioactive ^{61}Cu produced by IPCR 160 cm Cyclotron is under way in this Institute. Some of the preliminary results on magnetic oxides containing Ni will be briefly given in this report.

(2) Experimental

The decay scheme of ^{61}Ni is well known. There are two parent nuclides, ^{61}Cu and ^{61}Co, leading to the Mössbauer level of ^{61}Ni. ^{61}Co was utilized by many investigators,[1] because of its high signal-to-background ratio of the gamma ray spectrum. But we adopted ^{61}Cu because of its longer half life (3.3 h) than ^{61}Co (1.7 h). Two entirely different procedures were developed to prepare single-line gamma ray sources for Mössbauer experiments. The first one consists of irradiation of Ni metal by alpha particles, chemical separation of ^{61}Cu from the target, electroplating it on Cu metal, and annealing it at high temperature to diffuse ^{61}Cu into the host. Details of the procedure have been reported in a separate article.[2] The second one, which was used in the present experiments, is as follows:

The Ni-V alloy containing more than 16 % V is known to be non-ferromagnetic, which is a necessary condition as a host metal for the source. A circular plate 20 mm in diameter and 1.5 mm thick was cut from an ingot of 84 Ni-16 V alloy, fixed on a holder made of aluminium with water cooling, and irradiated with 20 MeV, ca. 20 μA alpha particle beam from the cyclotron for 3 ~ 4 h. The nuclear reactions are ^{58}Ni (α,p) ^{61}Cu and ^{58}Ni (α,n) ^{61}Zn $\xrightarrow{\beta^+}$ ^{61}Cu. It was then kept for about three hours in a shielded chamber to let spurious radioactive isotopes decay out. Earlier, the source was annealed to get rid of the effect of radiation damage, but this procedure is now eliminated after finding that it had no effect upon the obtained Mössbauer spectra. The source was mounted on the tip of a rod attached to the transducer extending into a liquid nitrogen cryostat to increase the fraction of recoilless emission of the 67.4 keV gamma ray. A 2 mm NaI scintillation counter was used with a 400 channel PHA. The energy spectrum of the source is shown in Fig. 1. The Mössbauer spectrometers were routine type commercial ones *,** in parabolic mode of operation.

* Elron Electronic Industries, Ltd.
** Hitachi Ltd.

(3) Results and discussion

Several oxides containing nickel with spinel (or distorted spinel) type crystal structure were prepared in small amount by firing appropriate mixtures of nitrates of constituent metals. Nickel metal enriched to 80 ~ 90 % in ^{61}Ni was used. The oxides investigated were, $NiFe_2O_4$, $NiCo_2O_4$, $NiMn_2O_4$, $GeNi_2O_4$, and $NiCr_2O_4$. Mössbauer absorption spectra were taken at liquid nitrogen temperature, and also at He temperature for some of them. As an example, the spectrum of $NiFe_2O_4$ at 80 ^{o}K is shown in Fig. 2. For all the oxides, because of the broad natural line-width of the 67.4 keV gamma ray, the twelve line spectra could not be resolved and showed a pattern with some structure and asymmetry. Thus, the computer fitting of the spectrum is an

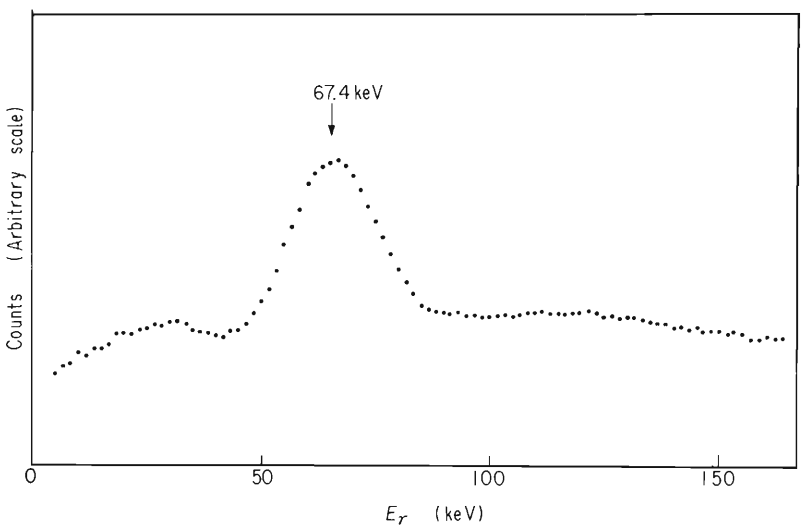

Fig. 1. Energy spectrum of the radiation from ^{61}Cu.

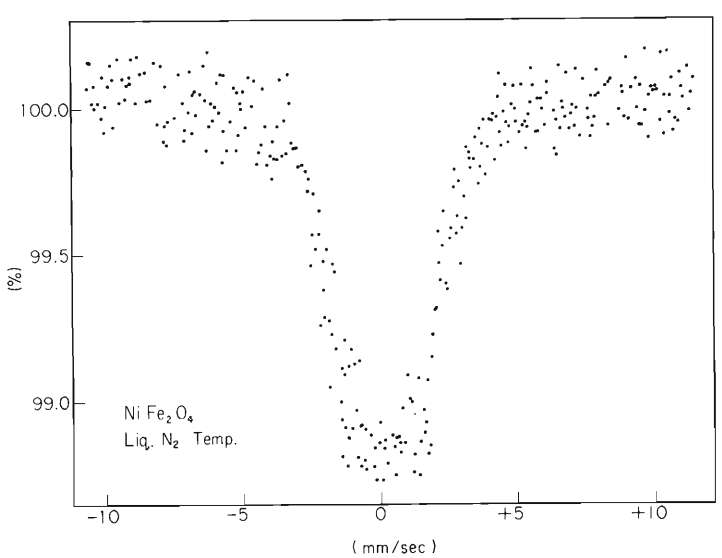

Fig. 2. ^{61}Ni Mössbauer absorption spectrum of $NiFe_2O_4$ at 80 ^{o}K.

unavoidable process in analyzing it. A computer program, in which the effect of electric field gradient was taken into account as a perturbation to the internal magnetic field effect, was made and tried to least-square fit the spectra. Unfortunately, it was found that the effect of the former is not so small and can not be treated as a perturbation. The preparation of an improved program without perturbation assumption is now in progress.

References

1) J. C. Travis and J. J. Spijkerman : "Mössbauer Effect Methodology", Plenum Publishing Corp., New York, N. Y., 4, 237 (1968).
2) F. Ambe, S. Ambe, M. Takeda, H. H. Wei, K. Ohki, and N. Saito : Radiochem. Radioanal. Letters, 1, 341 (1969).

10. RI PRODUCTION AND ITS APPLICATIONS

10-1. Preparation of ^{18}F-labelled Compounds and Production of ^{52}Fe

T. Nozaki and A. Shimamura

We have continued our studies of the preparation of ^{18}F-labelled compounds by use of the ^{3}He-bombardment of an oxygen stream.[1,2] A poly-perfluoroolefin bombardment box with a small metal beam-entrance window has been found to be very useful; about 80 % of all the ^{18}F formed in it can be carried away from the box with the stream. No other substance ever tested has had such a weak adsorptivity to the ^{18}F.

Thus, many inorganic fluorinating agents such as KF, SbF_3, AgF, and $NaBF_4$, can now be labelled easily and efficiently by the following procedure: (1) paint their aqueous or alcoholic solutions on glass wool and dry it; (2) place them in a small poly-perfluoroolefin tube and connect it to the stream-outlet of the bombardment box, and (3) bombard it with an oxygen stream. The labelled fluorinating agent with the glass wool is added to a reaction mixture for the halogen interchange or the Schiemann reaction.

This labelling method is usually superior to the inside-coating method reported previously,[2] because the fluorinating agent in the tube can be attached to or removed from the box without disturbing the box and the stream. A Teflon bombardment box is used now, but a metal box with Teflon-coated inside will soon be available; the latter is much superior in cooling efficiency.

The study of the production of ^{52}Fe has been almost completed.[3] Figs. 1 and 2 show the thick target yields of ^{52}Fe for the ^{3}He- and alpha-bombardments of chromium respectively. (The previously-described excitation curves for the formation of ^{52}Fe[3] should be slightly modified in absolute cross section, though their shapes are correct.) Although the alpha bombardment of an enriched ^{50}Cr gives a higher yield than does the ^{3}He-bombardment of natural chromium, we have adopted the latter because the enriched isotope is expensive.

Our chromium target for the ^{52}Fe production ($14 \times 1.5 \times 0.1$ cm in dimension) is prepared by electroplating onto a copper block of a standard size for the internal bombardment; after the electroplating, silver is electroplated onto the copper surface to give a target assembly from which the chromium is easily soluble in warm hydrochloric acid. The target is bombarded with the maximum available flux (about 30 μA) of 40 to 42 MeV ^{3}He-beam for a few hours. It is then taken away from the cyclotron by a remote-control operation and transported into a remote-operation chemistry cell.

Fig. 3 shows the apparatus used in the remote-controlled separation of the ^{52}Fe. The polyethylene bottle (700 mℓ in content) has been equipped with methyl isobutyl ketone (250 mℓ) and set on a motor-driven shaker in the chemistry cell; there, also, hydrochloric acid (8 N, 350 mℓ) containing KBr (3 g) has been heated to about 70 ^{o}C in a Teflon beaker on a hot plate. The target assembly is put into the beaker; the chromium is dissolved within about 20 min. Then, $KBrO_3$ (saturation solution, 1 mℓ) is added to the beaker, and its content is transferred into the bottle, which is stoppered and shaken for a few minutes. The stopper is then removed and a two-tubed glass lid

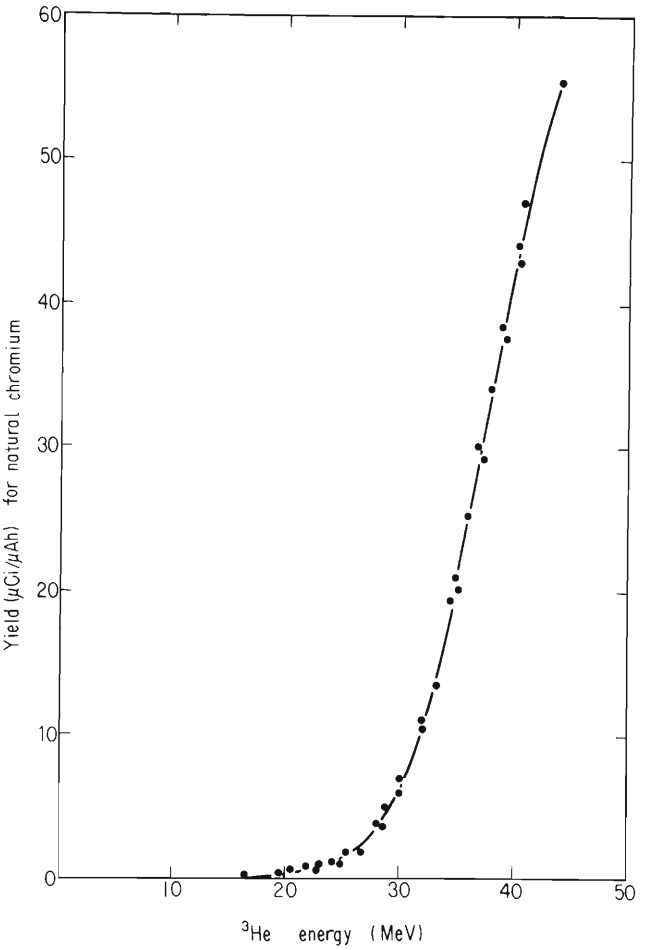

Fig. 1. Thick target yield for the Cr + ^{3}He ⟶ ^{52}Fe reaction.

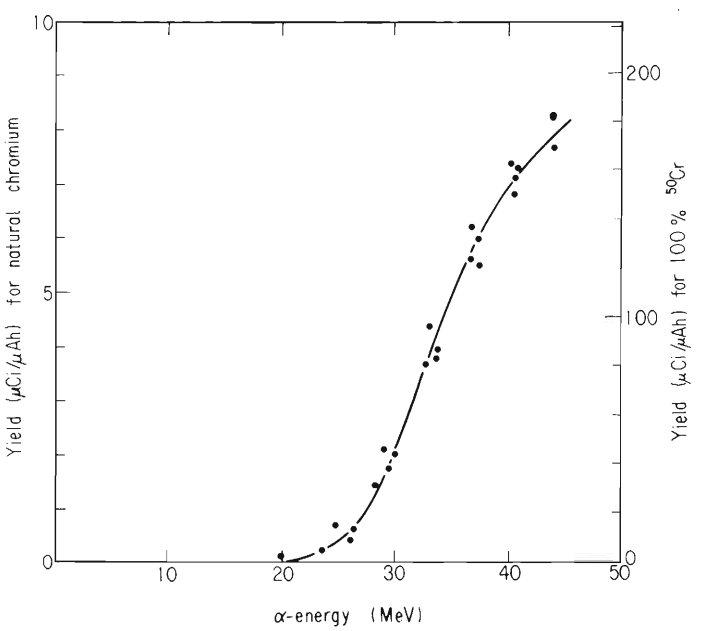

Fig. 2. Thick target yield for the Cr + α ⟶ ^{52}Fe reaction.

(Fig. 3) is set onto the bottle. Hydrochloric acid is added to the bottle through one tube until the entire organic phase has just overflowed through the other tube into a polyethylene beaker. The beaker is then taken away from the remote-separation cell, and the methyl isobutyl ketone is scrubbed with hydrochloric acid (5 N). The ^{52}Fe is then back-extracted into water (40 mℓ) and given to medical researchers.

It takes about one hour for the chemical process; the chemical yield and the radiochemical purity of the product have proved to be satisfactory. About 1 mCi of the processed ^{52}Fe is thus produced by one hour bombardment.

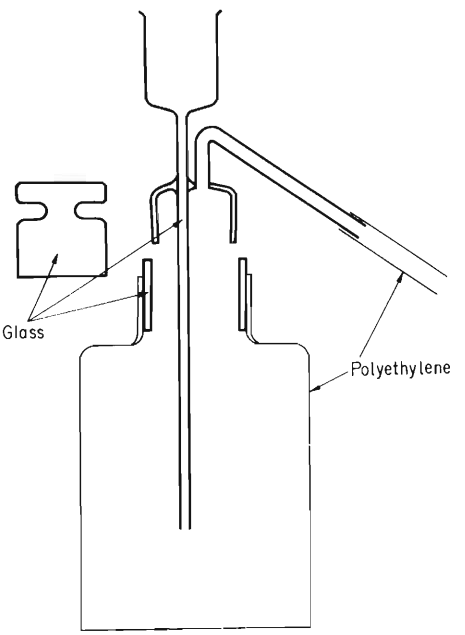

Fig. 3. Apparatus for remote-controlled separation of ^{52}Fe.

References

1) T. Nozaki : IPCR Cyclotron Progr. Rep., 1, 77 (1967).
2) T. Nozaki, A. Shimamura, and T. Karasawa : ibid., 2, 156 (1968).
3) T. Nozaki : ibid., p. 159.

10-2. Separation of Carrier-free ^{85}Sr from a Deuteron-bombarded Rubidium Target

M. Inarida and A. Shimamura

The 64-day ^{85}Sr, which is useful as a biological and medical tracer, was produced by the ^{85}Rb (d, 2n) ^{85}Sr reaction with a rubidium nitrate target. This report describes the separation of carrier-free ^{85}Sr from the irradiated target by means of solvent extraction.

The rubidium salt was wrapped in a 10 μm-thick aluminum foil and placed on a water-cooled brass target holder attached to the IPCR 160 cm Cyclotron. The target was then bombarded with 14 MeV deuterons through a window of 50 μm-thick aluminum foil for 40 min at a beam intensity of 1 ~ 3 μA. Under these conditions radioactive strontium isotopes were produced from ^{85}Rb and ^{87}Rb by the following reactions: ^{85}Rb (d, 2n) $^{85m}Sr \longrightarrow {}^{85}Sr$ and ^{87}Rb (d, 2n) ^{87m}Sr. After it has been cooled for 2 days to permit the decay of any short-lived nuclides, a 100 mg portion of the target was dissolved in 5 mℓ of a hydrochloric acid solution at pH 3. The method of separating carrier-free ^{85}Sr from the Rb target is shown below :

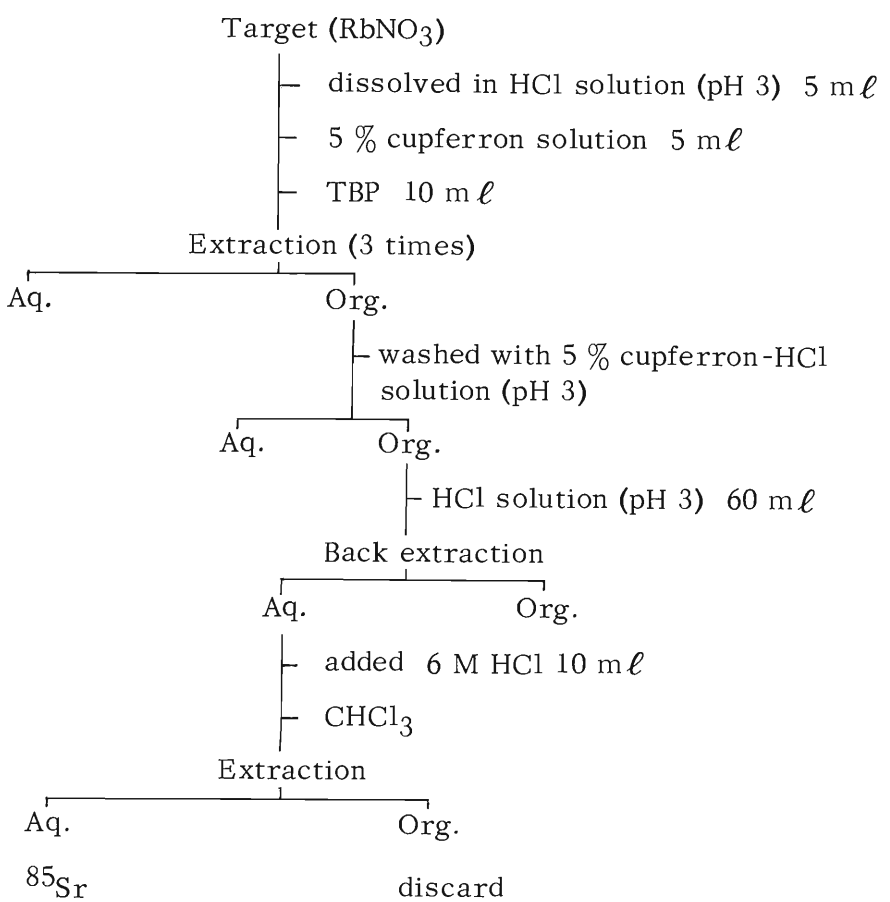

The radiochemical purity of the ^{85}Sr thus separated was checked by studying its gamma spectrum and decay curve and found to be higher than 99 %. The activity of the ^{85}Sr produced was about 0.02 millicurie. The radiochemical yield was about 95 %, and the time for separation was 10 min.

10-3. Separation of Carrier-free ^{89}Zr from a Deuteron-bombarded Yttrium Target

M. Inarida and A. Shimamura

The radionuclide, ^{89}Zr, produced by the ^{89}Y (d, 2n)^{89}Zr (79 h) nuclear reaction was isolated without an isotopic carrier by means of a solvent-extraction procedure.

The Y_2O_3 target was wrapped in a 10 μm-thick aluminum foil and placed on a water-cooled brass target holder attached to the IPCR 160 cm Cyclotron. The target was then bombarded with 15 MeV deuterons through a window of 50 μm-thick aluminum foil for 30 min at a beam intensity of $1 \sim 2$ μA. After the bombardment, the oxide powder was dissolved in a 10 M hydrochloric acid solution. The method of separating the carrier-free ^{89}Zr from the yttrium target is shown below :

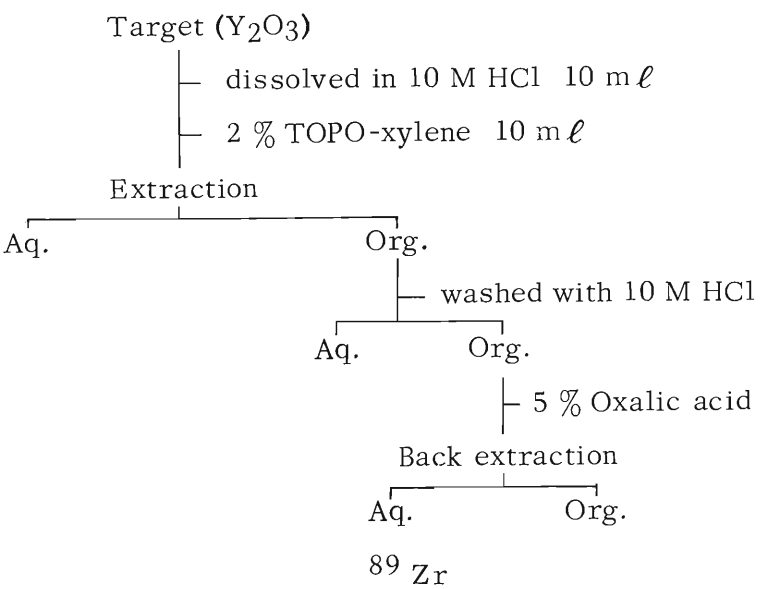

The radiochemical purity of the ^{89}Zr thus separated was checked by measuring its gamma spectrum and decay curve and found to be higher than 99 %. The ^{89}Zr produced amounted to about 0.3 millicurie. The radiochemical yield was about 93 %, and the time for separation was 6 min.

11. RADIATION MONITORING

11-1. Health Physics

K. Koda, I. Sakamoto, and I. Usuba

In this paper, the results of measurements made during a period from April 1968 to March 1969 are discribed on the dose distribution in the cyclotron room due to residual activities of the machine, radioactive concentration in the atmosphere, surface contamination, as well as the exposure of the workers.

(1) Residual activities

The distribution of dose rate due to residual activities of the machine measured 1 day after machine shutdown (the cyclotron had been operated for about 70 hours with deuteron of 20 MeV) is shown in Fig. 1. The highest dose rate of 6000 mR/h has been found at the baffle box.

(2) Air and surface contamination

When the accelerator chamber was opened, a slight contamination of the air in the cyclotron room was observed. The value of radioactive concentration (beta-gamma) ranged $10^{-6} \sim 10^{-7} \mu Ci/\ell$. The activity was identified by the gamma ray spectrometry to be of ^{65}Zn, ^{184}Re, ^{185}Os,and, probably, ^{7}Be, which could be eliminated with almost 100 % efficiency by filtration with the millipore filter AA (pore size : 0.8 μm).

The surface contamination on the floor of the cyclotron room was kept to be about $10^{-5} \mu Ci/cm^2$ (beta-gamma) throughout a year.

(3) Personnel monitoring

Concerning the external exposure in the yearlong measurement, the values of total dose of all personnel issued with the film badge are shown in Table 1. Average dose per person is 778 mrem which is 2.4 times of the value in the previous period. The gradual increase is considered to be mainly due to the increase of residual activities of the machine.

The neutron film badge is also supplied to all operators and accelerator physicists and some of the nuclear physicists, but they did not show any exposure to neutrons.

Measurements with the body counter have definitely shown that the workers are exposed to the radionuclides not only at their lungs but at other organs. Details of the results will be described on the next report.

An ordinary gauze mask having 20 leaves of gauze has been found to eliminate radioactive dusts in breathed air with an efficiency of about 90 % during works of the machine overhaul.

Table 1. Accumulated dose distribution of the staffs.

From Apr. 1968 to Mar. 1969

Group \ Dose (mrem)	Undetectable	10～100	101～300	301～1000	1001～
Operators				3	4
Nuclear physicists		5	8	7	
Accelerator physicists				5	1
Nuclear chemists		1	1	1	1
Radiochemists	1	2	2		
Health physicists			1	1	

Average dose per person : 778 mrem
Maximum dose : 1830 mrem

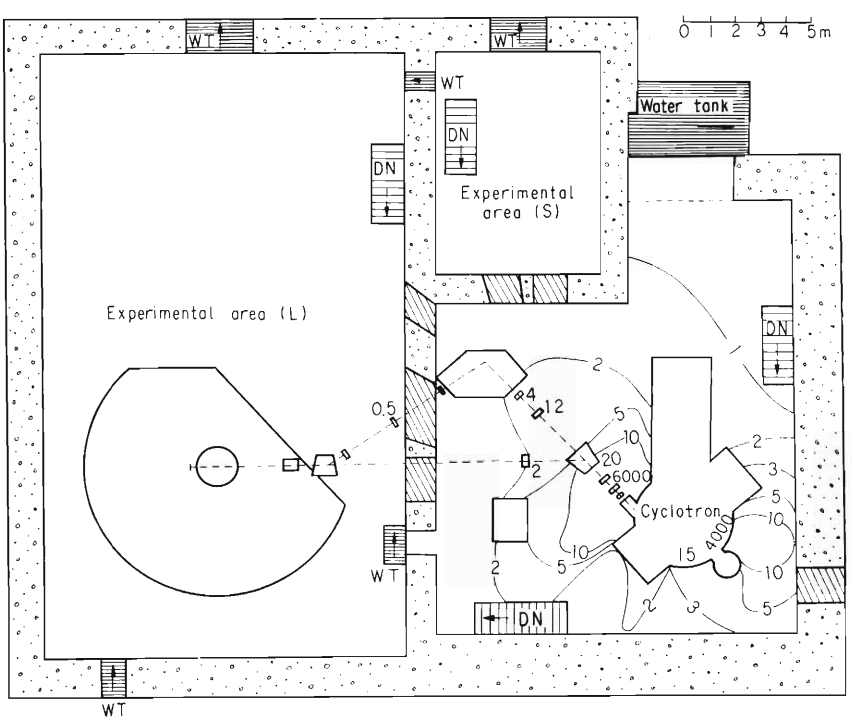

Fig. 1. Dose rate distribution in mR/h 1 day after the cyclotron had been operated for 70 h with deuteron of 20 MeV.

11-2. Gamma ray and Neutron Monitoring at the Monitoring Station

M. Wada, M. Okano, I. Sakamoto, M. Nisida,
and T. Hamada

Continuous records are taken for gamma rays and slow neutrons using two scintillation counters and a BF_3 counter at the monitoring station at 85 m apart from the cyclotron.

It was found that the gamma rays are mainly those from natural radioactive elements in the environments which sometimes vary during rain fall. The contribution of radioactive fallout was estimated by the gamma ray spectrometry.

During this period, gamma rays from the cyclotron operation could not be detected.

The slow neutron intensity depends upon the operating conditions of the cyclotron as was reported previously.[1] The integral gamma ray dose during the period from July 1968 to June 1969 was 24.6 mR within which the contributions of the environmental natural radioactive elements, of rain fall, and of the radioactive fallout are 22, 0.6, and 2 mR, respectively.

Reference

1) M. Wada et al.: IPCR Cyclotron Progr. Rep., 2, 163 (1968).

12. LIST OF PUBLICATIONS

1) M. Odera, Y. Miyazawa, T. Tonuma, M. Hemmi, and O. Terajima : "Design and Performance of a Focusing Magnetic Channel for a Variable Energy Multiparticle Cyclotron", Nucl. Instr. Methods, 65, 247 (1968).

2) I. Kohno, T. Tonuma, Y. Miyazawa, S. Nakajima, T. Inoue, A. Shimamura, and T. Karasawa : "A Multicharged Heavy Ion Source for the IPCR Cyclotron", Nucl. Instr. Methods, 66, 283 (1968).

3) N. Nakanishi, S. Motonaga, Y. Miyazawa, and T. Karasawa : "On Circular Trimming Coils Mounted on Magnet Pole Faces", Japan. J. Appl. Phys., 8, 1229 (1969).

4) M. Inarida and A. Shimamura : "Separation of Carrier-free ^{206}Bi from the ^{206}Pb Target", Radioisotopes, 18, 19 (1969).

5) F. Ambe, S. Ambe, M. Takeda, H. H. Wei, K. Ohki, and N. Saito : "Radiochemical Preparation of ^{61}Cu-Copper Single Line Source for the Measurement of the Mössbauer Effect in ^{61}Ni", Radiochem. Radioanal. Letters, 1, 341 (1969).

6) M. Inarida and A. Shimamura : "Separation of Carrier-free ^{76}As from the ^{78}Se Target", Radiochem. Radioanal. Letters, 2, 87 (1969).

7) H. Kamitsubo, T. Wada, T. Fujisawa, and M. Igarashi : "Large-Angle Scattering of ^{3}He Particles by ^{58}Ni", Phys. Letters, 28B, 408 (1969).

8) F. Ambe and N. Saito : "Chemical Effects of Neutron-Induced Nuclear Reactions in Halates and Related Compounds III, The (n, γ) and (n, 2n) Reactions in Iodates", Radiochim. Acta. (in press)

9) N. Nakanishi, Y. Chiba, Y. Awaya, and K. Matsuda: "Elastic Scattering of ^{3}He Particles on Ca at Five Incident Energies between 18.8 and 39.3 MeV", Nucl. Phys. (tobe published)

13. LIST OF PERSONNEL

IPCR Cyclotron Administration Committee

熊谷寛夫	Hiroo KUMAGAI (chairman)	浜田達二	Tatsuji HAMADA
橋口隆吉	Ryukiti R. HASIGUTI	今村昌	Masashi IMAMURA
唐沢孝	Takashi KARASAWA	松田一久	Kazuhisa MATSUDA
松山晃	Akira MATSUYAMA	斎藤信房	Nobufusa SAITO
杉本光男	Mitsuo SUGIMOTO	田中穣	Yutaka G. TANAKA

Managers of Users Group

野崎正	Tadashi NOZAKI	小寺正俊	Masatoshi ODERA

IPCR Cyclotron Operating Personnel

Management

唐沢孝	Takashi KARASAWA	小寺正俊	Masatoshi ODERA
元永昭七	Shoshichi MOTONAGA	河野功	Isao KOHNO
宮沢佳敏	Yoshitoshi MIYAZAWA		

Operation

藤田新	Shin FUJITA	池上九三男	Kumio IKEGAMI
中島尚雄	Hisao NAKAJIMA	荻原清	Kiyoshi OGIWARA
大沢信道	Nobumichi OSAWA	寺島為	Osamu TERAJIMA
吉田喜作	Kisaku YOSHIDA		

Scientific and Engineering Personnel

Cyclotron Lab.

熊谷寛夫	Hiroo KUMAGAI	千葉好明	Yoshiaki CHIBA
藤沢高志	Takashi FUJISAWA	藤田二郎	Jiro FUJITA
橋本房子	Fusako HASHIMOTO	逸見政武	Masatake HEMMI
稲村卓	Takashi INAMURA	井上敏彦	Toshihiko INOUE
上坪宏道	Hiromichi KAMITSUBO *	唐沢孝	Takashi KARASAWA
河野功	Isao KOHNO	松田一久	Kazuhisa MATSUDA
宮沢佳敏	Yoshitoshi MIYAZAWA	元永昭七	Shoshichi MOTONAGA
中島諄二	Shunji NAKAJIMA	中西紀喜	Noriyoshi NAKANISHI
小寺正俊	Masatoshi ODERA	島村晃	Akira SHIMAMURA
竹田繁	Shigeru TAKEDA	戸沼正雄	Tadao TONUMA
和田雄	Takeshi WADA	山路修平	Shuhei YAMAJI

* Present address: Saclay Lab.

(Visitors)

山崎敏光 Toshimitsu YAMAZAKI (Univ. of Tokyo)
野村　亨 Toru NOMURA (Univ. of Tokyo)
河合光路 Mitsuji KAWAI (Tokyo Inst. of Tech.)
小林晨作 Shinsaku KOBAYASHI (Inst. for Solid State Phys.)
鹿取謙二 Kenji KATORI (Tokyo Univ. of Educ.)
A. STRICKER (Univ. of Basel)

Radiation Lab.

浜田達二 Tatsuji HAMADA
岡野真治 Masaharu OKANO
天道芳彦 Yoshihiko TENDOW
粟屋容子 Yohko AWAYA
橋爪　朗 Akira HASHIZUME
加藤武雄 Takeo KATO

Nuclear Analytical Chemistry Lab.

斎藤信房 Nobufusa SAITO
荒谷美智 Michi ARATANI
安部静子 Shizuko AMBE
野崎　正 Tadashi NOZAKI
安部文敏 Fumitoshi AMBE
稲荷田万里子 Mariko INARIDA

(Visitors)

八剣吉文 Yoshifumi YATSURUGI (Komatsu Electronic Metals Co., Ltd.)
秋山信之 Nobuyuki AKIYAMA (Komatsu Electronic Metals Co., Ltd.)

Biochemistry I Lab.

田中　穣 Yutaka G. TANAKA

Radiobiology Lab.

松山　晃 Akira MATSUYAMA
竹下亮一 Ryoichi TAKESHITA
北山　滋 Shigeru KITAYAMA

Radiation Chemistry Lab.

今村　昌 Masashi IMAMURA
関　博之 Hiroshi SEKI
松井正夫 Masao MATSUI

Metal Physics Lab.

橋口隆吉 Ryukiti R. HASIGUTI
坂入英雄 Hideo SAKAIRI
八木栄一 Eiichi YAGI
塩谷亘弘 Nobuhiro SHIOTANI

(Visitors)

三島良績 Yoshitsugu MISHIMA (Univ. of Tokyo)
小林正俊 Masatoshi KOBAYASHI (Univ. of Tokyo)

Magnetic Materials Lab.

杉本光男 Mitsuo SUGIMOTO
岡本祥一 Shoichi OKAMOTO
岡田卓也 Takuya OKADA
関沢　尚 Hisashi SEKIZAWA

Radiation Monitors

甲田陸男	Kugao KODA	坂本一郎	Ichiro SAKAMOTO
薄葉勲	Isao USUBA		

(Editors of the Progress Report)

松田一久	Kazuhisa MATSUDA	野崎正	Tadashi NOZAKI
田中穣	Yutaka G. TANAKA		

IPCR Cyclotron Progress Report 1969

理化学研究所サイクロトロン年次報告 第3巻(1969)

印　刷　昭和45年（1970）　3月25日
発　行　昭和45年（1970）　3月30日
発行者　理化学研究所
　　代表者　赤　堀　四　郎
　　351　埼玉県北足立郡
　　大和町広沢2番1号
　　電話（0484）62－1111
編集者　理化学研究所サイクロトロン運営委員会
　　委員長　熊　谷　寛　夫
印刷所　丸星印刷株式会社
　　101　東京都千代田区
　　神田神保町1丁目42番地

定価 1,500 円

理化学研究所

埼玉県　北足立郡　大和町